ADVANCED INTELLIGENT SYSTEMS Open Access
www.advintellsyst.com

Poly(vinylidene Fluoride)-Based Ferroelectric Polymers for Electromechanical Transduction: A Systematic Review of Materials and Actuators

Giulio Gallucci and Andres Hunt*

Poly(vinylidene fluoride) (PVDF) and its derivatives are ferroelectric polymers (FPs) that combine high electric-field-induced strains with mechanical flexibility, light weight, and processability, making them attractive materials for actuator applications. This work reviews the state-of-the-art in PVDF-based electromechanical transduction, covering both reported materials and actuators. Materials are compared by maximum strains, energy densities, and coupling efficiencies and categorized as: 1) vinylidene fluoride (VDF) polymers, including PVDF and its co-, ter-, and tetrapolymers; 2) PVDF-based composites with ceramic, conductive, metal-organic, and organosilicate fillers; and 3) polymer blends with plasticizers or other electroactive polymers. The highest strains and energy densities have been respectively reported for P(VDF-DB) (13.4%) and TiO2/PVDF (11.3 J cm^{-3}) and highest coupling efficiencies for P(VDF-TrFE-CFE-FA), SWCNTs/P(VDF-TrFE), and TiO2/PVDF (0.88). Actuators are compared in terms of maximum displacements and categorized as unimorph and bimorph bending cantilevers, dilating diaphragms, plates, stacks, and tubular structures. Bending cantilevers are the most frequently reported actuators. The highest length-normalized displacements (δ/L) in quasi-static and resonant operation were reported for PVDF bimorphs (0.35 and 0.45 respectively), which can be significantly improved by optimizing the transducer design and employing more efficient materials. The findings further indicate several unexplored transducer material candidates that are anticipated to exhibit high transduction response.

1. Introduction

Emergence of smart material transducers stimulates development of new technologies in microfluidics,[1,2] tissue engineering,[3] organ-on-chips devices,[4] bio-inspired soft robotics,[5–7] and other fields.[8] Electroactive polymers (EAP) are a class of stimuli-responsive materials[9] that deform in response to electric field, making them directly compatible with electronic controls.[10–12] Their unique properties include softness, flexibility, high strains, light weight, simple construction, miniaturizability, and ease of shaping,[12–14] enabling innovative applications that require qualitatively different properties from conventional transducers. Achieving a versatile combination of electrical, mechanical and transduction properties is of critical importance in EAP utilization for practical applications.

EAPs are categorized as ionic and electronic materials that respectively rely on ionic current[15] and Coulomb forces.[11] Ionic EAPs (iEAPs) include conducting polymers,[16] ionic polymer gels,[17] ionic polymers,[18] and the related ionic-polymer-metal composites (IPMCs)[19] that produce large strains (up to 12%)[20] and bending displacement[21] at low voltages (typically <5 V or <25 mV μm^{-1}[19]), but limited coupling efficiency (<0.01) and response speed.[11,18,22] Electronic EAPs (eEAPs) include dielectric elastomers (DEs), ferroelectric polymers (FPs), liquid crystal elastomers (LCEs), electrostrictive graft elastomers (EGEs), and electrostrictive paper (EP)[11] that exhibit fast response, high strains and energy densities,[23] but generally require high activation voltages (>100 V μm^{-1}).[24]

While actuation of DEs, LCEs, and FPs[10,25] has been addressed in numerous studies, EGE[26] and EP[27] have received less attention. Dielectric elastomer actuators produce highest strains among EAPs (pre-streched acrylics can exceed 100%)[28], energy densities of up to 3.4 J cm^{-3} and coupling efficiencies of up to 0.7–0.8,[29–31] but require high electric fields (100–400 V μm^{-1}) and suffer from viscoelastic losses.[32–36] The electrically driven LCEs produce high strains (up to 4%) at very low field strengths (1.5 V μm^{-1}), but are limited in energy density (<0.1 J cm^{-3}) due to the low Young's modulus.[37,38] Ferroelectric polymers produce lower strains (up to 13.4% at 275 V μm^{-1})[39] than DEs, but similar energy densities (up to 3.1 J cm^{-3}), higher dielectric constant (50–60),[18] and high coupling efficiencies (up to 0.88).[40] Electromechanical transduction of LCEs[41–46] and DEs[30,31,35,47–60] has been reviewed in many reports, but has not been specifically reviewed for FPs.

G. Gallucci, A. Hunt
Department of Precision and Microsystems Engineering
Faculty of Mechanical Engineering
Delft University of Technology
Mekelweg 2, Delft 2628 CD, The Netherlands
E-mail: G.Gallucci@tudelft.nl

The ORCID identification number(s) for the author(s) of this article can be found under https://doi.org/10.1002/aisy.202500694.

DOI: 10.1002/aisy.202500694

Ferroelectric polymers include poly(vinylidenefluoride) (PVDF) and its derivatives,[61] odd-numbered Nylons,[62] amorphous polyamide blends,[63] polyimides,[64] polylactic acid (PLLA),[65] and chlorinated poly(*para*-xylylene) (PA-C),[66,67] exhibiting piezoelectric, pyroelectric, ferroelectric, and electrostrictive properties.[68] Polyvinylidene fluoride (PVDF) and its derivatives have received by far the most attention, as they exhibit strongest electromechanical transduction properties of the group. PVDF homopolymer has been reviewed in terms of its mechanical, physical, thermal, dielectric, and chemical characteristics.[69,70] Extensive summaries address the influence of manufacturing on the morphology[71] and crystalline properties[68,72–74] of PVDF and its copolymers. Other reviews have addressed strategies to enhance dielectric properties of PVDF-based polymers,[75] and their utilization in high-performance capacitors,[76–78] flexible nanogenerators,[79] and other applications.[80–83] While the materials have a strong position in actuation applications, no review summarizes the PVDF-based materials in terms of their electromechanical transduction properties for actuation.

This review addresses electromechanical transduction properties of PVDF-based ferroelectric materials and their application in actuators (**Figure 1**). It summarizes the most significant properties for the materials' transduction performance, such as dielectric permittivity, Young's modulus, strain, electrostrictive and piezoelectric coefficients, energy density, breakdown strength, and coupling efficiency. First, the transduction phenomena of ferroelectric polymers is addressed in Section 2, along with the functioning principles of the most common linear and bending actuators. Next, Section 3 reviews the polymers of vinylidene fluoride (VDF), covering PVDF and its co-, ter- and tetrapolymers. The modified PVDF-based materials include composites with ceramic, conductive or other fillers, and blends with plasticizers or other electroactive polymers, as further addressed in Section 4. Section 5 then reviews actuators that base on these pure and modified polymer materials, including unimorph and bimorph bending cantilevers, unimorph and dilating diaphragms, stacks, plates and tubular configurations. Section 6 discusses, compares and visualizes the electromechanical transduction properties of the reviewed PVDF-based materials and actuators, and highlights potential research opportunities for further improvements in transduction performance. Finally, the report is concluded in Section 7.

2. Actuation in Ferroelectric Polymer

2.1. Transduction and Properties

2.1.1. Piezoelectric Materials

Piezoelectricity is the ability of certain crystalline materials to convert mechanical energy into electrical energy and vice versa, respectively referred as direct and inverse piezoelectric effects. Out of 32 crystal classes, only 20 can exhibit piezoelectricity.[84] The constitutive equations for inverse and direct piezoelectric effects can be written in Voigt convention as follows.

$$S_{ij} = s^{E}_{ijkl} T_{kl} + d_{kij} E_k \quad (1)$$

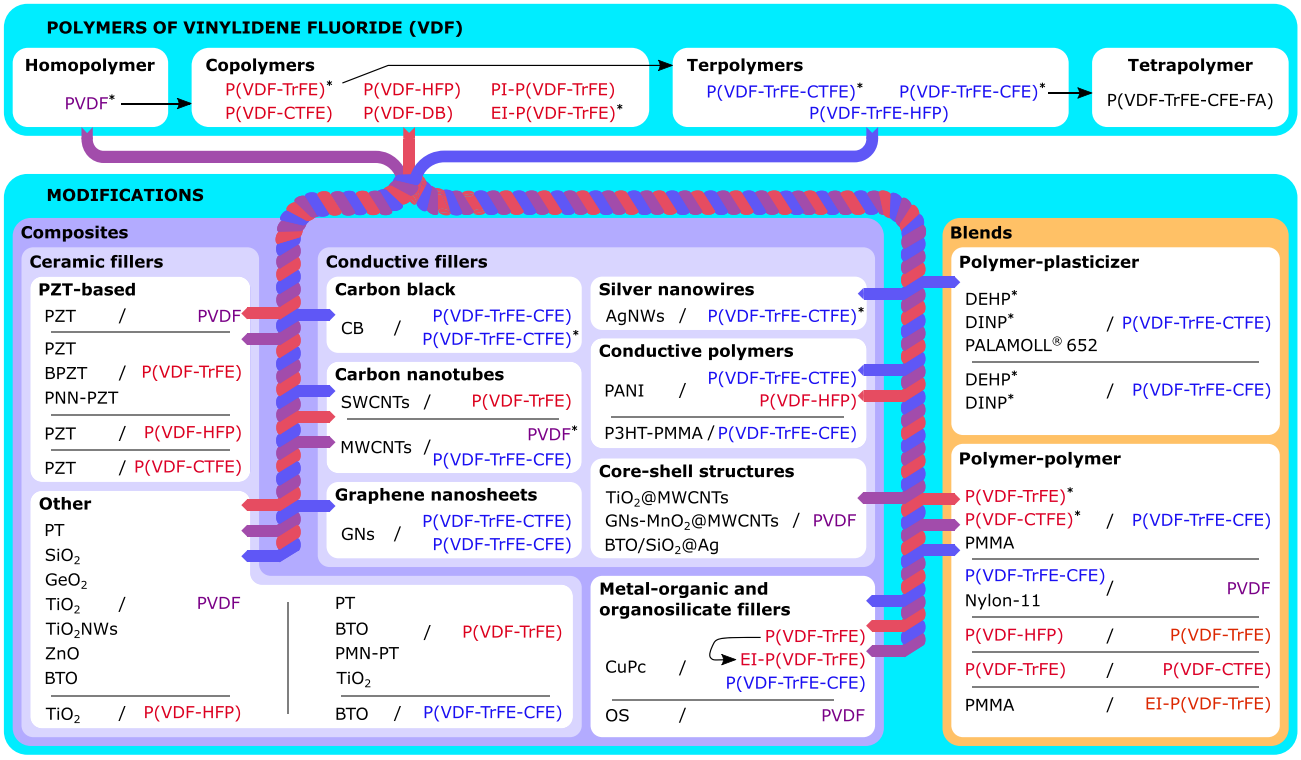

Figure 1. Schematic of the classification and derivation of the PVDF-based electromechanical transducer materials reviewed in this study. The marked materials (*) have been employed in actuators.

$$D_i = \varepsilon_{ik}^T E_k + d_{ikl} T_{kl} \tag{2}$$

where the mechanical strain S_{ij} and the dielectric displecement D_i are related to the applied mechanical stress T_{kl} and electric field E_k via the material compliance s_{ijkl}^E, dielectric permittivity ε_{ik}^T, and piezoelectric strain coefficient d_{ikl} (superscripts E and T respectively denote constant electric field and stress conditions).[85] Using Voigt convention, transduction is most commonly described in terms of transverse and longitudinal piezoelectric coefficients d_{31} and d_{33}, relating the applied electric field E_3 respectively to the transverse and longitudinal strains S_1 and S_3.[86] Substituting the stress T_{kl} from Equation (1) into 2 and omitting the tensor notation gives

$$D = d/s^E S + \varepsilon^T E(1 - k^2) \tag{3}$$

$$k^2 = \frac{d^2}{s^E \varepsilon^T} \tag{4}$$

Here, k denotes the electromechanical coupling factor describing the energy conversion efficiency, i.e., the ratio between the stored mechanical energy $U_S = 0.5YS^2$ and the input electric energy $U_E = 0.5\varepsilon E^2$ between the respective degrees of freedom.[87,88] Therefore, k remains between 0 and 1, and higher values mean more efficient transduction. Most of the research reports the k_{31} and k_{33} components, associated with d_{31} and d_{33} piezoelectric coefficients[89]

$$k_{31}^2 = \frac{d_{31}^2}{\varepsilon_{33}^T s_{11}^E} \tag{5}$$

$$k_{33}^2 = \frac{d_{33}^2}{\varepsilon_{33}^T s_{33}^E} \tag{6}$$

In eEAPs, the dielectric relaxation and viscoelasticity cause electrical and mechanical losses, lowering the electromechanical transduction efficiency, deviating from the proportional response, and producing hysteresis loops in the S-E plot.[90] The losses are described by the imaginary part of the dielectric permittivity and Young's modulus, allowing to describe the respective loss rates of energy as

$$\tan(\delta) = \frac{\mathrm{Im}(\varepsilon)}{\mathrm{Re}(\varepsilon)} \tag{7}$$

$$\tan(\delta_m) = \frac{\mathrm{Im}(Y)}{\mathrm{Re}(Y)} \tag{8}$$

where $\tan(\delta)$ and $\tan(\delta_m)$ respectively are the dielectric and mechanical loss tangents that depend on the operating conditions (e.g., frequency, temperature).[90–92]

The dielectric breakdown strength indicates the lowest electric field strength that causes irreversible material damage and therefore defines the admissible input voltages. The breakdown probability $\mathcal{P}(E)$ has been shown to follow the two-parameter Weibull distribution.[93,94]

$$\mathcal{P}(E) = 1 - \exp\left[-(E/\lambda)\right]^\beta \tag{9}$$

where E is the electric field, λ is the field strength that causes 63.2% of the breakdowns, and β defines the spread of the distribution.

2.1.2. Electrostrictive Materials

Electrostriction is an electromechanical coupling phenomenon that occurs in all dielectric materials (including piezoelectrics), characterized by a quadratic relation between the applied electric field and the induced strain.[95,96] Strain S_{ij} and electric displacement D_i are described by the constitutive equations of electrostriction as follows.[97,98]

$$S_{ij} = s_{ijkl}^E T_{kl} + M_{ijkl} E_k E_l \tag{10}$$

$$D_i = \varepsilon_{ij}^T E_j + 2M_{klij} T_{kl} E_j \tag{11}$$

where M_{ijkl} is the tensor of apparent electrostrictive coefficients (unit $\mathrm{m^2\,V^{-2}}$). Like d_{31} and d_{33} in piezoelectrics, M_{31} and M_{33} components of M_{ijkl} respectively describe the transverse and longitudinal response. In the absence of external stresses, the strain S can be decomposed into the electrostatic Maxwell component S_M and the true electrostriction component S_E.[99,100]

$$S = S_\mathrm{M} + S_\mathrm{E} \tag{12}$$

Maxwell strain is caused by the forces acting between the two charged faces of the dielectric, and can be expressed as[95,101]

$$S_\mathrm{M} = -\frac{\varepsilon_0 \varepsilon_r}{Y} E^2 \tag{13}$$

where ε_r and Y are the relative permittivity and Young's modulus of the material and $\varepsilon_0 = 8.85 \times 10^{-12}\mathrm{F/m}$ is the permittivity of free space. True electrosctrictive strain can be expressed as[99,102]

$$S_\mathrm{E} = QP^2 \tag{14}$$

where Q is the material's intrinsic electrostrictive coeffiecient (unit $\mathrm{m^4\,C^{-2}}$) and P is the polarization induced in the material by the applied electric field. In linear dielectric materials

$$P = \varepsilon_0(\varepsilon_r - 1)E \tag{15}$$

Therefore, the true electrostrictive strain can be given as[26,99,100]

$$S_\mathrm{E} = Q\varepsilon_0^2(\varepsilon_r - 1)^2 E^2 \tag{16}$$

In some electrostrictive eEAPs (e.g., polyurethane, graft elastomers, and PVDF-based FPs), the S_E term dominates the material deformations,[26,103–107] and S_M can be neglected. Then,

$$\begin{aligned} S &\approx Q\varepsilon_0^2(\varepsilon_r - 1)^2 E^2 \\ M &\approx Q\varepsilon_0^2(\varepsilon_r - 1)^2 \end{aligned} \tag{17}$$

It has been empirically shown that Q is inversely proportional to the product of dielectric permittivity ($\varepsilon_0\varepsilon_\mathrm{r}$) and Young's modulus ($Y$),[95,100,104,108–110] yielding (from Equation 17)

$$|M| \propto \frac{\varepsilon_0(\varepsilon_r - 1)^2}{Y\varepsilon_r}, \text{therefore} \tag{18}$$

$$|M| \propto \frac{\varepsilon_0 \varepsilon_r}{Y}, \text{for} \quad \varepsilon_r \gg 1 \tag{19}$$

For perovskites and PVDF-based materials, it has been shown that electrostriction (Q_{3i}) contributes to the piezoelectric effect (d_{3i}).[103,111] By taking a derivative of Equation (16) with respect to E (and considering $\frac{dS}{dE} = d$), this relation can be expressed as[112–115]

$$d_{3i} = 2Q_{3i}P_r\varepsilon_0\varepsilon_r \tag{20}$$

where P_r is the material's remanent polarization. In stretched PVDF copolymers, this electrostrictve coupling has been calculated to be approximately two times stronger[113] than the dimensional piezoelectric effect.[112,116]

The coupling coefficient k_{ij} of electrostrictive materials differs from the linear piezoelectrics (see Section 2.1.1), showing a rapid increase with the applied field, and a plateau once reaching saturation polarization.[117] Therefore, it is a function of induced polarization.[117,118]

$$k_{3i}^2 = \frac{kS_i^2}{s_{ii}^D\left[P_E \ln\left(\frac{P_S+P_E}{P_S-P_E}\right) + P_S \ln\left(1-\left(\frac{P_E}{P_S}\right)^2\right)\right]} \tag{21}$$

where the $i = 1$ and 3 respectively refer to transverse and longitudinal strains S_i, s_{ii}^D is the compliance at constant polarization, P_E is the induced polarization, P_S is the saturation polarization, and k is a material parameter that relates to its dielectric permittivity. The latter is an empirical parameter that stems from assuming a hypoerbolic behavior of the polarization.[119]

$$|P_E| = P_S \tanh(k|E|) \tag{22}$$

Therefore, good transducer material should exhibit large free strains S^0 ($T = 0$) and blocking stresses T^{bl} ($S = 0$) that associate with actuator free displacements (δ_0) and blocking forces (F_{bl}), respectively (see Section 2.2). High transduction coefficients d_{ij}, Q_{jj}, and M_{ij} allow to produce higher strains and stresses at a given field strength. High coupling coefficients k_{ij} (Equation 5, 6, and 21) allow to convert the most electrical energy into mechanical (Section 2.1.1). Furthermore, three figures of merit have been proposed to assess the overall performance of electrostrictive polymers, linking the squared electric field strength respectively to the strain (i.e., $\varepsilon_0\varepsilon_r Y^{-1}$), blocking stress (i.e., $\varepsilon_0\varepsilon_r$), and mechanical energy density (i.e., $\varepsilon_0^2\varepsilon_r^2 Y^{-1}$).[120]

2.2. Actuator Configurations

FPs have been employed in all common configurations of eEAP-based actuators,[31] i.e., unimorph and bimorph bending cantilevers, dilating and unimorph diaphragms, plates, stacks and tubular structures (see **Figure 2**). All these designs base on a layered structure, comprising at least one layer of active material and two layers of electrodes to deliver the electric field, and may further include constraining layers to induce bending, as in unimorph cantilevers and membranes (Section 2.2.2). Additional bonding layers may be required for adhesion between the components.[121]

Actuator capabilities are typically characterized by their free displacement δ_0 (i.e., the maximum induced displacement without external load) and blocking force F_{bl} (i.e., the maximum force that is generated by a blocked actuator at zero displacement). Force-displacement diagram visually represents the operating range of an actuator, as depicted for a linear transducer in **Figure 3**. While the transduction properties of an actuator design can be calculated from its active material properties (Section 2), accurate evaluation is complicated by the passive components (substrate, electrodes, bonding layers, etc.).[121–125]

2.2.1. Disk and Stack Actuators

The simplest piezoactuators consist of a thin piezoelectric disk coated with conductive electrodes, typically operating in the longitudinal (d_{33}) mode. Piezoelectric stack actuators are constructed by stacking a number of disk-electrode pairs mechanically in series and connecting them electrically in parallel.[126] In absence of external load, the quasi-static elongation of a linear actuator (Δl) upon applied voltage (V) can be expressed as[85,127]

$$\Delta l = n d_{33} V \tag{23}$$

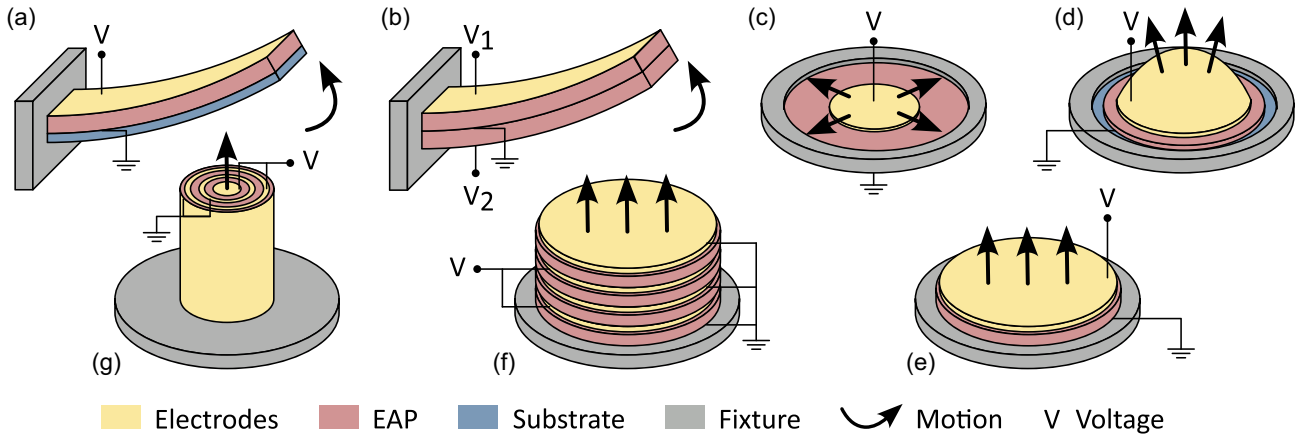

Figure 2. eEAP-based actuators configurations: a) unimorph and b) bimorph bending cantilevers, c) dilating and d) unimorph diaphragms, e) plates, f) stacks, and g) tubular structures.

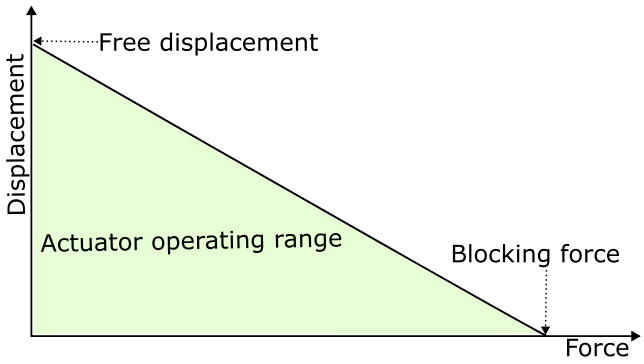

Figure 3. Force-displacement characteristics of a linear actuator.

where n is the number of disks in the stack (and $n = 1$ for disk transducer). For electrostrictive materials with a layered structure, the elongation can be expressed using Equation (17) and (19) as

$$\Delta l = \frac{\varepsilon_0 \varepsilon_r}{Yt} n V^2 \tag{24}$$

where t is the layer thickness. Actual behavior of such actuators deviates from Equation (23) and (24) due to additional nonlinearities, including hysteresis, creep, and energy dissipation (see Section 2.1.1).[126]

Similarly, blocking forces of piezoelectric and electrotrictive stack actuators can be written as[127]

$$F_{\mathrm{bl}} = \frac{YA}{t} d_{33} V = \frac{YA}{l} n d_{33} V \tag{25}$$

$$F_{\mathrm{bl}} = \frac{\varepsilon_0 \varepsilon_r A}{t^2} V^2 = \frac{\varepsilon_0 \varepsilon_r A}{l^2} n^2 V^2 \tag{26}$$

with l being the total free length of the stack (no field applied) and A the cross-section area of the actuator. The factor $k_{\mathrm{e}} = \frac{YA}{l}$ in Equation (25) is the actuator's effective stiffness. A more accurate expression that accounts for both active (k_{a}) and passive (k_{p}, i.e., bonding) layer stiffnesses has been derived for piezostacks.[128]

$$F_{\mathrm{bl}} = \frac{k_{\mathrm{a}} k_{\mathrm{p}}}{n k_{\mathrm{p}} + (n-1) k_{\mathrm{a}}} n d_{33} V \tag{27}$$

2.2.2. Bending Actuators

Bending unimorph and bimorph actuators produce large out-of-plane deflections at small material strains and are simple in structure. In bimorph configuration, two electroactive material layers are coated with thin electrodes and bonded together. In piezoelectric bimorphs, the polarization and electrodes are configured such that one layer contracts, while the other one expands, producing larger tip deflections. Tip deflection, blocking force, and electromechanical coupling coefficient k_{b} of such actuators can be written as[129]

$$\delta_0 = \frac{3L^2}{2t} S_1 \tag{28}$$

$$F_{\mathrm{bl}} = \frac{3wt^2 Y}{8L} S_1 \tag{29}$$

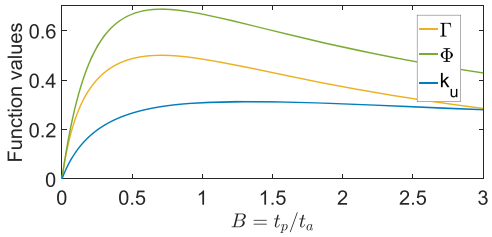

Figure 4. Dimensionless functions Γ, Φ, and k_{u} for unimorph cantilever design at $A = 2$ and $k_{31} = 0.5$. Maxima respectively indicate optimal actuator designs for highest deflection, force and coupling efficiency.

$$k_{\mathrm{b}}^2 = \frac{9}{16} \frac{k_{31}^2}{1 - k_{31}^2/4} \tag{30}$$

where L, t, and w are the length, thickness, and width of the bimorph.

In unimorph actuators, a single layer of electroactive material is coated with two electrodes and laminated on a flexible substrate. The field-induced active layer strain (S_1) is mechanically constrained by the substrate, inducing a bending moment. Unimorphs can be implemented in both cantilever and diaphragm (or membrane) configurations. For unimorph cantilever actuators, the tip deflection, blocking force, and coupling coefficient k_{u} can be written as[129,130]

$$\delta_0 = \frac{3L^2}{2(t_{\mathrm{a}} + t_{\mathrm{p}})} \Gamma(A, B) S_1 \tag{31}$$

$$\text{with } \Gamma(A,B) = \frac{2AB(1+B)^2}{A^2B^4 + 2AB(2+3B+2B^2) + 1}, \; F_{\mathrm{bl}} = \frac{3Y_{\mathrm{a}} w (t_{\mathrm{a}} + t_{\mathrm{p}})^2}{8L} \Phi(A,B) S_1 \tag{32}$$

$$\text{with } \Phi(A,B) = \frac{2AB}{(AB+1)(1+B)}, \quad k_{\mathrm{u}}^2 = \frac{9k_{31}^2}{4} \frac{A^2B^2(B+1)^2}{(AB+1)[A^2B^4 + 2A(2B+3B^2+2B^3) + 1 - k_{31}^2 AB(AB^3+1)]} \tag{33}$$

where $A = Y_{\mathrm{p}}/Y_{\mathrm{a}}$ and $B = t_{\mathrm{p}}/t_{\mathrm{a}}$ are the ratios of Young's moduli and thicknesses of the layers. The behavior of dimensionless functions Γ, Φ, and k_{u} is illustrated in **Figure 4**, while Equation (30) and (33) indicate that the actuator coupling efficiency always remains below the active material efficiency.

3. Polymers of Vinylidene Fluoride

This section addresses the electromechanical properties of PVDF (polyvinylidene fluoride) and its co-, ter- and tetrapolymers. Section 3.1 covers the PVDF homopolymer, Section 3.2 the copolymers, Section 3.3 the terpolymers, and Section 3.4 the P(VDF-TrFE-CFE-FA) tetrapolymer. Key mechanical, dielectric, and transduction properties are summarized in **Table 1** and **2**.

Table 1. Mechanical, dielectric, and transduction properties of PVDF and its copolymers.

Material	Y [MPa]	ε_r [a]	E [b] [V μm^{-1}]	S_{max} [b] [%]	U_s [b] [J cm^{-3}]	Other [c]	Ref.
PVDF	1500–5000	5.1–16 [e]	–	–	–	$d_{33} = 7.5$–34 pm/V $k_{33} = 0.038$–0.19 $d_{31} = 4.2$–37 pm/V $k_{31} = 0.018$–0.147	[78,148,154–160]
PVDF	4800 [d]	–	30	0.1 (S_3)	0.0024	$k_{33} = 0.0265$	[25,29,47]
PVDF	2100	5	150	0.14 (S_3)	0.002	$E_b = 150$ V μm^{-1}	[286]
PVDF	–	–	3.7	0.88 (S_3)	–	–	[161]
P(VDF-TrFE)	690	13.6	190	3.5 (S_3)	0.422	$Q_{33} = 9.51$ m^4 C^{-2}	[188]
P(VDF-TrFE)	–	–	40	1.2 (S_3)	–	–	[334]
P(VDF-TrFE)	–	20	16	0.01 (S_3)	–	–	[88]
P(VDF-TrFE)	457	9.6 (10 Hz)	90	0.82 (S_3)	0.0154	$M_{33} = 1.01 \times 10^{-18}$ m^2/V^2	[304]
P(VDF-TrFE)	450–1200	14.2–18	100	1.1 (S_3)	0.027	$d_{33} = 63.5$ pm V^{-1} $Q_{33} = 7$ m^4 C^{-2}	[176]
P(VDF-TrFE)	1300–3300	4–19 [e]	–	–	–	$d_{33} = 20$–38 pm V^{-1} $k_{33} = 0.27$–0.3 $Q_{33} = 12.65$–13.81 m^4 C^{-2} $d_{31} = 7$–49 pm V^{-1}	[78,114,154,162,166, 182–184,189,190,366]
P(VDF-CTFE)	850	–	220	5.5 (S_3)	1.1	$d_{33} = 140$ pm V^{-1} $k_{33} = 0.4$ $M_{33} = 1.2 \times 10^{-18}$ m^2 V^{-2}	[163,191]
P(VDF-CTFE)	38–230	7–9 (200 Hz)	–	–	–	$d_{33} = 4$ pm V^{-1}	[192]
P(VDF-CTFE)	5	15	100	4 (S_3)	0.004	–	[39]
P(VDF-DB)	320	61	275	13.4 (S_3)	3.1	$Q_{33} = 18$ m^4 C^{-2} $k_{33} = 0.5$ $E_b = 397$ V μm^{-1}	[39]
P(VDF-HFP)	500–1500	10–13.5	50	4.1 (S_3)	0.004–0.92	$d_{33} = 1700$ pm V^{-1} $d_{31} = 0.13$–2.3 pm V^{-1}	[164,197]
P(VDF-HFP)	450–2000	12 (1 Hz)	–	–	–	$d_{33} = 26.9$–32 pm V^{-1} $d_{31} = 39.3$–43.1 pm V^{-1} $k_{31} = 0.081$–0.187	[159]
P(VDF-HFP)	–	3.4	3	0.77 (S_3)	–	$M_{33} = 0.7 \times 10^{-15}$ m^2 V^{-2}	[196]
P(VDF-HFP) (nanofibers)	8–270	3.5–5.6	3	4 (S_3)	0.22	$M_{33} = 1.04 \times 10^{-14}$ m^2 V^{-2}	[196]
P(VDF-HFP) (nanofibers)	5	1.48	10.5	1.78 (S_3)	0.0008	$M_{33} = 1.28 \times 10^{-14}$ m^2 V^{-2}	[105]
P(VDF-HFP)	980	11–16 [e]	–	–	–	$d_{33} = 5.4$–24 pm V^{-1} $d_{31} = 30$ pm V^{-1} $E_b = 700$ V μm^{-1}	[193–195,198,199]
EI-P(VDF-TrFE) [f]	510	60	190 100	4.6 (S_3) 2.7 (S_1)	–	$M_{33} = 2.53 \times 10^{-18}$ m^2 V^{-1} $M_{31} = 2.75 \times 10^{-18}$ m^2 V^{-1} $Q_{33} = 4.5$ m^4 C^{-2} $Q_{31} = 4.6$ m^4 C^{-2}	[171]
EI-P(VDF-TrFE)	400–500	47–54	146	5 (S_3)	0.5	$d_{33} = 380$ pm V^{-1} $Q_{33} = 7$m^4 C^{-2} $k_{33} = 0.3$	[200,201]
EI-P(VDF-TrFE)	1000	54	144	4.3 (S_1)	0.92	$d_{31} = 300$ pm V^{-1} $k_{31} = 0.45$	[201]
EI-P(VDF-TrFE)	450	18.5	175	4.4 (S_3)	0.43	–	[213]
EI-P(VDF-TrFE)	1000	–	85	4.4 (S_1)	1.0	$k_{31} = 0.65$	[214,216]
EI-P(VDF-TrFE)	1000	–	110	3.5 (S_1)	0.61	$k_{31} = 0.45$ $Q_{33} = 4$–12 m^4/C^2	[215]
EI-P(VDF-TrFE)	–	59 (1 kHz)	150	2.55 (S_3)	–	–	[338]
PI-P(VDF-TrFE) [g]	–	20–30	100	2(S_3)	–	$d_{33} = 70$ pm V^{-1}	[204]

[a] Measured at 100 Hz if no frequency is indicated. [b] Maximum reported driving field, strain, and elastic energy density. [c] Absolute values of d_{ij} and Q_{ij} are given. [d] Estimated from the reported S and U_s. [e] Measurement frequency varies. [f] Electron-irradiated P(VDF-TrFE). [g] Proton-irradiated P(VDF-TrFE).

Table 2. Mechanical, dielectric and transduction properties of PVDF terpolymers.

Material	Y [MPa]	ε_r [a)]	E [b)] [V μm^{-1}]	S_{max} [b)] [%]	U_s [b)] [J cm^{-3}]	Other [c)]	Ref.
P(VDF-TrFE-CTFE)	129	14	200	9 (S_3)	0.51	$Q_{33} = 28.74$ m^4 C^{-2}	[188]
P(VDF-TrFE-CTFE)	400	30	120	4 (S_3)	0.30	$Q_{33} = 12$ m^4 C^{-2} $k_{33} = 0.32$ $E_b = 214$ V μm^{-1}	[39]
P(VDF-TrFE-CTFE)	400	51	150	4 (S_3)	0.32	–	[219]
P(VDF-TrFE-CTFE)	–	48	150	3 (S_1)	–	–	[201]
P(VDF-TrFE-CTFE)	64.9	19	25	0.3 (S_1)	0.0003	$M_{31} = 4.55 \times 10^{-18}$ m^2/V^2 $E_b = 223.9$ V μm^{-1}	[230]
P(VDF-TrFE-CTFE)	105–550	38	25	0.03–0.17 (S_1)	0.25–1.5 × 10^{-4}	$M_{31} = 0.03$–2.5×10^{-18} m^2/V^2	[224]
P(VDF-TrFE-CTFE)	163	26	20	0.094 (S_1)	7.16 × 10^{-5}	$M_{31} = 2.34 \times 10^{-18}$ m^2 V^{-2} $E_b = 269$ V μm^{-1}	[330]
P(VDF-TrFE-CTFE)	103	35	10	0.026 (S_1)	3.48 × 10^{-6}	$k_{31} = 0.0085$	[331]
P(VDF-TrFE-CTFE)	–	45	12	0.043 (S_1)	1.05 × 10^{-5}	$E_b = 165$ V μm^{-1}	[233]
P(VDF-TrFE-CTFE)	400	57	76	1.7 (S_3)	0.058	$E_b = 160$ V μm^{-1}	[232]
P(VDF-TrFE-CTFE)	160–260	–	20	1.2 (S_3)	0.019	$M_{33} = 4.4 \times 10^{-17}$ m^2 V^{-2}	[106]
P(VDF-TrFE-CTFE)	270	–	10	0.53 (S_3)	–	$M_{33} = 5.3 \times 10^{-17}$ m^2 V^{-2}	[107]
P(VDF-TrFE-CTFE)	–	–	10	0.9 (S_3, 1 mHz) 0.2 (S_3, 1 kHz)	–	$M_{33} = 9 \times 10^{-17}$ m^2 V^{-2} $M_{33} = 2 \times 10^{-17}$ m^2 V^{-2}	[244]
P(VDF-TrFE-CTFE)	120	41	100	2.2 (S_3)	0.03	$Q_{33} = 10$ m^4 C^{-2} $d_{33} = 55.4$ pm V^{-1}	[210]
P(VDF-TrFE-CFE)	1100	37	130	4.5 (S_3)	1.10	$k_{33} = 0.55$	[220]
P(VDF-TrFE-CFE)	132	57	95	2.5 (S_3)	0.04	$E_b > 300$ V μm^{-1}	[245]
P(VDF-TrFE-CFE)	160	45	25	0.19 (S_1)	2.88 × 10^{-4}	–	[224]
P(VDF-TrFE-CFE)	300	–	170	7 (S_3) 3 (S_1)	0.73	–	[214]
P(VDF-TrFE-CFE)	–	67.3	–	–	–	$E_b = 382.75$ V μm^{-1}	[229]
P(VDF-TrFE-CFE)	200–500	54	160	6.4 (S_3)	0.42	$Q_{33} = 7$ m^4 C^{-2}	[223]
P(VDF-TrFE-CFE)	–	40 (20 Hz)	100	4 (S_1)	–	–	[228]
P(VDF-TrFE-CFE)	65	50 (0.1 Hz)	12	0.08 (S_3)	2.3 × 10^{-5}	$k_{33} = 0.03$	[326]
P(VDF-TrFE-CFE)	110	50	10	0.06 (S_3)	2.25 × 10^{-5}	$E_b = 180$ V μm^{-1}	[329]
P(VDF-TrFE-CFE)	107	58	10	0.04 (S_3, 2.74 N preload)	–	$E_b = 100.4$ V μm^{-1}	[234]
P(VDF-TrFE-CFE)	165–690	10–20 (100 kHz)	80	0.5–1.6 (S_3)	0.0098–0.026	–	[235]
P(VDF-TrFE-CFE)	887.5	–	150	4 (S_1)	0.71	$k_{31} = 0.25$ $Q_{31} = 7.5$ m^4/C^2	[337]
P(VDF-TrFE-CFE)	147	49 (1 kHz)	150	3.9 (S_3)	0.113	$k_{33} = 0.17$	[236]
P(VDF-TrFE-CFE)	150	57	20	0.08 (S_1)	4.8 × 10^{-5}	$E_b = 276$ V μm^{-1}	[237]
P(VDF-TrFE-CFE)	80	54	56	0.66 (S_1)	0.0017	$M_{31} = 2.1 \times 10^{-18}$ m^2/V^2	[238]
P(VDF-TrFE-CFE)	80	39	106	4.4 (S_3)	0.077	–	[308]
P(VDF-TrFE-CFE-FA)	224	59	80	6 (S_3)	0.40	$Q_{33} = 45$ m^4/C^2 $d_{33} = 1050$ pm V^{-1} $k_{33} = 0.88$	[40]
P(VDF-TrFE-HFP)	–	24	70	2.8 (S_3)	–	–	[221]

[a)]Measured at 100 Hz if no frequency is indicated. [b)]Maximum reported driving field, strain, and elastic energy density. [c)]Absolute values of Q_{ij} are given.

3.1. PVDF

PVDF is a partially fluorinated thermoplastic polymer that can exhibit piezoelectric and ferroelectric behaviors.[131,132] Piezoelectric behavior of PVDF was first reported in 1969,[61] enabling a multitude of electromechanical and mechanoelectrical transduction applications.[80,133] As discussed in the following, properties of PVDF have been extensively studied, linking its piezoelectric behavior to the material structure and specific processing methods.

Piezoelectric behavior of PVDF arises from the high dipole moment of its monomers (4–7 × 10^{-30} C m), caused by the electronegativity difference between fluorine and hydrogen atoms within the monomer.[134,135] PVDF can exhibit multiple crystalline phases, depending on the fabrication process.[136–138] Among the five reported PVDF polymorphs (α, β, γ, δ, and ε), the

α, β, and γ phases are the most commonly found and most investigated for applications.[74,139,140] The α phase has a *trans–gauche* (TGTG′) conformation and is nonpolar (paraelectric), as the chains pack in opposite directions and their dipoles cancel. The β phase has an all-*trans* (TTTT) planar-zigzag chain conformation with the dipoles aligned in the same direction, resulting in a polar crystal with a net dipole moment of 7×10^{-30} C m per repeat unit.[134] The less common γ phase has an intermediate chain conformation (TTTGTTTG′, or T_3GT_3G'), with more *trans* bonds than α but fewer than β phase. In this helical arrangement, the dipoles are partially rotated, giving a lower polarity than the β phase.[140] Consequently, the β phase combines the highest polarization with the strongest piezoelectric behavior,[134,141–143] desirable for transducer applications.

Piezoelectric behavior in pure PVDF films is attained via two treatment steps: 1) mechanical stretching (aka drawing) in one or two in-plane directions (i.e., uniaxial and biaxial stretching, respectively) that induces conformational change in the polymer chains from TGTG′ (α phase) to all-*trans* (β phase)[144] and 2) poling in the thickness direction, causing the crystalline elements of the polar β phase to align in the electric field, and attaining a remanent polarization P_r after the electric field is removed.[145–147] In solution-cast PVDF films (i.e., mainly α phase,[68,81]) uniaxial stretching by 5× at 80 °C has been shown to produce up to 80% of β phase content.[148] Poling is implemented at electric field strengths of $>10\ \mathrm{V\ \mu m^{-1}}$ at temperatures of 20–110 °C,[61,149–151] attaining typical remanent polarizations of 4–10 $\mu\mathrm{C\ cm^{-2}}$.[148,152,153]

PVDF is characterized by a dielectric constant of 5.1–16[78,154–157] and Young's modulus of 1.5 to 5 GPa.[47,78,154,155,158–160] The reported (absolute) values for the d_{31} and d_{33} coefficients are respectively in the range of 4.2–37 and 7.5–34 $\mathrm{pm\ V^{-1}}$, depending on the crystalline structure, stretching ratio, and poling conditions.[148,154,155,157–160] The longitudinal electromechanical coupling coefficient $k_{33} = 0.19$ has been shown to be temperature-invariant and stronger than the transverse coefficient k_{31},[155,157] which has been shown to vary from 0.02 to 0.16 between −170 and 100 °C.[157] Maximum strains are rarely reported for PVDF. Pelrine et al.[29,47] and Bar–Cohen[25] indicated typical strains of 0.1% ($30\ \mathrm{V\ \mu m^{-1}}$), while Burnham–Fay et al. reported S_3 of up to 0.88% ($3.7\ \mathrm{V\ \mu m^{-1}}$) in 3D-printed films.[161]

3.2. PVDF Copolymers

Forming PVDF copolymers with different bulky fluorinated monomers has been investigated in order to enhance the piezoelectric properties of PVDF. Section 3.2.1 addresses the PVDF copolymers with triffiuoroethylene (TrFE),[162] Section 3.2.2 with chloride triffiuoride ethylene (CTFE),[163] and Section 3.2.3 with hexaffiuoropropene (HFP).[164] Irradiating P(VDF-TrFE) with high-energy electrons and ions promotes relaxor ferroelectric behavior, addressed in Section 3.2.4.

3.2.1. P(VDF-TrFE)

The P(VDF-TrFE) copolymer is among the most studied ferroelectric polymers for transducer applications. P(VDF-TrFE) exhibits higher crystallinity, better temperature stability, smaller dielectric losses and lower viscous losses than PVDF homopolymer.[165,166] Additionally, it is easy to process, and commercially available in various molar ratios. Introduction of TrFE causes steric hindrance in the polymer structure, promoting and stabilizing the ferroelectric β phase at room temperature.[167–169] A well-defined transition from ferroelectric (FE) to paraelectric (PE) phase occurs at TrFE molar contents above ≈18% (i.e., 82% VDF content), below which the melting and Curie temperatures of the polymer coincide.[166,170,171]

Thin films of PVDF-TrFE are typically cast from molten or dissolved materials, and their behavior stongly depend on TrFE content. At TrFE content below 10%, the melt crystallizes mainly into the paralectric α phase, and β phase formation requires mechanical stretching.[172] Between 10% and 18% TrFE content, a mixture of α-, β- and γ-phases is obtained, which can be transformed into β phase by a cyclic application of a strong electric field ($>100\ \mathrm{V\ \mu m^{-1}}$).[172,173] TrFE contents of 18% to 40% exhibit stable ferroelectric β phase without the need of mechanical stretching,[166,169] whereas the Curie temperature decreases with increasing TrFE content, from about 140–150 °C (18% TrFE) to 70–80 °C (40% TrFE).[170,173] For TrFE concentrations above 40 mol%, early studies reported a mixture of β (all-*trans*) phase and a disordered paraelectric phase[167,174] that convert into β phase upon mechanical stretching or poling.[174,175] More recent work shows that TrFE content >45 mol% produces a distorted 3/1-helix structure with $(TG)_3$ chain conformation.[176] Behavior of these polymers resembles inorganic relaxor ferroelectrics,[176–178] characterized by a slim hysteresis loop and a similar dependence of the dielectric constant on temperature and frequency.[179,180]

The piezoelectric properties of P(VDF-TrFE) thin films are significantly enhanced upon thermal annealing (>110 °C)[166,181,182] and electrical poling (typically at $40–100\ \mathrm{V\ \mu m^{-1}}$),[183–186] respectively increasing the polymer crystallinity and dipole alignment.[182,187] For example, Ducrot et al. reported a 95% increase in the free deflection of P(VDF-TrFE) actuators after poling at $100\ \mathrm{V\ \mu m^{-1}}$ and annealing at 140 °C.[165] Depending on TrFE content and processing, typical P(VDF-TrFE) films achieve longitudinal strains of up to 3.5% ($190\ \mathrm{V\ \mu m^{-1}}$),[188] piezoelectric coefficients of 12–38 $\mathrm{pm\ V^{-1}}$ for d_{33} and 7–49 $\mathrm{pm\ V^{-1}}$ for d_{31} and elastic energy densities of up to $0.42\ \mathrm{J\ cm^{-3}}$.[154,162,166,176,182,183,188–190]

Compositions near 50% TrFE content exhibit the highest piezoelectric coefficients[166,176,183,184] with d_{33} of up to 63.5 $\mathrm{pm\ V^{-1}}$ (unstretched P(VDF-TrFE) film)[176] and d_{31} further increasing by 3x upon stretching (4–6×).[166,184] Enhanced piezoelectricity has been attributed to the formation of a morphotropic phase boundary (MPB) in the TrFE content range of 45%–51%, where all-*trans* and disordered helical conformations coexist.[176] The highest electromechanical coupling coefficients have been reported in the interval of 18%–25% TrFE content, attaining a k_{33} of 0.27–0.3 both in stretched and unstretched samples.[166] While higher TrFE concentrations result in lower values, the stretching significantly improves k_{33} in the 25%–60% interval.[166]

3.2.2. P(VDF-CTFE) and P(VDF-DB)

Incorporating CTFE monomer into the PVDF chain induces a transition from the TGTG conformation toward a disordered helical chain conformation, resulting in relaxor

ferroelectric properties[177] and high electrostrictive response.[163,191] Uniaxially drawn and annealed P(VDF-CTFE) films (25–35 μm in thickness) with 12 mol% CTFE content have been reported to exhibit strains of up to 5.5% (220 V μm^{-1}), electrostrictive coefficient M_{33} of 1.23×10^{-18}m^2/V^2, piezoelectric coefficient d_{33} of up to 140 pm V^{-1}, elastic energy density of up to 1.1 J cm^{-3}, and longitudinal coupling efficiency (k_{33}) as high as 0.4.[163,191] Without annealing and stretching steps, the similarly manufactured P(VDF-CTFE) films (solution-cast) exhibited lower d_{33} values (up to 4 pm V^{-1}).[192]

P(VDF-CTFE) has been further used as a basis for polymeric blends (addressed in Section 4.3.2) and as a precursor to obtain double-bonded (DB) PVDF.[39] Namely, CTFE units can be converted into CH═CF bonds through a dehydrochlorination reaction, resulting in P(VDF-DB), where the rigid double bonds act as molecular defects that improve crystallinity and promote ferroelectric phase formation upon stretching.[39] The solution-cast P(VDF-DB) films displayed maximum strain S_3 of 13.4% (at 275 V μm^{-1}), energy density of 3.1 J cm^{-3}, k_{33} coefficient of 0.5, and breakdown strength of close to 400 V μm^{-1}.[39]

3.2.3. P(VDF-HFP)

PVDF copolymers with HFP have been shown to exhibit strong piezoelectric and electrostrictive response.[159,164] Depending on film processing, P(VDF–HFP) have been reported to adopt a paraelectric α-like phase or a ferroelectric β-like phase.[159,164,193–196] The latter, typically targeted for transduction, can be promoted by mechanical stretching and poling,[159,193,194] annealing,[193] or thermal compression.[196]

In the early 2000s, transduction properties of 50–60 μm thick P(VDF-HFP) films (fabricated both by solution-casting and melt-pressing) were first studied, reporting S_3 strains of up to 4.1% (<100 V μm^{-1}), elastic energy densities of up to 0.92 J cm^{-3}, and high d_{33} values of up to 1700 pm V^{-1}.[164,197]

He et al. reported a maximum d_{33} coefficient of 12.6 pm V^{-1} for melt-quenched P(VDF-HFP) (90/10) films that were stretched by 3–4× and poled at 250 V μm^{-1}.[193] Huan et al. fabricated P(VDF-HFP) (90/10) films via resin extrusion and stretched the film in a static electric field (stretch ratio 4.5, 160 V μm^{-1}, 60 °C), attaining a d_{33} of 24 pm V^{-1}.[194] Künstler et al. studied the effect of stretching on the transverse piezoelectric coefficient of P(VDF-HFP) (85/15) films, reporting d_{31} coefficients of up to 30 pm V^{-1} in 4× uniaxially drawn samples, indicating a fivefold improvement over the unstretched samples upon identical poling conditions (350 V μm^{-1}, room temperature).[198] Zhou et al. reported that P(VDF-HFP) exhibits elevated breakdown strengths of up to 700 V μm^{-1} and associated this to the extrusion and stretching steps of the fabrication (uniaxial, 110 °C).[199]

Neese et al. studied quasi-static and high-frequency (50 kHz) response in melt-pressed, stretched (4–5×, 100 °C) and corona-poled (30 kV) films of P(VDF-HFP),[159] reporting that the d_{31} and k_{31} respectively decrease by 52% and 41% between 1 and 50 kHz (d_{31} from 43.1 to 20.5 pm/V, k_{31} from 0.187 to 0.110). Further, Sousa et al. studied the effect of polymer concentration (up to 20 wt% in DMF), drying temperature (25–100 °C), and poling temperature (80–120 °C) of solution-cast P(VDF-HFP) films (thickness 9–76 μm) on their piezoelectric properties.[195] The highest d_{33} (12 pm V^{-1}) was reported for 10 wt% P(VDF-HFP) samples that were dried and poled at 100 °C.[195]

Tohluebaji et al. investigated P(VDF-HFP) nanofiber mats, showing that combining electrospinning and hot-pressing (at 80 °C) increases the β phase content and dielectric constant of the mats.[196] Electrostrictive strains of up to 4% ($M_{33} = 1.04 \times 10^{-14}$m^2/V^2) were reported at very low field strengths (3 V μm^{-1}), showing an ≈15× improvement over the solution-cast films.[196] In a later study, the S_3 was reported to saturate at 1.78% above 10.5 V μm^{-1} (M_{33} 1.28×10^{-14}m^2/V^2).[105]

3.2.4. Irradiated P(VDF-TrFE)

Ferroelectric hysteresis in P(VDF-TrFE) causes dielectric losses and heat dissipation (see Section 2.1.1). These losses can be mitigated by introducing defects into polymer chains via high-energy electron[171,200–203] and ion[204] irradiation, promoting the transition from normal ferroelectric to relaxor ferroelectric (RFE) behavior.[205] The defects break the long-range ferroelectric domains into polar nanodomains, reducing the energy barrier of paraelectric to ferroelectric phase transition.[206–210]

The large electrostriction observed in relaxor ferroelectric polymers (RFPs), such as irradiated P(VDF-TrFE) and terpolymers (see Section 3.3), has been attributed to field-induced reversible conformational changes from $(TG)_3$ (3/1-helix, see Section 3.2.1) to all-*trans* conformation.[204,210] Therefore, electrostrictive response in RFPs can be enhanced by promoting formation of distorted helical conformation over long all-*trans* sequences.[177,211]

Electron-irradiation of P(VDF-TrFE) has been shown to improve the dielectric constant (e.g., ε_r from 15 to 26 at 10 Hz)[212,213] and electromechanical coupling efficiency (e.g., k_{31} and k_{33} of up to 0.65 and 0.3, respectively),[201,214] producing longitudinal strains S_3 as high as 5% (150 V μm^{-1}), and elastic energy densities of up to 1 J cm^{-3}.[200,201,214–216] In unstretched P(VDF-TrFE) films, the ratio between the transverse and longitudinal strains S_1/S_3 is below 0.33,[171,215] while stretching has been shown to improve the transverse strains by ≈3× (S_1 up to 3.5% at 110 V μm^{-1} and 5× uniaxial streching).[215] Introducing a two-step annealing procedure (between stretching and electron-irradiation steps) has been shown to further improve the transverse strains in solution-cast P(VDF-TrFE) films, attaining S_1 of up to 4.4% (85 V μm^{-1}) and energy densities of up to 1 J cm^{-3}.[214,216] The first annealing step at lower temperature (115–125 °C) was argued to release the stored stress in the stretched films, and the second step (134 °C) to promote crystallization.[216]

The effects of ion irradiation on P(VDF–TrFE) were recently studied by Liu et al.[204] The 65/35 mol% polymer composition was exposed to proton irradiation doses of up to 50 Mrad. Doses of 20–40 Mrad induced an all-*trans*/helix MPB (see Section 3.2.1), enhancing the piezoelectric response (d_{33} of up to 70 pm V^{-1} for 30 Mrad). At higher irradiation doses, the 3/1-helix becomes the dominant phase, producing electrostrictive behavior with S_3 of up to 2% (100 V μm^{-1} for 50 Mrad).

3.3. PVDF Terpolymers

While high-energy electron irradiation produces improved electromechanical properties in P(VDF-TrFE), it also causes

undesirable changes, such as cross-linking, radical formation, chain-scission, and amorphization.[217,218] Alternatively, defects required to attain RFE behavior in P(VDF-TrFE) can be obtained by introducing another bulky monomer (e.g., CTFE,[219] CFE (chlorofluoroethylene),[220] or HFP[221]) into the copolymer chains, obtaining PVDF terpolymers. Such terpolymers are less crystalline than the starting copolymers, and possess smaller polar domains.[39,222,223] PVDF terpolymers exhibit higher dielectric permittivity and lower elastic modulus than PVDF and P(VDF-TrFE) (see Section 3.1 and 3.2.1).[78,223,224]

The minimum molar fraction of third monomer required to convert the P(VDF-TrFE) from normal ferroelectric to RFE depends on the monomer type. For CTFE, a significant decrease in polarization hysteresis occurs at about 7.6–10 mol%.[210,219,225] For CFE and HFP, 4 mol% and 2.5 mol% respectively are sufficient to achieve the same effect.[220,221,226] Earlier studies linked the RFE behavior in these polymers to an increase in $T3GT_3G'$ conformation at the expense of all-*trans* conformation, upon incorporation of the ter-monomer.[220,221,227] Later it was shown that these RFE properties instead originate from a disordered helical conformation, as also observed in certain compositions of P(VDF–TrFE) and P(VDF–CTFE) (see Section 3.2.1 and 3.2.2).[177,204,210,211]

A number of different terpolymer films have been manufactured with thicknesses spanning from 1 to 250 μm.[39,188,221,224,225,228–238] The films are fabricated most commonly by solution-casting,[188,210,214,221] and less frequently by screen-printing,[225] stencil-printing,[239] spin-coating,[240,241] melt-extrusion,[231] hot-pressing,[210] inkjet printing,[242] and spray-coating.[243] The films does not require poling and stretching,[188,214,221] and their crystallinity is usually improved via thermal annealing (90–130 °C, 2–12 h).[39,219–221,223,229,240]

3.3.1. P(VDF-TrFE-CTFE)

P(VDF-TrFE-CTFE) exhibits high dielectric permittivities (e.g. 57, 100 Hz[232]) and low Young's moduli (e.g., 0.065–0.55 GPa).[39,106,188,224,230] Increasing the CTFE content stabilizes the RFE phase (distorted 3/1-helix), lowers Young's modulus and crystallinity, and increases ε_r and S_3.[188,210] For CTFE content of 1.7–5 mol%, both all-*trans* and helical conformations have been shown to coexist, resulting in an enhanced d_{33} of up to 55.4 pm V^{-1}.[210] Maximum S_3 values of up to 9% have been reported for solution-cast P(VDF-TrFE-CTFE) (12 mol% CTFE, 200 V μm^{-1}, $Y = 129$ MPa),[188] meaning an energy density of 0.51 J cm^{-3}, while the S_1 of up to 3% (10 mol% CTFE, 150 V μm^{-1})[201] and coupling efficiency k_{33} of up to 0.32[39] have been reported. Stretching the P(VDF-TrFE-CTFE) films has been shown to enhance the breakdown strength E_b (e.g., from 190 to 230 V μm^{-1}) and slightly improve the ε_r and Y.[188] Similarly, thermal annealing (2 h, 120 °C) was reported to improve the ε_r by 50% (to 40.6 at 0.1 Hz), Y by 180% (to 0.18 GPa), and E_b by 52% (to 340.4 ± 18).[230]

Buckley et al. used a combination of bulk copolymerization and oxygen-activated free-radical initiation to synthesize compositionally homogenous P(VDF-TrFE-CTFE) that operates at low field strengths. They reported strains (S_3) of up to 1.2% at 20 V μm^{-1} (2 mHz), yielding an M_{33} coefficient of $4.4 \cdot 10^{-17} m^2/V^2$.[106] Garrett et al. further studied how the response of this material dependent on the temperature and frequency,[107] reporting a 1.85-fold increase in M_{33} from room temperature to ≈42 °C (up to $9.8 \cdot 10^{-17} m^2/V^2$, 10 V μm^{-1}), and a >5-fold decrease with frequency between 10 mHz and 1 kHz at fixed temperature (50 °C). Roland et al. later reported an M_{33} of up to $9 \cdot 10^{-17} m^2/V^2$ for 1 mHz (10 V μm^{-1}), and a 4.5x decrease as the frequency was increased to 1 kHz.[244]

3.3.2. P(VDF-TrFE-CFE)

P(VDF-TrFE-CFE) achieve higher energy densities and coupling efficiencies than CTFE terpolymers, attributable to the larger ε_r (up to 67.3, 100 Hz),[229] breakdown strength (>300 V μm^{-1}[229,245]) and Young's modulus (up to 1.1 GPa).[220] For P(VDF-TrFE-CFE) with 62/38/4 mol% composition, S_3 strains of 4.5%, Young's modulus of 1.1 GPa, energy density of 1.1 J cm^{-3} and k_{33} of 0.55 have been reported (130 V μm^{-1}).[220] Huang et al. studied the 68/32/9 mol% composition and reported S_3 of 7% (170 V μm^{-1}), Y of 0.3 GPa and U_S of 0.73 J cm^{-3}.[214] Klein et al. investigated a range of CFE content (0 to 9 mol%), reporting S_3 strains of up to 6.4% (65/35/8.6 mol%, 160 V μm^{-1}).[223] For 58.3/34.2/7 mol% composition, S_3 of 2.5% and energy density of 0.04 J cm^{-3} were observed at lower field strengths of 95 V μm^{-1}.[245]

Transverse strains (S_1) have been shown to improve with stretching, increasing from 1.3% to 3% (125 V μm^{-1}) upon 5× uniaxial stretching.[214] S_1 of up to 4% (100 V μm^{-1}) has been reported[228] for uniaxially stretched films that were drawn from 60 to 6 μm thickness, and a breakdown strength E_b of up to 382.75 V μm^{-1} has been reported in uniaxially stretched films (>5×, 63/37/7.5 mol%).[229]

3.3.3. P(VDF-TrFE-HFP)

The introduction of a small amounts of HFP into P(VDF-TrFE) (i.e., <3 mol%) has been reported to reduce the fraction of long all-*trans* sequences and promote changes in conformation, turning the material into a RFP.[221] A 62/38/2.5 mol% P(VDF-TrFE-HFP) has been shown to exhibit a dielectric constant of up to 24 (100 Hz, room temperature) and S_3 of up to 2.8% (70 V μm^{-1}).[221]

3.4. P(VDF-TrFE-CFE-FA)

Chen et al. introduced a small amount of fluorinated alkyne (FA) monomers (1.9 mol%) into P(VDF-TrFE-CFE) terpolymer, producing a P(VDF-TrFE-CFE-FA) tetrapolymer.[40] Comparing the tetrapolymer to the terpolymer films indicated an improved S_3 (2.7% vs. <1%) at significantly lower field strengths (40 V μm^{-1}), an improved Q_{33} (>40m^4/C^2, i.e., ≈4× improvement) and estimated an exceptionally high d_{33} of 1050 pm V^{-1} ($k_{33} = 0.88$).[40]

4. Modified PVDF-Based Materials

Modifying the FPs and DEs with micro/nanofillers, plasticizers, or other polymers allows to enhance their dielectric and

electroactive properties for actuation,[100,246–248] sensing,[249,250] energy storage,[251–253] and energy harvesting[146] purposes. Such modifications allow to alter the crystalline structure, dielectric constant (ε_r), breakdown strength (E_b), and Young's modulus (Y) of FPs to enhance their transduction properties. Improvement of the ε_r is commonly ascribed to the percolation phenomenon and interfacial polarization effect, as explained in Section 4.1. Modified PVDF-based materials can be divided into polymer matrix composites with micro- and nanoscale fillers (Section 4.2) and polymer blends with platicizers or other EAPs (Section 4.3).

4.1. Interfacial Polarization and Percolation Effects

Electrostrictive and piezoelectric effects in FPs directly relate to their dielectric permittivity (see Section 2.1.2). Microscale modification to the FPs result in an improved dielectric permittivity, commonly explained through the interfacial polarization and percolation effects.

The Maxwell–Wagner–Sillars (MWS) interfacial polarization occurs in electrically heterogeneous materials where free charges segregate at the interfaces between the different phases,[254–256] allowing to attain improved dielectric permittivity.[251,257–259] MWS occurs in polymers due to the presence of additives (such as plasticizers, conductive, and ceramic fillers), impurities, or their semicrystalline structure.[260–264] Charge segregation locally intensifies the electric field, leading to the undesirable effects of elevated dielectric losses and decreased breakdown strength.[265,266]

In percolation approach, a significantly improved dielectric permittivity can be achieved by introducing small amounts of conductive particle fillers (i.e., below percolation threshold) into the polymer matrix. Dielectric constant of such composites is a function of the mass fraction of the filler in the composite f:[267–269]

$$\varepsilon_r = \varepsilon_{r,m}\left[\frac{(f_c - f)}{f_c}\right]^{-q}, \qquad f \leq f_c \tag{34}$$

where $\varepsilon_{r,m}$ is the dielectric constant of the polymer matrix, q is the critical exponent, and f_c is the percolation threshold. Filler loading fractions nearby f_c form a network of micro/nanocapacitors (i.e., conductive particles and thin layer of dielectric polymer)[270] as illustrated in **Figure 5**, enhancing the material's effective dielectric permittivity. Exceeding percolation threshold leads to an insulator–conductor transition due to the formation of conductive pathways.[271]

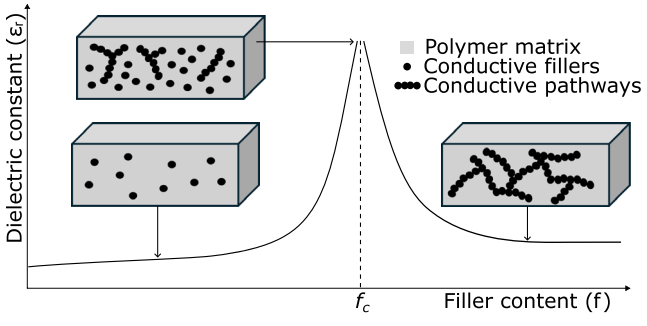

Figure 5. Percolation in polymer composites with conductive fillers.

4.2. Composites

Different type of filler materials have been incorporated into EAP-based matrices to fabricate flexible composite materials with enhanced electromechanical properties, including piezoceramic powders, carbon-based and metallic nanoparticles, conductive polymers, core-shell structures, metal-organic compounds, and organically modified silicates. Mechanical, dielectric, and transduction properties of these composites are summarized in **Table 3** and **4**.

4.2.1. PZT-Based Ceramics

Several studies have investigated embedding PZT (lead zirconate titanate) fillers in PVDF and its copolymers. The dielectric constant, Young's modulus, and piezoelectric coefficient d_{33} have been shown to increase with PZT concentration,[272–274] and also depend the PZT particle size, manufacturing process and poling conditions.[275]

Multiple studies have addressed embedding PVDF homopolymer with PZT powders to improve its piezoelectric properties for transducer applications.[274,276–279] Cai et al. investigated composites of PZT/PVDF.[277] The PZT/PVDF films (65 vol%, hot-rolled, hot-pressed and poled) exhibited d_{33} of up to 33 pm V^{-1} and k_{33} of up to 0.45. Chen et al. studied the piezoelectric properties of PZT/PVDF composites.[278] The 100–200 μm thick films (55 wt% of PZT, ≈3 μm particles) attained d_{33} of up to 27 pm V^{-1}, showing an 80% improvement over their pure PVDF samples. Tiwari and Srivastava studied PZT/PVDF composite films (solution-cast, poled and annealed) with up to 30 vol% PZT.[279] They reported an increase in β-phase content and ε_r with an increasing PZT volume fractions, attaining highest ε_r of 72 and d_{33} of 84 pm V^{-1} (30 vol% PZT). Zhang et al. studied fabricating PZT/PVDF composite films with 0–45 wt% PZT content (30–100 μm thickness) and reported that the extrusion-cast samples produce higher longitudinal strains than solution-cast ones.[274] The 25%wt composites exhibited S_3 of up to 1.6% and d_{33} of 35 pm V^{-1} (200 V μm^{-1}), about 7× higher than their pure PVDF samples.

PZT-based fillers have been embedded in P(VDF-TrFE),[189,273,280,281] P(VDF-HFP),[282] and P(VDF-CTFE)[283] copolymers. Ng et al. showed that poling conditions and PZT content can tailor the piezoelectric and pyroelectric properties of PZT/P(VDF-TrFE) composites.[273] Poling the copolymer matrix and PZT fillers in the same direction decreased the d_{33} of the composite with increasing PZT volume fraction, reaching complete loss of piezoelectricity at 45 vol% PZT content (purely pyroelectric behavior) due to the opposite signs of d_{33} coefficients in the host and filler phases. Poling the two phases in opposite directions (i.e., anti-parallel poling) attained up to 14% higher d_{33} than the pure copolymer (60 vol% PZT). Wegener and Arlt studied the piezoelectric response of solution-cast PZT/P(VDF-HFP) films (100 μm thick) at 19–67 vol% PZT concentration. The highest d_{33} of 11 pm V^{-1} was reported at 48 vol% PZT, whereas higher PZT concentrations resulted in porous and brittle films.[282] Choi et al. investigated the effect of PZT particle sizes

Table 3. Electromechanical transduction properties of PVDF-based composites with ceramic fillers.

Matrix	Filler	ε_r [a)]	d_{33} [b)] [pm V^{-1}]	Other	Ref.
PVDF	PZT (65 vol%)	–	33	$k_{33} = 0.45$	[277]
PVDF	PZT (55 wt%)	60	27	$k_{33} = 0.105$	[278]
PVDF	PZT (30 vol%)	72	84	–	[279]
PVDF	PZT (25 wt%)	–	35	$S_3 = 1.6\%$ (200 V μm^{-1})	[274]
PVDF	TiO_2 (14.9 vol%)	13	–	$S_3 = 8.1\%$(40 V μm^{-1}) $Y = 3.46$ GPa, $U_s = 11.3$ J cm^{-3} $k_{33} = 0.88$, $E_b = 52$ V μm^{-1}	[286]
PVDF	TiO_2 (NWs, 2.1 vol%)	–	–	$S_3 = 0.2\%$ (50 V μm^{-1}), $E_b = 50$ V μm^{-1}	[286]
PVDF	ZnO (14.9 vol%)	–	–	S_3=5.4% (34 V/μm)	[286]
P(VDF-TrFE)	PZT (50 vol%)	48	–	$Y = 1.3$ GPa, $d_{31} = 17$ pm V^{-1}	[280]
P(VDF-TrFE)	PZT (60 vol%)	124.2	42	–	[273]
P(VDF-CTFE)	PZT (80 vol%)	181	98	–	[283]
P(VDF-HFP)	PZT (48 vol%)	62.6	11	–	[282]
P(VDF-HFP)	TiO_2 (14.9 vol%)	–	–	$S_3 = 3.9\%$ (80 V μm^{-1})	[286]
P(VDF-TrFE)	TiO_2 (14.9 vol%)	–	–	$S_3 = 0.5\%$ (170 V/μm)	[286]
P(VDF-TrFE)	PNN-PZT (50 vol%)	81	100	$Y = 1.6$ GPa	[281]
P(VDF-TrFE)	BPZT (10 vol%)	12 (0.48 MHz)	37	–	[189]
P(VDF-TrFE)	PT (27 vol%)	–	20	–	[284]
PVDF	PT (65 vol%)	–	30	$Y = 1.98$ GPa, $k_{33} = 0.486$	[277]
P(VDF-TrFE)	PMN-PT (40 vol%)	37.3	31	–	[285]
P(VDF-TrFE)	BTO (60 vol%)	80 (50 kHz)	22	–	[256]

[a)]Measured at 1 kHz if no frequency is indicated. [b)]Absoulte values of d_{33} are given.

(<53, 53–106, and 106–212 μm) and volume fraction (50 to 80 vol%) on PZT/P(VDF-CTFE) transduction properties[283] and observed d_{33} to increase with particle size, attaining up to 98 pm V^{-1} (hot-pressed films, 80 vol% of 106–212 μm PZT particles, poled at 5 V μm^{-1} and 120 °C). Siponkoski et al. studied PZT/P(VDF-TrFE) composites (30–70 vol% PZT), estimating the highest d_{31} value of 17 pm/V at 50 vol% of PZT.[280] Concentrations >50 vol% were reported to cause fabrication defects (stencil-printing). Belovickis et al. investigated P(VDF-TrFE) composites with barium lead zirconate titanate (BPZT, up to 50 vol%).[189] The solution-cast thin films of BPZT/P(VDF-TrFE) displayed improved dielectric permittivity ($\varepsilon_r = 27$ at 50 vol% BPZT, 0.48 MHz) compared with the pure copolymer ($\varepsilon_r = 9$), and a d_{33} of up to 37 pm V^{-1} was observed (10 vol% BPZT). Dietze and Es-Souni introduced PNN-PZT (PNN - lead nickel niobate) into the P(VDF-TrFE) matrix, producing d_{33} values of up to 100 pm V^{-1} (50 vol% PNN-PZT, solution-cast film, anti-parallel poling) and elevated Young's modulus (1.6 GPa).[281]

4.2.2. Other Ceramics

Electromechanical enhancements comparable to those in PZT-filled composites can also be realized using other piezoceramic fillers, such as lead-titanate (PT),[277,284] lead magnesium niobate-lead titanate (PMN-PT),[285] barium titanate ($BaTiO_3$, BTO in short),[190,256] and semiconductor oxides (SiO_2, GeO_2, TiO_2, ZnO).[286,287]

Cai et al. investigated PVDF composites with lead-titanate (65 vol% PT).[277] The PT/PVDF films attained d_{33} and k_{33} of up to 30 pm V^{-1} and 0.486, respectively. Chan et al. studied P(VDF-TrFE) composites with barium titanate (up to 50 vol% BTO).[190] A diminishing piezoelectric behavior (d_{33}) was reported with increasing BTO concentrations, attributed to the parallel poling of copolymer and ceramic phases. Dalle Vacche et al. reported that similar BTO/P(VDF-TrFE) composites (60 vol% BTO) exhibited a d_{33} of up to ≈22 pm V^{-1}, which then decreased to 7–10 pm V^{-1} within 1 week.[256] Liu et al. investigated the interfacial effect in BTO/PVDF and BTO/P(VDF–TrFE–CFE) composites, reporting that BTO nanoparticles locally stabilize the all-*trans* polar conformation at the filler–polymer interface.[288]

Ploss et al. produced P(VDF-TrFE) composites with 27 vol% of lead titanate (PT), attaining pyroelectric (d_{33} of 1 pm V^{-1}) and piezoelectric (d_{33} of 20 pm V^{-1}) behavior upon parallel and anti-parallel poling conditions, respectively.[284] Lam and Chan studied P(VDF-TrFE) composites with PMN-PT (5 vol% to 40 vol%), reporting that ε_r and d_{33} increase with PMN-PT volume fraction in the hot-pressed films (anti-parallel poling, 50 V μm^{-1}).[285] The 40 vol% composite films (30 μm thickness) exhibited the highest d_{33} coefficient of 31 pm V^{-1} and ε_r of 37.3.[285] Kar et al. studied PVDF composites with semiconductor oxide nanoparticles (up to 15 wt% SiO_2 and GeO_2), indicating a

Table 4. Mechanical, dielectric, and transduction properties of PVDF-based composites with carbon-based, conductive polymer, core-shell, metal-organic, and OS fillers.

Matrix	Filler	Y [MPa]	ε_r [a)]	E [b)] [V μm^{-1}]	S_{max} [b)] [%]	U_s [b)] [J cm^{-3}]	Other [c,d)]	Ref.
P(VDF-TrFE-CTFE)	CB (2.75 wt%)	–	71	12	0.069 (S_1)	3.59×10^{-5}	$E_b = 30$ V μm^{-1}	[233]
P(VDF-TrFE-CTFE)	CB (4.5 wt%)	400	140	–	–	–	$E_b = 9.6$ V μm^{-1} $f_c = 4.68$ wt%	[292]
P(VDF-TrFE-CTFE)	PANI (23 vol%)	535	1900	16	2.65 (S_3)	0.18	$E_b = 16$ V μm^{-1} $f_c = 25.9$ vol%	[232]
P(VDF-HFP) (nanofibers)	PANI (5 wt%)	50	2.58	9	3.65 (S_3)	0.03	$M_{33} = 2.53 \times 10^{-14}$ m^2/V^2	[105]
P(VDF-TrFE-CFE)	P3HT-PMMA (1.5 wt%)	132	89.6	60	1.1 (S_1)	0.008	$E_b = 60$ V μm^{-1} $M_{31} = 3.05 \times 10^{-16}$ m^2/V^2	[238]
P(VDF-TrFE)	P3HT-PMMA@SWCNTs (0.05 wt%)	571	76.3 (10 Hz)	50	5.1 (S_3)	0.74	$E_b = 50$ V μm^{-1} $M_{33} = 2.04 \times 10^{-15}$ m^2/V^2 $k_{33} = 0.88$	[304]
PVDF	MWCNTs (0.075 wt%)	–	21.5	–	–	–	$E_b = 340$ V μm^{-1} $d_{33} = 33$ pm V^{-1}	[305]
P(VDF-TrFE-CFE)	MWCNTs (1 wt%)	159	74	72	2.5 (S_3)	0.05	$E_b = 72$ V μm^{-1}	[245]
P(VDF-TrFE-CFE)	GNs (2.75 vol%)	–	102 (1 kHz)	–	–	–	$f_c = 3$ vol% $M_{33} = 3 \times 10^{-15}$ m^2/V^2	[307]
P(VDF-TrFE-CFE)	GNs (1.09 vol%)	550	40 200	23	4.1 (S_3)	0.47	$E_b = 23$ V μm^{-1}	[308]
PVDF	TiO_2@MWCNTs (0.3 wt%)	–	16 (1 kHz)	–	–	–	$E_b = 320$ V μm^{-1} $d_{33} = 41$ pm V^{-1}	[311]
PVDF	GNs-MnO_2@MWCNTs (0.1-0.2 wt%)	–	26	–	–	–	$E_b = 213$ V μm^{-1} $d_{33} = 48$ pm V^{-1}	[315]
EI-P(VDF-TrFE)	CuPc (40 wt%)	750	101	13	1.91 (S_3)	0.13	$E_b = 13$ V μm^{-1}	[88]
PVDF	OS (4 wt%)	880	10 (1 kHz)	–	–	–	$d_{33} = 22.2$ pm V^{-1}	[321]

[a)] Measured at 100 Hz if no frequency is indicated. [b)] Maximum reported driving field, strain, and elastic energy density. [c)] Absolute values of d_{33} are given. [d)] f_c – Percolation threshold.

significantly improved β-phase formation at 5 wt% concentrations (SiO_2 or GeO_2) without the need of stretching.[287]

Liu et al. studied TiO_2/PVDF, TiO_2NWs/PVDF, ZnO/PVDF, TiO_2/P(VDF-HFP), and TiO_2/P(VDF-TrFE) nanocomposites,[286,289] reporting that the highest S_3 (8.1% at 40 V μm^{-1}), U_s (11.3 J cm^{-3}), and k_{33} (0.88) are exhibited by TiO_2/PVDF at 14.9 vol% TiO_2 (see Table 3). The large strains were ascribed to the electrothermal all-*trans* (β) ↔ TGTG′ (α) phase transition near the percolation threshold (14.9 vol% TiO_2), as the β-rich regions at the polymer-filler interfaces overlap and form a polar network.[286,289] The increased strains were accompanied by a reduction in breakdown strength, showing a ≈3× lower E_b for 14.9 vol% TiO_2/PVDF compared with the neat PVDF.[286,289] In a later study, Li et al. showed that the β-rich interfacial regions in TiO_2/PVDF originate from in-plane strains due to the polymer and nanofiller lattice mismatch.[290]

4.2.3. Carbon Black

Incorporating small amounts (≤5 wt%) of carbon black (CB) nanoparticles into PVDF terpolymers can significantly enhance their dielectric permittivity due to percolation phenomenon.

Lallart et al. studied carbon black (CB) nanoparticle composites with P(VDF-TrFE-CFE) for energy harvesting use and reported the increase in dielectric permittivity ε_r from 40 to 70 (100 Hz, 1 vol% 30 nm CB particles, 50 μm-thick solution-cast film) compared with the neat terpolymer, while tan(δ) (dielectric losses) increased from ≈0.02 to 0.07 (20–120 Hz).[291] Yin et al. studied dielectric and mechanical properties of CB/P(VDF-TrFE-CFE) composites (0–5 wt% 30 nm CB NPs, 100–200 μm thick solution-cast films), reporting a percolation threshold of $f_c = 4.68$ wt%.[292] The 4.5 wt% CB composites exhibited an ε_r of up to 140, a dielectric loss of 0.05 (100 Hz), and similar mechanical properties to the neat polymer, while significantly decreasing in dielectric breakdown strength (from 80.2 V μm^{-1} in neat polymer to 9.6 V μm^{-1} for 4.5 wt% CB).

Tu et al. hypothesized that the low E_b in such composites originates from the poor dispersion of CB NPs and studied grafting functional groups (-COOH- and -OH-) on the -NPs- to enhance dispersion quality.[233] The thin P(VDF-TrFE-CTFE) composite films (8 μm thick, solution-cast, 2.75 wt% CB) exhibited ε_r of 71 (≈1.6x higher than the neat terpolymer) and dielectric loss of 0.071 (100 Hz), while the E_b decreased from 165 V μm^{-1} (neat polymer) to 30 V μm^{-1} (2.75 wt% CB). From the unimorph actuator performance they estimated the strain S_1 of up to 0.069% and elastic energy density of up to 3.59×10^{-5} J/cm^3 at 12 V μm^{-1}.[233]

4.2.4. High Aspect-Ratio Conductive Fillers

The percolation threshold depends on the conductive nanofiller geometry, and it can be lowered using high aspect ratio

particles.[293,294] Carbon-based nanofillers such as graphene nanosheets (GNs), single-walled carbon nanotubes (SWCNTs), and multiwalled carbon nanotubes (MWCNTs) further offer improved thermal, electrical, and mechanical properties[295–297] and have been investigated as fillers in EAPs.[247,298–301] Besides the carbon-based materials, introducing Ag nanowires (NWs) has been shown to improve dielectric properties of the EAP matrix.[302]

The influence of SWCNTs on FPs' electromechanical transduction properties has been studied only basing on the P(VDF-TrFE) polymer matrix. Levi et al. observed a 25% increase of transverse piezoelectric response (d_{31} of up to ≈25 pm V^{-1}) upon incorporation of 0.0072 wt% ($f_c = 0.1$ wt%) of SWCNTs in P(VDF-TrFE).[303] This was ascribed to the dispersed nano-inclusions that nucleated higher β phase content than the pure polymer. Cho et al. studied using compatibilizer (P3HT-PMMA block copolymer) to improve dispersion of SWCNTs in P(VDF-TrFE).[247,304] Addition of 0.05 wt% SWCNTs attained dielectric constant (10 Hz) of 11.3 for SWCNTs and 76.3 for SWCNTs with P3HT-PMMA, compared with the 9.59 of pure P(VDF-TrFE).[304] The solution-cast films of SWCNTs/P(VDF-TrFE) with P3HT-PMMA exhibited electrostrictive strains S_3 of up to 5.1% (50 V μm^{-1}) and elastic energy density U_s of 0.74 J cm^{-3}.[304]

Multiwalled carbon nanotubes (MWCNTs) have been investigated in percolative composites basing on both PVDF and P(VDF-TrFE-CFE) matrices. Zhang et al. investigated P(VDF-TrFE-CFE) composites with functionalized MWCNTs (up to 2 wt%).[245] MWCNTs were chemically grafted with fluorinated silane molecules prior to blending with P(VDF-TrFE-CFE) in DMF and formed into films via anti-solvent precipitation and hot-pressing (200 °C). This increased the degree of crystallinity from 51% (neat polymer) to 60% (2 wt%), producing the highest strains of 2.5% (72 V μm^{-1}) at 1 wt% MWCNT content (compared to S_3 of 1.8% in neat polymer at the same field strength). Yang et al. observed a significant increase in β phase content upon addition of small amounts (0.05–0.075%wt.) of MWCNTS into PVDF.[305] While the low breakdown strength of the solution-cast MWCNTS/PVDF films (≈50 V μm^{-1}) limited the poling, the mechanical rolling of the MWCNTS/PVDF films increased the E_b to 340 V μm^{-1}, enabling higher poling fields and producing d_{33} of up to 33 pm V^{-1}. Sharafkhani and Kokabi studied nanofiber mats of MWCNTs/PVDF composite.[299] They reported that 1.5 wt% of MWCNTs content produces a higher crystallinity, β phase fraction, and Young's modulus (up to ≈0.2 GPa) than the pure PVDF nanofibers mats and employed the composite for actuator fabrication (Section 5.5).

Incorporation of graphene nanosheets (GNs) has been shown to significantly enhance the dielectric constant and electrostrictive response of PVDF terpolymers. Wen et al. investigated dielectric properties of P(VDF-TrFE-CTFE) composites with surface-modified GNs (up to 4 wt%).[306] The 24 μm thick solution-cast films exhibited a 14-fold increase in dielectric constant (1 kHz) from 10 (neat polymer) to 144 (4 wt% GNs), while the dielectric losses increased to 0.56. Seveyrat et al. studied P(VDF-TrFE-CFE) composites with 60 nm-thick GNs (up to 5 vol%) and reported a percolation threshold of 3 vol%.[307] The dielectric permittivity (0.1–10 kHz) of the solution-cast films increased with the filler content, and 2.75 vol% GNs composite exhibited an electrostrictive coefficient M_{33} of 3×10^{-15} m^2/V^2 (2× increase compared to the pure terpolymer). Javadi et al. reported a significant improvement in the P(VDF-TrFE-CFE) actuation response at low field strengths upon introduction of small amounts (up to 1.37 vol%) of functionalized GNs.[308] The 1.09 vol% GNs composite exhibited a ε_r of 40 200 (100 Hz), Y of 550 MPa and S_3 of up to 4.1% (23 V μm^{-1}, U_S of 0.47 J cm^{-3}), but a reduced breakdown field strength from 100 to 23 V μm^{-1}.

As an alternative to blended nanocomposites, Fook et al. proposed to combine a layer of Ag nanowires (NWs) between two layers of P(VDF-TrFE-CTFE) to form a modified EAP film.[302] They attained an increase in the dielectric constant ε_r from 34.5 (neat terpolymer, 1 kHz) to 75.5 (3.81 μg cm^{-2} Ag NWs, 1 kHz), and in maximum polarization from 3.4 to 5.1 μC cm^{-2}, accompanied by a 39% decrease in breakdown strength. These effects were argued to be induced by MWS effect at the interface between the polymer matrix and the conductive interlayer, and the material was further employed as an EAP in actuators (see Section 5.5.1).

4.2.5. Conductive Polymers

Similarly to carbon black, conductive polymer fillers produce enhanced dielectric properties, without significantly impacting the mechanical flexibility of the composites.

Huang et al. investigated fully polymeric P(VDF-TrFE-CTFE) composites with polyaniline (PANI), indicating a very high percolation threshold of $f_c = 25.9$ vol% and dielectric permittivity of up to 1400 (1 kHz, 23 vol% PANI).[232] The composite films (50 μm thickness, solution-cast, 23 vol% PANI) exhibited high longitudinal strains S_3 of up to 2.65% at very low field strengths (16 V μm^{-1}, $U_s = 0.18$ J/cm^3), while the breakdown strength decreased from 160 V μm^{-1} (neat terpolymer) to 16 V μm^{-1} (see **Figure 6**).

Tohluebaji et al. investigated electrospun nanofiber mats of PANI/P(VDF-HFP) composites (up to 5 wt% PANI), reporting increased ε_r (up to 2.58, 100 Hz), tan(δ) (up to 0.024),

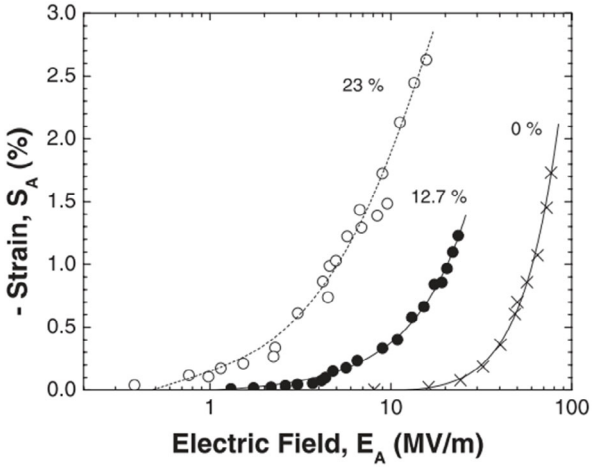

Figure 6. S-E curves for PANI/P(VDF-TrFE-CTFE) composites with different PANI content. Reproduced with permission.[232] Copyright 2004, WILEY-VCH Verlag GmbH & Co.

conductivity (up to 9.18×10^{-10}S/m), Young's modulus (50 MPa), and M_{33} coefficient (up to 2.53×10^{-14}m^2/V^2) with increasing PANI content.[105]

Kim et al. studied fully organic relaxor ferroelectric composites that consisted of micelle-structured block copolymer (poly(3-hexylthiophene)-b-poly(methyl methacrylate), i.e., P3HT-PMMA) dispersed in P(VDF-TrFE-CFE).[238] The composite (2 wt% of P3HT-PMMA) exhibited a twofold increase in transverse strain (S_1 of 0.44%) and eightfold increase in energy density (1.52 mJ cm^{-3}) compared with the pure terpolymer at the same field strength (30 V μm^{-1}), while a maximum S_1 of up to 1.1% was attained by the 1.5 wt% P3HT-PMMA composite at higher field strength (60 V μm^{-1}).

4.2.6. Core-Shell Structures

Conductive fillers deteriorate the dielectric losses and breakdown strength of eEAPs composites due to the local field intensification at matrix-filler interfaces (see Section 4.1). To mitigate this, it has been proposed to employ core-shell structure fillers, where the conductive particles are coated with a thin insulating layer that prevents formation of conductive paths.[309–312]

Yang et al. investigated PVDF composites with up to 1 wt% TiO_2@MWCNTs fillers (i.e., MWCNTs with TiO_2 coating) to improve the ε_r and lower the tan(δ).[311] The 0.3 wt% TiO_2@MWCNTs composite breakdown field strengths were reported to be ≈24% higher than in pure PVDF (210 and 170 V μm^{-1}, respectively). The low d_{33} of the solution-cast and poled TiO_2@MWCNTs/PVDF films (14 pm V^{-1}, 0.3 wt% TiO_2@MWCNTs) was addressed in a follow-up study, where mechanical rolling was applied to align the TiO_2@MWCNTs particles.[313] The rolled samples (0.3 wt% of MWCNTs@TiO_2, ≈20 μm thickness) exhibited higher β-phase content and d_{33} of up to 41 pm V^{-1} (ca 2x higher than in rolled films of pure PVDF).

Yang et al. investigated PVDF composites with nanohybrid fillers of MWCNTs covered with graphene and manganese oxide (MnO_2) nanoflakes, aiming to attain uniform particle dispersion in the PVDF matrix.[314] The 12 μm films (solution-cast and rolled) with 0.3 wt% nanohybrid filler content (with 66 wt% of MnO_2) exhibited d_{33} of 17–33 pm V^{-1}, depending on the poling field (50–80 V μm^{-1}). The rolled films of pure PVDF required poling at >100 V/μm to achieve similar d_{33}.[314] In a follow-up study, the same materials were further used to form three-layer composite films, where the middle layer (0.2 wt% filler content at 66 wt% MnO_2) served to elevate the breakdown field strength and the outer layers (0.1 wt% filler content at 23 wt% MnO_2) to enhance piezoelectric response.[315] The 20–25 μm thick films were manufactured separately, laminated together by compression molding and rolling, and poled at 70 V μm^{-1}. This resulted in d_{33} of up to 48 pm V^{-1}, exhibiting small variations over the temperature range of 10–60 °C.[315]

Liang et al. investigated loading PVDF with a combination $BaTiO_3$ (20 vol%) and SiO_2@Ag (i.e., SiO_2-coated Ag) nanoparticles (0 to 45 vol%).[316] The solution-cast and hot-pressed films (1 mm thickness) with 40 vol% of SiO_2@Ag content attained ε_r of up to 723 and tan(δ) of 0.82 (100 Hz). The high ε_r was attributed to the formation of a microcapacitor network, enhancing the MWS effect (see Section 4.1).[316]

4.2.7. Metal-Organic Compounds and Organically Modified Silicates

Metal-organic compounds and organically modified silicates (OS) have also been employed as dispersed phases within PVDF-based matrices in order to facilitate β phase nucleation and enhance the dielectric constant of the polymer matrix.

Zhang et al. studied composites of electron-irradiated P(VDF-TrFE) with high-ε_r copper phthalocyanine (CuPc).[88] The solution-cast 40 wt% CuPc composite exhibited an ε_r of 101 (100 Hz) and an S_3 of up to 1.91% (13 V μm^{-1}), while increasing the dielectric losses and decreasing the E_b down to 13 V μm^{-1}. These shortcomings were later addressed via chemically grafting CuPc oligomer onto P(VDF-TrFE)[317] and P(VDF-TrFE-CFE)[318] backbones, while transduction properties of these materials were not reported.

Geng et al. and Zhang et al. studied PVDF composites with OS fillers.[319,320] OS fillers were reported to promote β and γ phase formation in PVDF composites, but the unstreched films produced low d_{33} values (2–6 pm V^{-1}).[319,320] He et al. showed that stretching OS/PVDF composites (melt-extruded, hot-pressed, and poled films, 4 wt% of OS) further improves the d_{33} (22.2 pm V^{-1}) by ≈3× over the unstretched films.[321]

4.3. Blends

Blending ferroelectric polymers (FPs) with plasticizers (Section 4.3.1) or other EAPs (Section 4.3.2) aims to enhance achievable strains and energy densities via tuning the material's Young's modulus and dielectric constant. The findings of this section are summarized in **Table 5**.

4.3.1. Polymer-Plasticizer

Blending eEAPs with plasticizing agents has been shown to be an efficient way to improve actuation performance.[322–324] Plasticizer molecules expand the free volume between the eEAP polymer chains, increasing their mobility and causing decrease in viscosity and Young's modulus.[325] In semicrystalline polymers, the plasticizers additionally enhance the dielectric constant at low frequencies due to the interfacial polarization effects at the filler-polymer boundaries (MWS, see Section 4.1).[326–328]

Capsal et al. proposed to blend PVDF terpolymers with small molecular phthalates and investigated the electromechanical properties of P(VDF-TrFE-CFE) blends with di-2-ethylhexyl phthalate (DEHP).[326] DEHP was reported to reduce the Young's modulus and increase the dielectric constant of the polymer, and 70 μm thick solution-cast films with 15 wt% DEHP attained energy densities of up to 5 mJ cm^{-3} (11 V μm^{-1}). Up to 2% strains (S_3) were measured at 10 V μm^{-1}, in contrast to the pure P(VDF-TrFE-CFE) that required 55 V μm^{-1} to produce similar strains. Le et al. later reported that introducing 15 wt% DEHP into P(VDF-TrFE-CFE) decreases its E_b from 180 V μm^{-1} (neat terpolymer) to 150 V μm^{-1}.[329]

Table 5. Mechanical, dielectric, and transduction properties of PVDF-based blends.

Blend	Y [MPa]	ε_r [a)]	E [b)] [V μm^{-1}]	S_{max} [b)] [%]	U_s [b)] [J cm^{-3}]	Others	Ref.
DEHP (15 wt%)/P(VDF-TrFE-CFE)	20	725 (0.1 Hz)	10	2 (S_3)	0.005	$k_{33} = 0.12$	[326]
DEHP (15 wt%)/P(VDF-TrFE-CFE)	44	820 (0.1 Hz), 50	10	1.8 (S_3)	0.0071	$E_b = 150$ V μm^{-1}	[329]
DEHP (15 wt%)/P(VDF-TrFE-CFE)	50	4800 (0.1 Hz), 47	25	1.6 (S_1)	0.0064	–	[224]
DEHP (15 wt%)/P(VDF-TrFE-CTFE)	45	2000 (0.1 Hz), 38	25	1.6 (S_1)	0.0058	$M_{31} = 2.56 \times 10^{-17}$ m^2/V^2	[224]
DEHP (10 wt%)/P(VDF-TrFE-CTFE)	95.7	651.2 (0.1 Hz), 29	30	1 (S_1)	0.0048	$E_b = 207$ V μm^{-1} $M_{31} = 1.57 \times 10^{-17}$ m^2/V^2	[330]
DEHP (15 wt%)/P(VDF-TrFE-CTFE)	45	1200 (0.1 Hz), 35	10	0.41 (S_1)	0.00038	–	[331]
DINP (15 wt%)/P(VDF-TrFE-CTFE)	35	1900 (0.1 Hz), 95	10	0.51 (S_1)	0.00045	$k_{31} = 0.053$	[331]
Palamoll 652 (15 wt%)/P(VDF-TrFE-CTFE)	17	200 (0.1 Hz), 35	10	0.21 (S_1)	0.000037	–	[331]
DINP (8 wt%)/P(VDF-TrFE-CFE)	67	330 (0.1 Hz), 48	25	1.3 (S_3, 0.76 N preload)	–	$E_b = 70$ V μm^{-1}	[234]
DINP (10 wt%)/P(VDF-TrFE-CFE)	50	290 (0.1 Hz), 51	20	0.35 (S_1)	0.0003	$E_b = 119$ V μm^{-1}	[237]
Nylon 11 (2.5 wt%)/PVDF	2650	11	–	–	–	$d_{31} = 31.5$ pm V^{-1}	[333]
P(VDF-HFP) (15 wt%)/P(VDF-TrFE)	–	–	40	3.5 (S_3)	–	–	[334]
P(VDF-TrFE) (10 wt%)/P(VDF-CTFE)	490	–	170	5 (S_3)	0.6	$d_{33} = 100$ pm V^{-1} $k_{33} = 0.2$	[335]
P(VDF-TrFE) (20 wt%)/P(VDF-TrFE-CFE)	520	–	110	1.6 (S_3)	0.0145	–	[336]
P(VDF-TrFE) (20 wt%)/P(VDF-TrFE-CFE)	660	13.46 (10 kHz)	80	0.64 (S_3)	0.0135	–	[235]
P(VDF-CTFE) (5 wt%)/P(VDF-TrFE-CFE)	1050	–	150	3.7 (S_1)	0.73	$k_{31} = 0.31$ $Q_{31} = 6.8$ m^4/C^2	[337]
PMMA (5 wt%)/P(VDF-TrFE-CFE)	439	37 (1 kHz)	150	3.5 (S_3)	0.269	$k_{33} = 0.27$	[236]
EI-PMMA (7 wt%)/P(VDF-TrFE)	–	23 (1 kHz)	150	2.25 (S_3, 25 °C) 6.1 (S_3, 70 °C)	–	–	[338]

[a)]Measured at 100 Hz if no frequency is indicated. [b)]Maximum reported driving field, strain and elastic energy density.

Capsal et al. further studied adding DEHP (15 wt%) both in P(VDF-TrFE-CFE) and P(VDF-TrFE-CTFE).[224] DEHP was reported to improve the strains and energy densities of both the polymers, while DEHP/P(VDF-TrFE-CFE) exhibited ≈3× higher strains than DEHP/P(VDF-TrFE-CTFE) at up to 25 V μm^{-1}. Commercial availability of P(VDF-TrFE-CTFE) with different compositions allowed to further study the effect of CTFE content in DEHP/P(VDF-TrFE-CTFE) blends (15 wt% DEHP). Increasing CTFE content (3.2 to 8.9%) resulted in an increasing transverse strain (up to 1.6 %, 25 V μm^{-1}), energy density (up to 5.8 mJ cm^{-3}), and electrostrictive coefficient (up to $2.56 \cdot 10^{-17}$m^2/V^2). Yin et al. explored the influence of DEHP concentration on the DEHP/P(VDF-TrFE-CTFE) transduction properties.[330] They reported a decreasing Young's modulus (from 163 to 87.8 MPa) and increasing dielectric constant (from 36.8 to 2127, 0.1 Hz) with increasing DEHP concentration (0–15 wt%), accompanied by a reduction in breakdown strength (from 269 to 79 V μm^{-1}). A sharp decrease in breakdown field strength (from 207 to 79 V μm^{-1}) occurred between DEHP concentrations of 10 wt% and 15 wt%, while at low field strengths (20 V μm^{-1} at 0.1 Hz), similar transverse strains of 0.63% (M_{31} of $1.57 \cdot 10^{-17}$m^2/V^2) and 0.66% (M_{31} of $1.63 \cdot 10^{-17}$m^2/V^2) were respectively reported. At higher field strengths (30 V μm^{-1}), the 10 wt% DEHP blends exhibited transverse strains of up to 1%, representing a 10-fold improvement compared to the neat terpolymer.

Della Schiava et al. investigated how diisononyl phthalate (DINP), Palamoll 652, and DEHP plasticizers (15 wt%) compare in enhancing the transduction properties of P(VDF-TrFE-CTFE), as illustrated in **Figure 7**.[331] All plasticizers caused a decrease in Young's modulus and increase in ε_r, whereas the DINP/P(VDF-TrFE-CTFE) composite exhibited the highest S_1 (0.51%, 15 wt%, 10 V μm^{-1}) and energy density (0.47 mJ cm^{-3}). The impact of DINP concentration (0 to 16 wt%) was further studied, indicating a positive impact on actuation properties. In a separate study, increasing the DINP concentration (0 to 12 wt%) was reported to decrease E_b of the DINP/P(VDF-TrFE-CFE) films (200 μm thickness).[234] DINP concentrations in the range of 8–10 wt% were reported to be a good trade-off between the material strain (S_3 of up to 1.3%, 25 V μm^{-1}, 0.76 N pre-loading, 8 wt% DINP) and breakdown strength (70 V μm^{-1}, 8 wt% DINP).

Della Schiava et al. further reported enhanced low-frequency (0.1 Hz) dielectric constant (up to 290) and transduction response (S_1 of up to 0.35% at 20 V μm^{-1}) in DINP/P(VDF-TrFE-CFE) blends (10 wt% DINP) at the cost of a steep decrease in the breakdown strength (from 276 to 119 V/μm).[237] The plasticized terpolymer retained its electromechanical properties upon exposure to β-radiation and was proposed for the construction of medical devices (see Section 5.5.2).

4.3.2. Polymer-Polymer

Similarly to doping with micro/nanoparticles and plasticizers (Section 4.2 and 4.3.1), it is possible to obtain EAPs with tailored properties by blending two or more polymers with distinct electrical and mechanical characteristics.

Gao et al. investigated PVDF blends with Nylon-11 that were fabricated as thin films (≈20 μm) via melt-pressing and

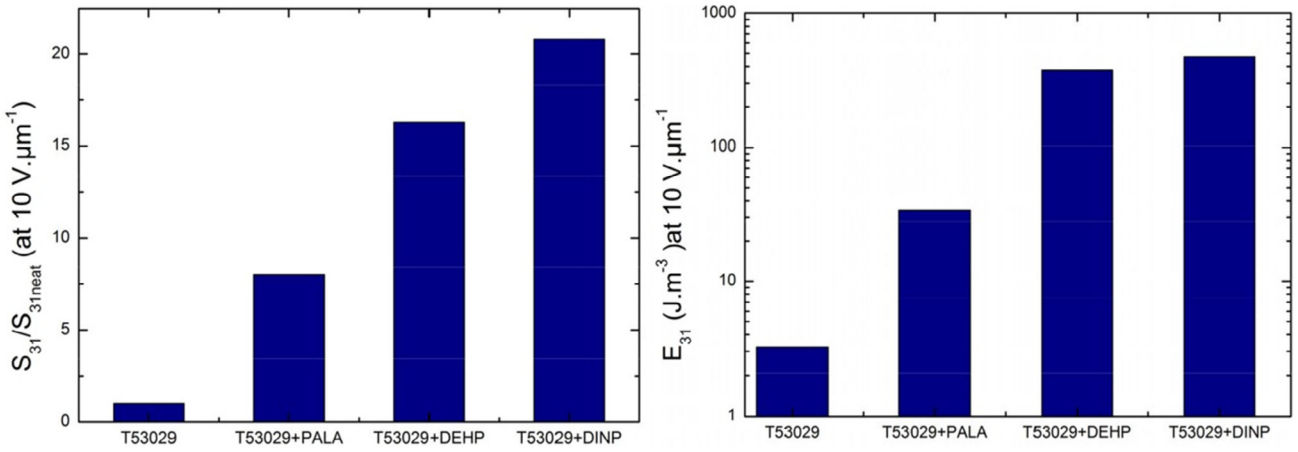

Figure 7. Transverse strain and energy density in P(VDF-TrFE-CTFE) can be improved via blending with DEHP, DINP, and Palamoll plasticizers. Reproduced with permission.[331] Copyright 2017, Wiley Periodicals, Inc.

ice-quenching the blended polymer powders and further uniaxially drawing and poling the films (220 V μm^{-1}).[332,333] It was reported that 50 wt% Nylon-11 concentration attains a ≈60% increase in remnant polarization P_r (up to 90 mC m^{-2}) over the pure PVDF and Nylon-11 polymers, while the ϵ_r decreases with increasing Nylon-11 content (from ≈11.7 at 0 wt% to ≈4 at 100 wt%).[332] Low Nylon-11 concentrations attained up to 15% improvement in d_{31} at room temperature (from 27.5 pm V^{-1} for pure PVDF to 31.5 pm V^{-1} for 2.5 wt% Nylon-11), and 6.8× improvement at 160 °C (from 8.5 pm V^{-1} for pure PVDF to 58 pm V^{-1} for 20 wt% Nylon-11).[333]

Jayasuriya et al. investigated blends of P(VDF-TrFE) with up to 25 wt% P(VDF-HFP) content.[334] The solution-cast, melt-pressed, and quenched films with 15 wt% P(VDF-HFP) concentration showed higest S_3 of 3.5% at low field strengths (40 V μm^{-1}), a 2.9-fold increase over pure the P(VDF-TrFE) (S_3 of 1.2% at 40 V μm^{-1}). Higher P(VDF-HFP) concentrations deteriorated the Curie temperature, melting point, and electrostrictive strain of the materials.

Li et al. studied the electrostrictive response of P(VDF-TrFE)/P(VDF-CTFE) blends in different weight ratios (75/25, 50/50, 25/75, and 10/90 wt%).[335] The solution-cast, uniaxially stretched, and annealed films with 10/90 wt% composition attained the highest longitudinal strains of up to 5% with the corresponding energy density of 0.6 J cm^{-3} (170 V μm^{-1}), and k_{33} of up to 0.2.

Van Duong et al. studied P(VDF-TrFE)/P(VDF-TrFE-CFE) blends with up to 20 wt% P(VDF-TrFE) copolymers (45 and 25 wt% TrFE content).[336] The longitudinal strains S_3 of the 3.6 μm thick films were reported to decrease compared with the neat terpolymer (up to 2.2% at 0 wt% P(VDF-TrFE), 1.8% at 10 wt% and 1.6% at 20 wt%, 110 V μm^{-1}, 25 °C), while the film stresses ($\sigma = YS$) varied with the amount and composition of P(VDF-TrFE) due to the changing Young's modulus. In a follow-up study, P(VDF-TrFE)/P(VDF-TrFE-CFE) blends (20 wt% copolymer, 45 mol.% TrFE) were reported to exhibit an increased mechanical energy density over the neat terpolymer both at the room temperature (from 9.8 to 13.5 mJ cm^{-3}) and at 60 °C (from 15.6 to 24.7 mJ cm^{-3}).[235]

Gorny et al. investigated the electrostrictive response of P(VDF-CTFE)/P(VDF-TrFE-CFE) with up to 10 wt% of P(VDF-CTFE) content.[337] At room temperature and 150 V μm^{-1}, the uniaxially stretched films (25 μm thickness) attained transverse strains S_1 of up to 4% (both at 0 and 2.5 wt% P(VDF-CTFE)), energy densities of up to 0.73 J cm^{-3} (in contrast to 0.71 J cm^{-3} for neat terpolymer) and k_{31} of 0.31 at 5 wt% P(VDF-CTFE).

Bharti et al. investigated the electrostrictive response of PMMA/P(VDF-TrFE) blends containing up to 7 wt% PMMA.[338] The solution-cast, annealed, and electron-irradiated films with 7 wt% PMMA exhibited slightly lower room-temperature strains (S_3) compared with the P(VDF-TrFE) matrix (2.25% vs. 2.55% at 150 V μm^{-1}), but showed a 126% increase in S_3 at 70 °C (up to 6.1%, 150 V μm^{-1}). This enhancement was attributed to the increased contribution of Maxwell stress at elevated temperatures.

Zhang et al. investigated blending P(VDF-TrFE-CFE) with up to 10 wt% of PMMA.[236] The 20 μm-thick solution-cast PMMA/P(VDF-TrFE-CFE) films with 5 wt% PMMA content attained a 137% improvement in energy density (from 0.113 to 0.269 J cm^{-3}) and a 59% improvement in coupling factor k_{33} (from 0.17 to 0.27) under a 150 V μm^{-1} excitation.

Dielectric properties of FP blends have been addressed in several studies without characterizing the electromechanical transduction. Chu et al. studied P(VDF-TrFE-CFE) blends with up to 20 wt% of P(VDF-CTFE), reporting an improved breakdown strength of up to 358 V μm^{-1} at 5 wt% P(VDF-CTFE), over the 262 V μm^{-1} of the pure terpolymer.[339] This was hypothesized to stem from the increased Young's modulus, as explained by the Stark–Garton model.[199,340] Casar et al. investigated dielectric properties of P(VDF-TrFE-CFE) blends with up to 50 wt% P(VDF-TrFE) over a range of temperatures (225 to 350 K), reporting a purely RFE behavior at <20 wt% P(VDF-TrFE) concentrations, and a concurrent RFE and FE behaviors at higher concentrations.[341] Ullah et al. manufactured 800 nm thick films of P(VDF-TrFE)/P(VDF-TrFE-CFE) blends (0 to 100 wt% P(VDF-TrFE)) via spin-coating, and reported an up to 13% improvement in ϵ_r at 40 wt% P(VDF-TrFE) over the neat terpolymer (i.e., from

47 to 53, 10 kHz).[342] Zhang et al. investigated blending P(VDF-TrFE-CFE) with PVDF homopolymer in 0 to 100 vol% composition,[343] reporting an improvement in the breakdown field strength (up to 665.1 V μm^{-1} for 40/60 vol% P(VDF-TrFE-CFE)/PVDF).

5. Actuators and Devices

Various PVDF-based materials have been also used to construct actuators and devices. Actuators basing on PVDF, P(VDF-TrFE) and EI-P(VDF-TrFE) are addressed in Sections 5.1, 5.2, and 5.3, and their characteristics are summarized in **Table 6**. PVDF terpolymer actuators base on P(VDF-TrFE-CTFE) and P(VDF-TrFE-CFE), as addressed in Section 5.4 and summarized in **Table 7**. Actuators of PVDF-based composites and blends are covered in Section 5.5 and compared in **Table 8**.

5.1. PVDF

Utilization of PVDF as transducer material dates back to 1972, when thin PVDF films were patented for ultrasound applications,[344] and functional MHz-range transducers (in d_{33} configuration) were first reported in 1973.[345] In 1975, electroacoustic transducers were introduced and commercialized for microphone and speaker applications, utilizing stretched PVDF membranes (8–30 μm in thickness) in d_{31} mode.[346] Since the late 1970s, PVDF homopolymer has been investigated as an active material for the construction of both bimorph[347–356] and unimorph[357–361] actuators, respectively addressed in Section 5.1.1 and 5.1.2. PVDF has also been proposed for plate actuators (d_{33} mode).[161] Namely, Burnham–Fay et al. 3D-printed 230 μm thick PVDF films and used Cu tape for electrodes, attaining actuators that exhibited longitudinal displacements of up to 2.02 μm under 860 V excitation (≈3.7 V μm^{-1}).[161]

5.1.1. Bimorphs

Bending PVDF transducers were first introduced in 1979 to amplify the small field-induced strains of PVDF films employing bimorph structure.[350–353] Two sheets of metalized PVDF (9 μm thick) were stretched, poled, and bonded together using a thin layer of epoxy resin.[352] Upon 10 V excitation, the 2 cm long benders achieved 1 mm tip deflections and 4 μN blocking forces.[350] Such actuators were further employed in double-supported configuration to construct a seven-segment alphanumeric display.[354] The 4 cm long bimorph actuators produced 1.8 cm deflections at 120 V (60–100 ms response time).

Toda et al. stacked multiple metalized PVDF sheets to construct bimorph cantilever actuators.[350,351,353] The actuators used four to six layers of 9 μm thick metalized PVDF sheets that were glued together using epoxy resin. The vibrating cantilevers were proposed for ventilating applications and were demonstrated to generate air flows of ≈7 L s^{-1} (resonant operation, 150 V amplitude). Electromechanical coupling efficiencies of 0.33–0.5 were estimated.[351,353]

Bohannan et al. used PVDF bimorph cantilevers to construct actuators in a leaf-spring configuration.[347] Two bimorph beams with Ag electrodes were glued together in the ends and pressed to form the curved leaf-spring shape. The actuators were proposed for vibration isolation applications and reported a measurable damping at 5 Hz and above.

Schmidt et al. fabricated bending bimorph actuators basing on commercial PVDF sheets.[349,355] They used both the inkjet printing and air-brushing techniques to deposit

Table 6. Constituent materials and performance of PVDF homopolymer and copolymer actuators.

Configuration	Size[a)]	Active layer[b)]	Substrate	Electrodes	E [V m^{-1}]	Actuation[c)]	Ref.
Bimorph	$L = 20$ mm	PVDF	none	–	1.1	$\delta = 1$ mm $F_{bl} = 0.004$ mN	[350]
Bimorph	$L = 40$ mm	PVDF	none	–	13.3	δ = 18 mm (3 Hz)	[354]
Bimorph	$L = 45$ mm	PVDF	none	PEDOT:PSS	30.3	δ = 16 mm	[355]
Bimorph	$L = 60$ mm	PVDF	none	Ag, Al	3.7	$\delta = 0.3$ mm	[356]
Unimorph	$L = 6$ mm	PVDF	Ni-Fe alloy	–	6.4	$\delta = 0.16$ mm	[358]
Unimorph	$L = 53$ mm	PVDF	PI	Metal, CP	40	$\delta = 10$ mm	[357]
Plate	35 × 35 mm	PVDF	none	Cu	3.7	$\Delta = 0.00202$ mm	[161]
Unimorph	$L = 40$ mm	P(VDF-TrFE)	PC	Ag	20–40	$\delta = 0.02$ mm $F_{bl} = 2.8$ mN	[365]
Unimorph	$L = 15$ mm	P(VDF-TrFE)	PET	Ag	44.4 11.1	$\delta = 0.145$ mm $\delta = 0.3$ mm (160 Hz)	[366]
Unimorph	$L = 11$ mm	P(VDF-TrFE) $N = 5$	P(VDF-TrFE)	Al	6.7 0.7	δ = 0.015 mm δ = 0.056 mm (225 Hz)	[364]
Unimorph diaphragm	$D = 10$ mm	P(VDF-TrFE)	PET	Ag	8.3	$\delta = 0.0015$ mm (5.8 kHz)	[366]
Unimorph diaphragm	$D = 100$ mm	P(VDF-TrFE)	Si	Au	25	$\delta = 0.02$ mm	[367]
Unimorph diaphragm	2.2 × 2.2 mm	EI-P(VDF-TrFE) $N = 2$	PVDF	Au	90	$\delta = 0.08$ mm	[369]
Unimorph	$L = 22$ mm	EI-P(VDF-TrFE)	–	Au	65	–	[215]
Unimorph diaphragm	4.5 × 1 mm	EI-P(VDF-TrFE)	P(VDF-TrFE)	Au	135	$\delta = 0.06$ mm	[370,371]

[a)] L is the length of the bender and D is the diameter of the diaphragm. [b)]Number of layers (only given if $N > 1$). [c)] δ is the displacement of the actuator (quasi-static operation unless specified otherwise) and F_{bl} is its blocking force.

Table 7. Constituent materials and performance of PVDF terpolymer actuators.

Configuration	Size[a)]	Active layer[b)]	Substrate	Electrodes	E [V μm^{-1}]	Actuation[e)]	Ref.
Tubular	$L = 30$ mm	P(VDF-TrFE-CFE)	none	Al or CPS[c)]	100	$\delta = 1.2$ mm F_{bl}=1300 mN	[228]
Unimorph	$L = 10$ mm	P(VDF-TrFE-CFE) $N = 2$	Scotch tape	MWCNTs/ silicone	50	$\delta = 3$ mm $F_{bl} = 2.5$ mN	[373]
Unimorph	$L = 10$–20 mm	P(VDF-TrFE-CTFE)	PEN	PEDOT:PSS	100	$\delta = 0.014$ mm	[225]
Unimorph	$L = 41$ mm	P(VDF-TrFE-CTFE)	PET	Au	20	$\delta = 1.706$ mm	[230]
Unimorph	$L = 63$ mm	P(VDF-TrFE-CTFE)	PI	Al	15	$\delta = 1.6$ mm $\delta = 1.8$ mm $F_{bl} = 2.4$ mN (film) $F_{bl} = 1.5$ mN (fibers)	[231]
Unimorph	$L = 45$ mm	P(VDF-TrFE-CTFE)	PI	CB/PDMS	25	$\delta = 5.14$ mm $F_{bl} = 0.4$ mN (fibers)	[374]
Unimorph	$L = 18$ mm	P(VDF-TrFE-CTFE)	PET-based	CB	–[d)]	$\delta = 0.206$ mm $\delta = 3$ mm (110–130 Hz)	[240]
Unimorph	$L = 18$ mm	P(VDF-TrFE-CTFE)	PEN	Ag	60	$\delta = 0.759$ mm $\delta = 5.95$ mm (52 Hz)	[239]
Unimorph	$L = 18$ mm	P(VDF-TrFE-CTFE)	PET-based	Ag	43.1 31.3	$\delta = 0.224$ mm $\delta = 1.72$ mm (114 Hz)	[242]
Unimorph	$L = 40$	P(VDF-TrFE-CTFE)	PET	Au	40	$\delta = 3.25$ mm $F_{bl} = 1$ mN	[120]
Unimorph	$L = 18$ mm	P(VDF-TrFE-CTFE)	PET-based	CB	31.5 30	$\delta = 0.179$ mm $\delta = 2$ mm (107 Hz)	[243]
Unimorph	$L = 18$ mm	P(VDF-TrFE-CTFE) $N = 2$	PET-based	CB	44 40	$\delta = 0.34$ mm $\delta = 3.7$ mm (104 Hz)	[243]
Unimorph	$L = 30$ mm	P(VDF-TrFE-CTFE)	Scotch tape	Ag	50	$F_{bl} = 3$ mN	[372]
Unimorph	$L = 30$ mm	P(VDF-TrFE-CTFE) $N = 6$	Scotch tape	Ag	50	$F_{bl} = 26$ mN	[372]
Unimorph diaphragm	85 mm × 60 mm	P(VDF-TrFE-CTFE)	PET	ITO, PEDOT: PSS	20	$\delta = 0.0024$ mm (220 Hz)	[377]
Unimorph diaphragm	85 mm × 60 mm	P(VDF-TrFE-CTFE) $N = 2$	PET	ITO, PEDOT: PSS	25	$\delta = 0.0033$ mm (220 Hz)	[377]
Unimorph diaphragm	7 mm × 7 mm	P(VDF-TrFE-CTFE) $N = 12$	P(VDF-TrFE-CTFE)	Al	32	$\delta = 0.009$ mm	[376]

[a)] L is the length of the bender. [b)]Number of layers (only given if $N > 1$). [c)]Conductive polymer solution. [d)]300 V excitation. [e)] δ is the displacement of the actuator (quasi-static operation unless specified otherwise) and F_{bl} is its blocking force.

Table 8. Constituent materials and performance of modified PVDF-based actuators.

Configuration	Size[a)]	Active layer[b)]	Substrate	Electrodes	E (V μm^{-1})	Actuation[c)]	Ref.
Unimorph	$L = 17.5$ mm	CB/P(VDF-TrFE-CTFE)	Cu foil	Cu, Ag	12	$\delta = 0.248$ mm (13 Hz)	[233]
Unimorph	$L = 35$ mm	Ag NWs/P(VDF-TrFE-CTFE)	PET	ITO, PEDOT:PSS	25	$F_{bl} = 2$ mN	[302]
Unimorph	$L = 40$ mm	MWCNTs/PVDF (fibers)	PET	Ag	4	$\delta = 0.024$ mm (200 Hz)	[299]
Unimorph	$L = 40$ mm	DEHP/P(VDF-TrFE-CTFE)	PET	Au	40	$\delta = 6$ mm $F_{bl} = 2.5$ mN	[120]
Tubular	$L = 65$ mm	DEHP/P(VDF-TrFE-CTFE)	none	Carbon, Au	60	–[d)]	[379]
Tubular	$L = 60$ mm	DINP/P(VDF-TrFE-CFE)	none	Carbon, Au	5–50	–	[237]
Stack	$D = 13$ mm	DINP/P(VDF-TrFE-CFE) $N = 8$	Glass	Au	20	$\delta = 0.01$ mm	[378]
Unimorph diaphragm	$D = 40$ mm	DINP/P(VDF-TrFE-CFE) $N = 5$	Glass	Au	15	$\delta = 0.003$ mm	[234]
Diaphragm	5 × 5 mm	DEHP/P(VDF-TrFE-CFE)	none	Au	15	–	[329]
Unimorph	$L = 45$ mm	P(VDF-TrFE)/P(VDF-TrFE-CFE)	PET	Ag NWs, Au	110	$\delta = 0.471$ mm	[336]
Tubular	$L = 40$–45 mm	P(VDF-CTFE)/P(VDF-TrFE-CFE) $N = 2$	none	Al	60	$\delta = 0.5$ mm $F_{bl} = 1100$ mN	[380]

[a)] L is the length of the bender and D is the diameter of the diaphragm. [b)]Number of layers (only given if $N > 1$). [c)] δ is the displacement of the actuator (quasi-static operation unless specified otherwise) and F_{bl} is its blocking force. [d)]Bending angle of 85°.

poly(3,4-ethylenedioxythiophene)-poly(styrenesulfonate) (i.e., PEDOT:PSS) electrodes on PVDF films (28 μm thickness) and epoxy glues (3–8 μm thickness) to bond the two sheets together. The 45 mm long actuators produced maximum deflections of up to 16 mm (850 V excitation, i.e., 30.3 V μm^{-1}) and were further creased and folded to realize bellows actuator.

Pérez et al. proposed the use of a PVDF bimorph actuator to steer a laser beam.[348] Their actuator consisted of two commercial metalized PVDF films (52 μm thickness) glued together using a conductive Ag epoxy resin. The actuator was able to deflect a 0.16 g mirror by $\pm 5 \times 10^{-6}$ rad upon a ±15 V stimulus.

Liu et al. proposed to use PVDF actuators for driving solar sails and made a 20 cm diameter sail demonstrator that was deformed by eight PVDF actuators (6 × 2 cm).[356] PVDF films (160 μm thickness) were solution-casted, stretched, coated with Ag on both sides, and poled. Bimorph actuators were formed by bonding two of these films together (Al foil in between) and then attached to a Kapton sail. Up to 0.3 mm sail displacements were measured upon a 600 V stimulus.

5.1.2. Unimorphs

Unimorph actuators are simpler in structure than bimorphs, as explained in Section 2.2.2. In 1980, Sato et al. investigated a unimorph-based deformable mirror system, made by bonding an electroded 32 μm thick PVDF membrane on the back of a 120 μm thick mirror.[359] Triangular and rectangular actuators were operated at up to 30 V μm^{-1} and 200 Hz excitation to alter the wavefront of the light.

Unimorphs were further studied in mid-2000s, when Fu et al. proposed fabricating unimorph PVDF actuators from commercial 28 μm-thick metallized PVDF membranes.[358] PVDF sheet was cut into samples (6 mm by 1 mm) and one electrode of each sample was electroplated with a 5 μm permalloy (Ni-Fe) layer to produce the passive layer of the unimorph. The resulting actuators achieved maximum tip deflections of up to 160 μm upon 180 V driving voltage (i.e., 6.4 V μm^{-1}).

Chen et al. studied manufacturing actuators from both the solution-cast and melt-pressed PVDF films of 25 μm thickness.[357] The stretched and poled samples were coated with metal and conductive polymer electrodes (respectively via sputter-coating and screen-printing) and bonded on a polyimide (PI) substrate using an epoxy resin. The resulting unimorph cantilevers (length 5.3 cm) exhibited up to 1 cm displacements (40 V μm^{-1}) and were used to actuate a membrane reflector of 0.2 m diameter.

Zhang et al. proposed multilayer PVDF actuators for active vibration control of curved surfaces.[360,361] Up to five layers of PVDF patches (200 μm each) were bonded on one end of a thin elastic cylinder. Vibrations were applied in the middle of the cylinder and active control was reported to effectively attenuate three vibration modes in closed-loop operation.

5.2. P(VDF-TrFE)

Among PVDF copolymers, actuation applications have only employed P(VDF-TrFE). Edqvist et al. fabricated P(VDF-TrFE) multilayer unimorph actuators by recursively spin-coating thin copolymer films (2–10 μm) and depositing Al electrodes on different flexible substrates.[362–364] The 11 × 2 mm cantilevers showed quasi-static and resonant deflections of up to 15 μm (20 V) and 56 μm (2 V, 225 Hz), respectively.[364] A locomotion unit (10 × 10 mm) was built from three of such actuators, demonstrating motion in different directions at speeds of up to 730 μm s^{-1} (32 V square wave, 540 Hz) and carrying more than 9× of its own weight (40 V, 13 V μm^{-1}).

Pabst et al. fabricated bending unimorph actuators comprising of a polycarbonate (PC) substrate, a sputter-coated Ag bottom electrode, an inkjet-printed P(VDF-TrFE) active layer (5–10 μm thickness) and an inkjet-printed Ag top electrode.[365] After prost-processing (thermal annealing for 60 min at 140 °C, sintering the Ag ink in Ar plasma), the 4 cm long actuator showed tip deflections of 20 μm and blocking forces of 2.8 mN (200 V excitation).

In a later study, Pabst et al. developed a process for fully inkjet-printing P(VDF-TrFE) unimorph cantilevers and membrane actuators.[366] The Ag bottom electrodes were printed on polyethylene terephthalate (PET) substrates and sintered in Ar plasma. Printing the EAP layer (9 μm in thickness) and the top electrode followed a similar procedure to their earlier study.[365] The 1.5 cm long cantilever actuators exhibited quasi-static and dynamic tip displacements of 145 μm (400 V, i.e., 44.4 V μm^{-1}) and 0.3 mm (100 V, 11.1 V μm^{-1}, 160 Hz), respectively. The membrane actuators of 10 mm diameter showed resonant deflections of up to 1.5 μm (75 V, 5.8 kHz, operated in air) and were proposed for lab-on-chip micropump applications.[366]

Patterson and Pellegrino investigated using P(VDF-TrFE) for actuating lightweight deformable mirrors.[367] The actuator was formed by spin-coating the P(VDF-TrFE) layer (20 μm thickness) on a metalized (Ti/Au/Ti) silicon substrate and sputter-coating the other electrode (Ti/Au). Shadow masks were used to pattern one of the electrode into separate actuation segments, and the EAP layer was poled (50–100 V μm^{-1}). The deformable mirror was able to produce peak-to-valley deflections of 20 μm (25 V μm^{-1}).

Similarly, Wang et al. employed P(VDF-TrFE) for activating their spherical adaptive reflectors.[114,368] PET substrates were sputter-coated with Al to form a keystone pattern of bottom electrode segments, and a thin P(VDF-TrFE) film (4–5 μm) was applied using either spin-coating or spray-coating method, using a P(VDF-TrFE) solution in methyl ethyl ketone (MEK) and methyl isobutyl ketone (MIBK). After annealing (140 °C) and poling (5–62 V μm^{-1}), Al was sputtered on the EAP to form the top electrode, and on the other side of the PET layer to form the reflective mirror (**Figure 8**a). Samples with spin-coated EAP layer displayed a ≈24% higher ε_r and a ≈ 8% higher d_{31} than the samples that were made by spray-coating.

5.3. Electron-Irradiated P(VDF-TrFE)

Electron-irradiated P(VDF-TrFE) (aka EI-P(VDF-TrFE)) films have been employed as active layers in unimorph diaphragm actuators[369–371] and bending cantilevers.[215] Xia et al. utilized EI-P(VDF-TrFE) bilayer unimorph actuators to construct a microfluidic pump.[369] The active bilayer was constructed by sputter-coating Cr and Au electrodes on both sides of two 20 μm-thick electron-irradiated P(VDF-TrFE) films, and gluing them together. The resulting bilayer was further bonded on a passive PVDF membrane, completing the unimorph actuator of the membrane pump. The 2.2 × 2.2 mm membranes deflected by up to 80 μm (90 V μm^{-1}) in air. The respective pump produced

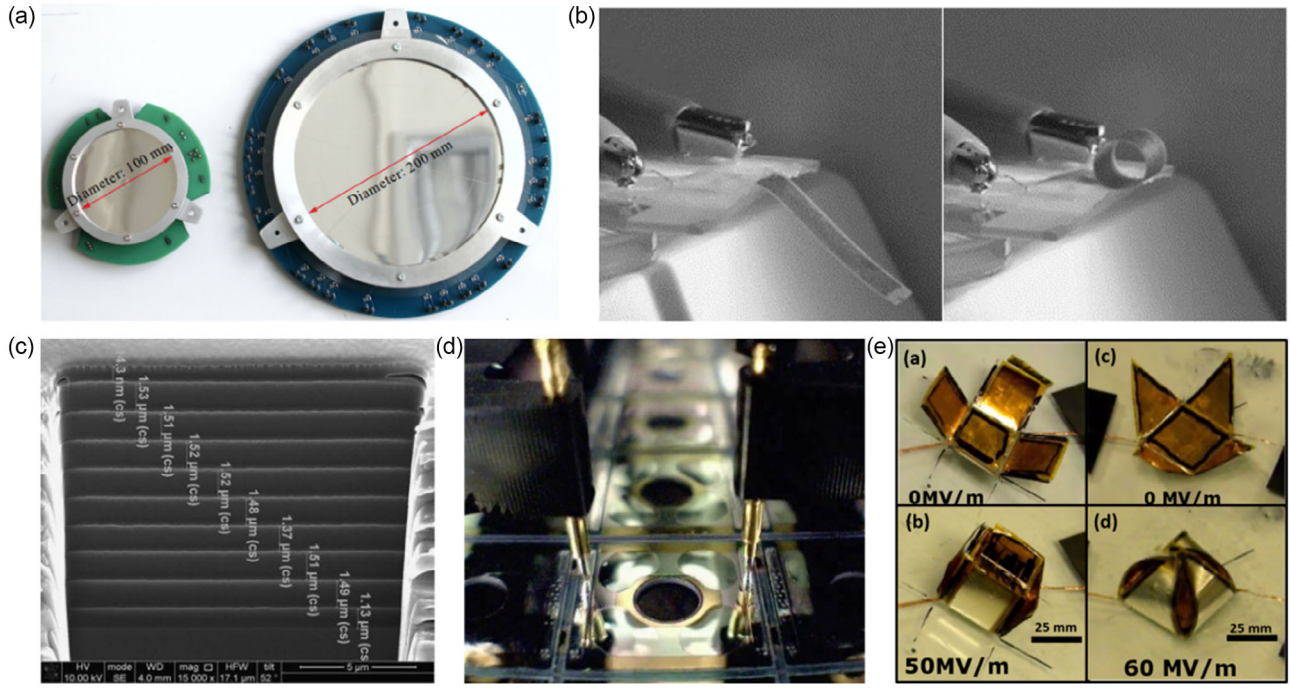

Figure 8. Actuators basing on PVDF co- and terpolymers: a) Wang et al. proposed to use P(VDF-TrFE) in adaptive shell spherical reflectors. Reproduced under CC-BY 4.0 license from.[114] b) Actuation of an EI-P(VDF-TrFE) bending unimorph actuator. Reproduced with permission.[215] Copyright 2001, Elsevier. c) Cross section and d) operation of a multilayer P(VDF-TrFE-CTFE) diaphragm actuator with 12 active layers and Al electrodes. Reproduced with permission.[376] Copyright 2013, Elsevier. e) Self-folding cube and pyramid structures that are actuated by P(VDF-TrFE-CTFE) unimorph actuators. Reproduced with permission.[372] Copyright 2017, Elsevier.

flow rates of up to 25 µml mi^{-1}n and static pressures of up to 350 Pa (63 Hz).[369]

Cheng et al. fabricated bending unimorph actuators by sputter-coating Au electrodes on stretched and electron-irradiated P(VDF-TrFE) layers (22 µm thickness) and bonding them to polymeric substrates of equal thickness.[215] Transverse strains (S_1) of up to 1.7% were produced upon 65 V µm^{-1} excitation, causing the actuator tip to bend by a full turn (see Figure 8b).

Similarly, Xu et al. fabricated unimorph membrane actuators (4.5 × 1 mm) by sputtering Au electrodes on 10 µm thick irradiated and stretched P(VDF-TrFE) films and epoxy bonding (1 µm layer thickness) them on passive layers of the same material and thickness.[370,371] With both ends fixed to a silicon substrate, the membranes achieved maximum deflections of 60 µm in air (135 V µm^{-1}, 10 Hz). Operating in silicone oil caused a slight decrease in actuation magnitude and reduced resonance frequency from 86 kHz (in air) to 13.2 kHz.[371]

5.4. Terpolymers

P(VDF-TrFE-CFE) and P(VDF-TrFE-CTFE) terpolymers have been employed in unimorph cantilever,[39,225,230,231,239–243,372–375] unimorph diaphragm,[235,376,377] and tubular[228] actuators, as summarized in Table 7.

Levard et al. used P(VDF-TrFE-CFE) films to build tubular actuators for Braille displays.[228] Terpolymer films were solution-cast, annealed, uniaxially drawn, and poled. Both sides of the films were coated with conductive polymer or Al electrodes, and two sheets were laminated together, and further rolled up and bonded. The resulting tubular actuators exhibited displacements and blocking forces of up to 1.2 mm and 1.3 N (100 V µm^{-1}), respectively.

Choi et al. proposed an adhesion-mediated film transfer (AMFT) technique to deposit thin P(VDF-TrFE-CTFE) layers (1 to 1.5 µm) on glass substrates, using silicone elastomer support layer and water for film separation.[376] Multilayer unimorph diaphragm actuators were fabricated by laminating 5 µm thick substrate of the same terpolymer on a Si wafer, further recursively sputter-coating Al electrodes and laminating the P(VDF-TrFE-CTFE) films on it, and finally exposing the diaphragm actuator via deep-reactive ion etching. The 12-layer unimorph actuators (Figure 8c,d) attained quasi-static deflections of 9 µm (40 V excitation) and allowed to vary optical power of a vari-focal liquid-filled microlens over 50 diopters.

Ju et al. employed the AMFT technique to manufacture P(VDF-TrFE-CTFE) unimorph membrane actuators for vibrotactile interfaces.[377] The resulting terpolymer films (4 and 8 µm in thickness) were laminated at 110 °C on ITO-covered PET substrates (188 µm thick) and spray-coated with PEDOT:PSS for top electrodes. Single- and double-layer membrane designs (85 × 60 mm) were manufactured, achieving maximum resonant deflections of up to 2.4 µm (220 Hz, 20 V µm^{-1}, 8 µm thick EAP) and 3.3 µm (220 Hz, 25 V µm^{-1}, 4 µm thick EAP), respectively.

Kadooka et al. studied multilayer unimorph actuators basing on P(VDF-TrFE-CFE).[373] A pneumatic dispenser system was used to deposit the layers of EAP (10 µm) and MWCNTs/silicone

composite electrodes (10–15 μm). Stacks of 2 to 10 active layers were applied on glass substrates and transferred to scotch tape (passive layer) to form 10 × 10 mm unimorphs. The 2- and 10-layer samples respectively produced F_{bl} of up to 2.5 and 20 mN (50 V μm^{-1}), and tip displacements of up to 3 and 0.9 mm.

Liu et al. manufactured unimorph cantilever actuators in their study on annealing of P(VDF-TrFE-CTFE).[230] 60 μm thick terpolymer membranes were solution-cast, annealed under different conditions, sputter-coated with Au electrodes, and attached to 100-μm-thick PET substrates using an adhesive tape. The 41 mm long annealed actuators (90 °C, 1 h) displayed maximum tip displacements δ of 1.706 mm (20 V μm^{-1}), performing significantly better than the 0.823 mm in unannealed samples.

Ahmed et al. studied P(VDF-TrFE-CTFE) unimorph actuators basing on paper and scotch tape substrates and used them in self-folding structures (Figure 8e).[372] The 35-μm thick EAP films were solution-cast and annealed, sputtered with Ag electrodes, and laminated both on paper ($Y = 5.5$ GPa) and scotch tape (1.6 GPa) substrates. Both cantilever types curled into a full loop, whereas the scotch tape actuators achieved this at lower field strengths (up to 80 V μm^{-1}). Multilayer unimorph actuators were also constructed employing a similar manufacturing process.[372] The six-layer samples (3× 1 cm) produced blocking forces of up to 26 mN (50 V μm^{-1}), providing a 8.7× higher forces and 1.5× lower displacements than the monolayer transducers and were further used to actuate paper origami structures (butterfly, catapult, and barking dog).

Lheritier et al. screen-printed 1.2–4 μm thick P(VDF-TrFE-CTFE) films and PEDOT:PSS electrodes on 125-μm-thick PEN substrates to form unimorph actuators.[225] The 1–2 cm long actuators produced tip deflections of up to 14 μm (100 V μm^{-1}), while the actuator efficiencies remained <0.01.

Baelz and Hunt produced unimorph cantilever actuators by inkjet-printing carbon black electrodes and spin-coating P(VDF-TrFE-CTFE) on 140-μm-thick PET-based substrates.[240,241] The 18 mm long annealed and poled actuators produced 206 μm quasi-static (300 V) and 3 mm resonant (115 Hz) displacements.

Sekar and Hunt developed a process for fully inkjet-printing similar actuators (using Ag for electrodes), and their 18 × 3 mm cantilevers attained maximum quasi-static and resonant deflections of up to 224 μm (275 V) and 1.72 mm (200 V, 114 Hz), respectively.[242]

Gallucci et al. combined inkjet-printing (Ag electrodes) and stencil-printing (P(VDF-TrFE-CTFE) layer) to manufacture unimorph cantilevers (18 × 3 mm) on both PET-based (140 μm) and PEN (polyethylene naphthalate, 50 μm) substrates.[239] P(VDF-TrFE-CTFE) layer thicknesses of 5–24 μm were studied, and the actuators exhibited up to 759 μm quasi-static (560 V) and 5.95 mm resonant (550 V, 52 Hz) displacements.

IJssel de Schepper and Hunt developed an automated airbrush 3D printer and used it to print single- and dual-layer P(VDF-TrFE-CTFE) unimorph actuators (18 × 4 mm) with CB electrodes (≈1 μm) on PET-based substrates.[243] The single-layer actuators (20 μm EAP thickness) produced maximum quasi-static and resonant displacements respectively of 179 μm (630 V) and 2 mm (600 V, 107 Hz). Dual-layer actuators (10 μm EAP thickness) showed higher deflections at lower activation voltages (**Figure 9**), reaching up to 340 μm (440 V) and

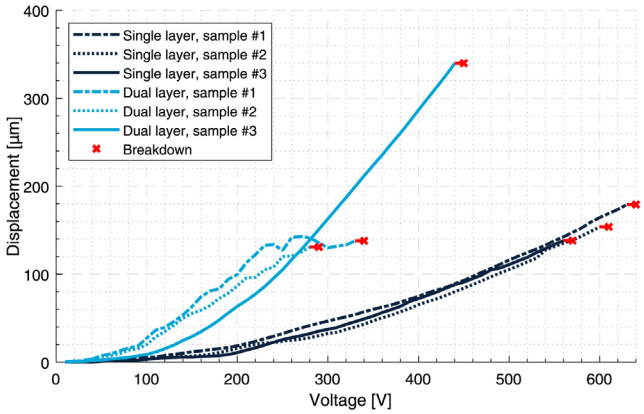

Figure 9. Spray-printed dual-layer P(VDF-TrFE-CTFE) unimorph cantilever actuators exhibiting higher displacements than single-layer counterparts. Reproduced under CC-BY 4.0 license from.[243]

3.7 mm (104 Hz, 400 V) in quasi-static and dynamic operation, respectively.

D'Anniballe et al. proposed P(VDF-TrFE-CTFE) unimorph actuators basing on electrospun aligned nanofiber mats, and compared them against melt-extruded P(VDF-TrFE-CTFE) film actuators.[231] Both the electrospun mats and melt-extruded films (50–80 μm thickness) were produced, sandwiched between aluminum tape, and laminated on a PI (polyimide, thickness 57-μm) substrate. The 63 mm long nanofiber- and film-based actuators (thickness 50 μm, 15 V μm^{-1}) respectively produced maximum tip deflections of 1.8 and 1.6 mm. Maximum forces of 1.5 mN (80 μm nanofiber mat) and 2.4 mN (60 μm film) were reported.

In a follow-up study, D'Anniballe et al. filled the nanofiber mat cavities with PDMS (polydimethylsiloxane) to improve dielectric strength[374,375] and used conductive CB/PDMS composite for the electrodes to improve actuator flexibility. The resulting 45 mm long actuators achieved maximum deflections of 5.14 mm (25 V μm^{-1}) and blocking force of up to 0.4 mN.[374]

Van Duong et al. investigated the performance of microfluidic pumps based on P(VDF-TrFE-CFE) unimorph diaphragms.[235] The unimorph actuators were fabricated by sputter-coating the EAP films with Au electrodes and laminating them onto a PET membrane. Under 600 V sinusoidal excitation (0.5 Hz), the pumps achieved a silicon oil column height of up to 678 μm.

5.5. Composites and Blends

A number of studies have employed PVDF-based polymer matrix composites (Section 5.5.1) and blends (Section 5.5.2) to construct functional actuators, as summarized in Table 8. These can be broken down into bending unimorph cantilevers[120,233,299,302,331,336] and diaphragms,[234,235] dilating diaphragms,[329] stacks,[378] and tubular[237,379,380] configurations.

5.5.1. Composites

Tu et al. fabricated unimorph bending cantilever actuators basing on CB/P(VDF-TrFE-CTFE).[233] 8 μm thick CB/P(VDF-TrFE-CTFE) layers were solution-cast on 12-μm copper foils, annealed,

and further coated with 0.15 μm thick Ag top electrodes. The 17.5 mm long actuators achieved resonant tip displacements of up to 248 μm (13 Hz) upon 12 V μm^{-1} electric field.

Sharafkhani and Kokabi manufactured bending unimorph actuators basing on MWCNTs/PVDF composite nanofibers.[299] Rectangular nanofiber mats (40 × 15 × 0.1 mm) were electrospun, coated with Ag paste on both sides to form electrodes, and attached on flexible Al substrates. The finished actuators exhibited tip displacements of up to 24 μm upon 4 V μm^{-1} excitation.

Fook et al. introduced Ag NW interlayer into P(VDF-TrFE-CTFE) unimorph actuators.[302] The actuators were fabricated by doctor-blading the P(VDF-TrFE-CTFE), Ag NW ink and another P(VDF-TrFE-CTFE) layers on ITO-coated PET substrates (125 μm), and further depositing PEDOT:PSS top electrodes. The 25 × 35 mm actuators with a 10 μm thick active layer produced a blocking force of up to 2 mN (25 V μm^{-1}).

5.5.2. Blends

Le et al. employed 50 μm DEHP/P(VDF-TrFE-CFE) films with sputter-coated Au electrodes to form diaphragm actuators for microfluidic pumps (**Figure 10**).[329] The micropumps were reported to attain flow rates of up to 8 μl min^{-1} and back pressures of up to 250 Pa (15 V μm^{-1}, 1 Hz).

Della Schiava et al. sputter-coated thin DEHP/P(VDF-TrFE-CTFE) films with Au electrodes and laminated them on PET substrates (adhesive tape and pressing), forming bending unimorph actuators (**Figure 11**).[120] The 40 mm long actuators (25 μm EAP) attained up to 6 mm tip displacements (0.1 Hz, 40 V μm^{-1}) and 2.5 mN blocking forces (2.5× higher than pure terpolymer actuators at the same field), while the breakdown strength was reported to deteriorate with increasing EAP layer thickness (25 to 60 μm) and remained lower than in pure terpolymer.

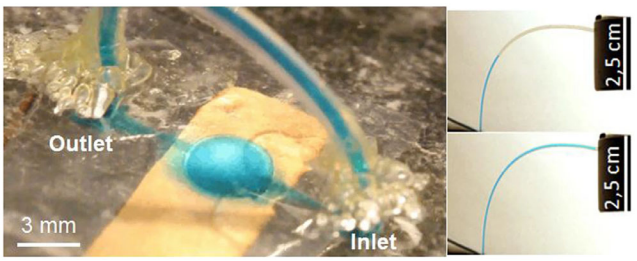

Figure 10. A diaphragm micropump that is driven by a DEHP/.P(VDF-TrFE-CFE) actuator. Reproduced under CC-BY 4.0 license from.[329]

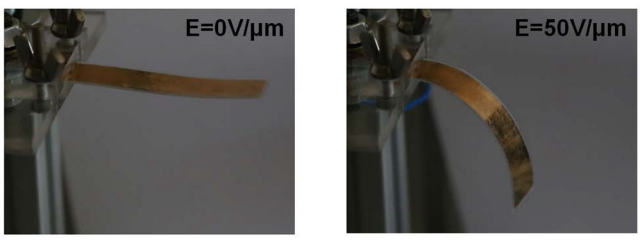

Figure 11. Operation of a DEHP/.P(VDF-TrFE-CTFE) bending unimorph cantilever actuator. Reproduced under CC-BY 4.0 license from.[120]

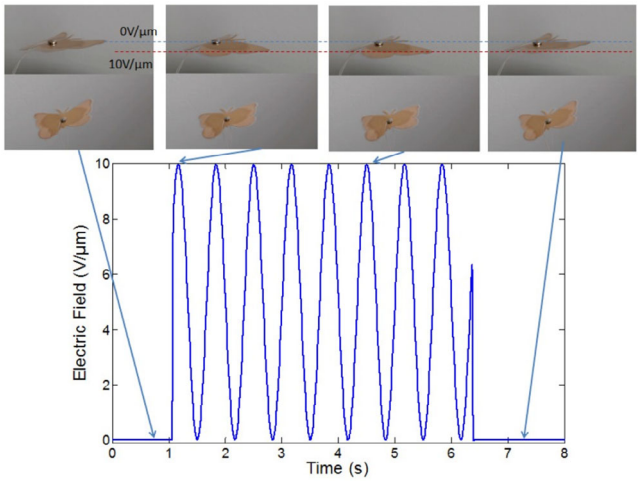

Figure 12. Butterfly-shaped structure are activated by DINP/P(VDF-TrFE-CTFE) transducers. Reproduced with permission.[331] Copyright 2017, Wiley Periodicals, Inc.

DINP/P(VDF-TrFE-CTFE) actuators have been proposed to make butterfly-shaped morphing structures, as shown in **Figure 12**.[331] An EAP layer was sandwiched between Au electrodes (sputter-coated) and glued on a PET substrate. The butterfly-shaped actuators were demostrated to mimic flapping motion in response to 10 V μm^{-1} stimulation at ≈1.5 Hz.

PVDF terpolymer blends with DEHP and DINP have been proposed for smart guidewire applications in endovascular surgery.[237,379] Ganet et al. constructed smart guidewires of 1.4 mm diameter by melt-extruding hollow tubular DEHP/P(VDF-TrFE-CTFE) structures, filling them with carbon grease for central electrodes, and sputter-coating two semicircular Au electrodes on the outer surfaces.[379] Activating opposite actuator segments allowed to bend the guidewires in opposite directions, and 65 mm long samples showed 85° bending angles upon 60 V μm^{-1} excitation. Della Schiava et al. based on the same design to make a DINP/P(VDF-TrFE-CFE) guidewire with improved biocompatibility.[237] Under 25 to 50 V μm^{-1} excitation a 60 mm long guidewire was visually confirmed to bend.

Thetpraphi et al. fabricated multilayer actuators basing on 10 wt% DINP/P(VDF-TrFE-CFE) blends (Section 4.3.1) by solution-casting 200–250 μm thick EAP films, sputtering them with Au electrodes, and bonding them into multi-layer stacks.[234,378] These actuators were then used for deforming optical surfaces in longitudinal[234,378] and shear[234] configurations. In longitudinal mode, a single eight-layer actuator deformed a 3 mm thick glass sheet by up to 10 μm (20 V μm^{-1}),[378] and a four-actuator design was further demonstrated effective in altering the surface deformation profile.[234] In shear configuration, a five-layer actuator (4 cm diameter) produced up to 3 μm (15 V μm^{-1}) out-of-plane deformations in a 2 mm thick glass sheet.[234]

Lu et al. fabricated core-free tubular actuators of P(VDF-CTFE)/P(VDF-TrFE-CFE) blends for activating Braille display.[380] Two sheets of 4 wt% P(VDF-CTFE) blend were solution-cast, mechanically stretched (4 to 6 μm net layer thickness), coated with Al electrodes, laminated together, annealed thermally and rolled into tubes. The resulting 40–45 mm long actuators (2.2 mm diameter)

produced displacements of up to 0.5 mm and forces of up to 1.1 N upon 300 V excitation.

Van Duong et al. studied unimorph bending cantilever actuators basing on P(VDF-TrFE)/P(VDF-TrFE-CFE) blends.[336] The 45 × 5 mm actuators were fabricated by coating 130 µm PET substrates with Ag NWs to form bottom electrodes, laminating 3.6 µm thick EAP films (20 wt% P(VDF-TrFE) content) on them, and sputtering Au to form the top electrodes. The resulting actuators produced up to 0.47 mm tip displacements (110 V µm^{-1}, 0.1 Hz), an improvement of up to 16.5% over the neat terpolymer samples. The same EAP was further used to build a pressure-responsive vibrotactile device (5 µm thick EAP) that is activated by touch and produces vibrational stimulus on a human fingertip. The device produced quasi-static and dynamic deformations of 3.5 µm (1 Hz) and 1 µm (500 Hz), respectively (40 V µm^{-1}).

In a later study, Van Duong et al. employed P(VDF-TrFE)/P(VDF-TrFE-CFE) blends to actuate microfluidic membrane pumps,[235] achieving a silicon oil column height of up to 778 µm (600 V excitation, 0.5 Hz). This resulted in a 14.7% performance increase compared with reference pumps based on pure P(VDF-TrFE-CFE) films (see Section 5.4).

6. Highlights and Perspectives

This section will discuss, compare, and visualize the findings of this review on electromechanical transduction properties of PVDF-based materials (Section 6.1) and the respective actuators and devices (Section 6.2). It summarizes the current state-of-the-art of the field, and provides insights into possible future developments in terms of improving the material performance, actuator design and fabrication.

6.1. Materials

Making versatile actuators from ferroelectric polymers requires the materials to exhibit high strains, high elastic energy density, efficient electromechanical coupling, and low losses (both mechanical and electric).

The maximum strains for all PVDF-based materials are plotted in **Figure 13**, and the highest strains of up to 13.4% have been reported for P(VDF-DB).[39] The maximum strain depends on the electrostrictive coefficient and the applied electric field ($S_{max} = ME^2_{max}$), the latter being constrained by the dielectric breakdown strength (E_b).

The electrostrictive coefficient is further proportional to the compliance (i.e., $1/Y$) and dielectric permittivity ($\varepsilon = \varepsilon_0\varepsilon_r$), as described by Equation (19). This relationship is illustrated in **Figure 14**, indicating incremental improvement by an order of magnitude between PVDF, copolymers, terpolymers, composites, and blends.

The electromechanical coupling coefficients (k_{33} and k_{31}) indicate the efficiency in converting the electrical energy into mechanical output, commonly estimated for quasi-static operation. Identical values of up to 0.88 have been reported for P(VDF-TrFE-CFE-FA),[40] P3HT-PMMA@SWCNTs/P(VDF-TrFE), and TiO_2/PVDF,[286,304] while typical values remain between 0.1 and 0.65 (see Table 1, 2, 3, 4, and 5).

Elastic energy densities of the reviewed materials are plotted against the respective driving field strengths in **Figure 15**, with the highest values of up to 11.3 and 3.1 J cm^{-3} being reported for TiO_2/PVDF[286] and P(VDF-DB),[39] respectively. While high energy densities typically correlate with high activation field strengths (see Figure 15), it is possible attain high energy densities at low field strengths by modifying the base materials. Energy density depends linearly on the Young's modulus and quadratically on the strain of the material ($U_S = 0.5YS^2$), as illustrated in **Figure 16**. In practice, stiffer materials tend to exhibit higher elastic energy density than softer ones, as the material strains are generally limited below 10%.

Some properties of practical significance are rarely studied in the reviewed works, such as power density and reliability. While the power density could be assumed proportional to the energy density, it depends on the operating frequency and is limited by

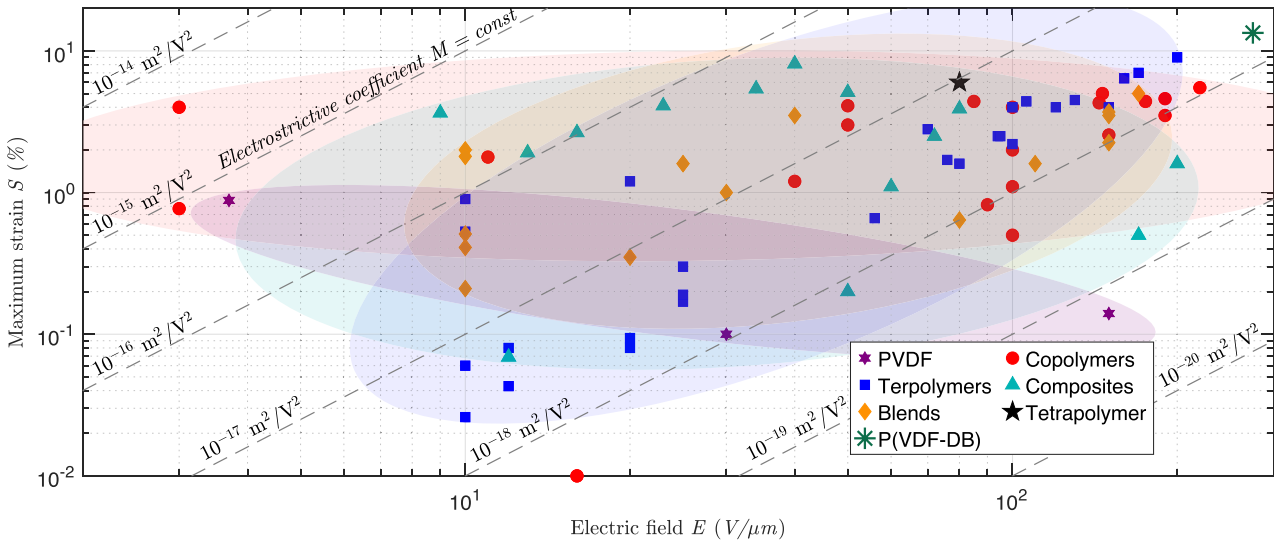

Figure 13. Maximum strain (S) versus driving electric field (E) of PVDF-based actuator materials.

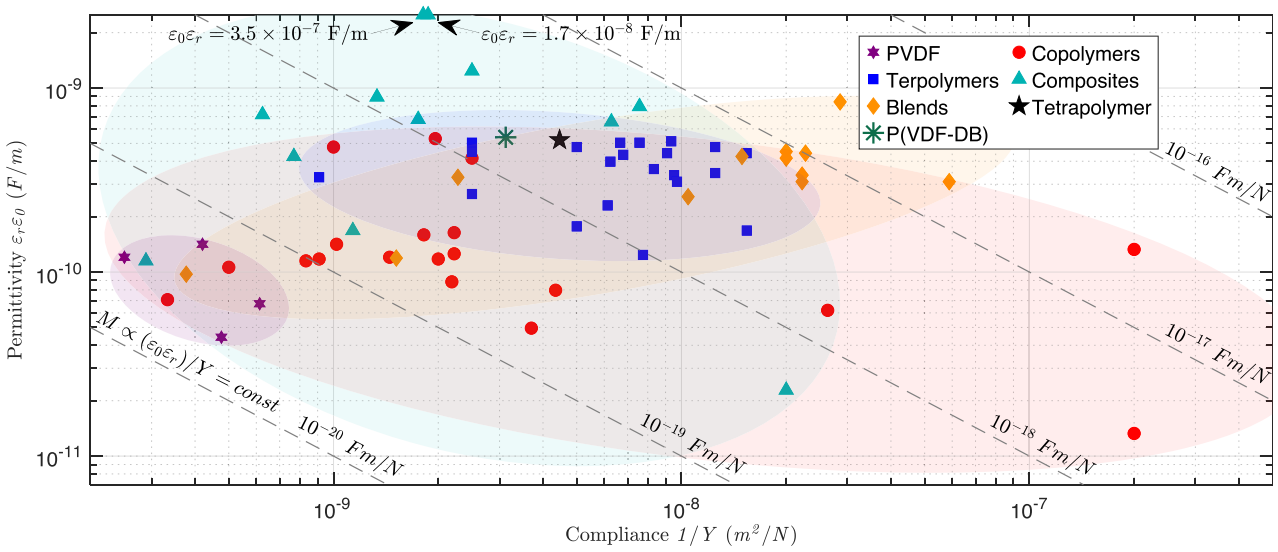

Figure 14. Permittivity ($\varepsilon_0\varepsilon_r$) versus compliance ($1/Y$) of PVDF-based actuator materials.

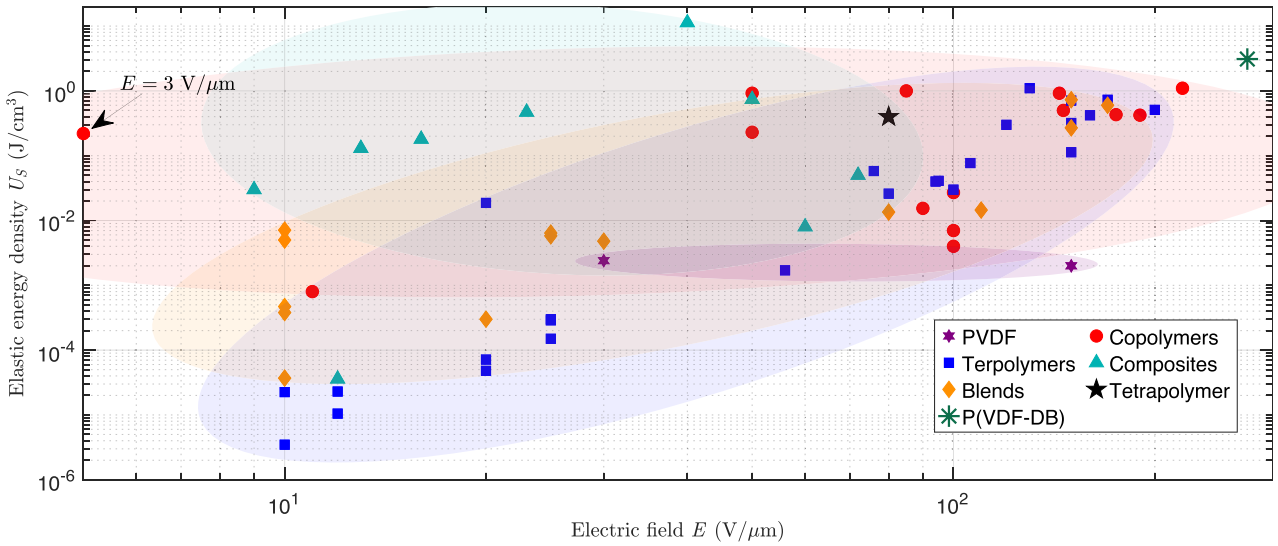

Figure 15. Elastic energy density (U_S) versus driving electric field (E) of PVDF-based actuator materials.

the transduction dynamics (e.g., viscoelastic losses), as has been indicated for the strain, piezoelectric and electrostrictive coefficients, and coupling efficiency.[107,159,215,244] It is further important to study the actuator lifespan and stability of properties (mechanical, electrical, transduction) to guarantee reliable and robust operation.

6.1.1. PVDF

Strong piezoelectric response, mechanical flexibility and a wide commercial availability has led to a wide use of PVDF in sensing and energy harvesting applications.[83,381] In contrast, the pure PVDF polymer is used in limited actuator studies (see Section 5.1), ascribable to the elaborate preparation (stretching and poling), high driving fields, low strains, and energy conversion efficiency (see Table 1). Very limited studies report the strains for PVDF, indicating up to 0.88% at $\approx$3.7 V μm^{-1}.[161] The need for higher electromechanical coupling performance in actuation applications has inspired a number of alterations to develop better-suited materials.

6.1.2. Copolymers

PVDF copolymers, with P(VDF-TrFE) being the most studied, offer significant advantages over PVDF in both ease of processing and performance. P(VDF-TrFE) can crystallize directly into the stable electroactive β-phase without requiring mechanical stretching, although stretching, poling, and annealing steps have

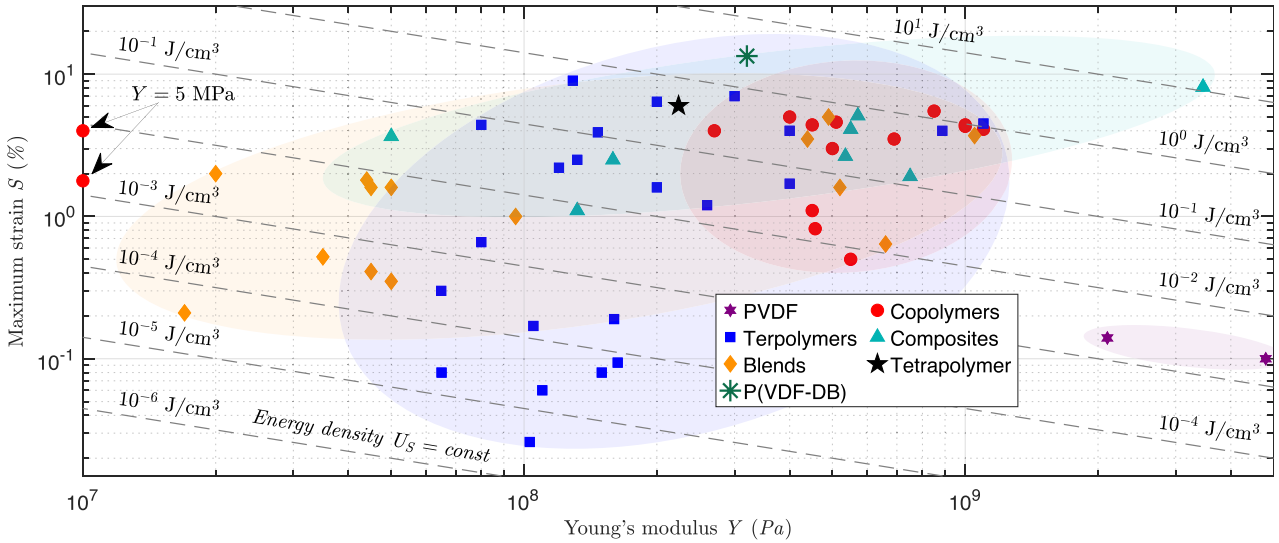

Figure 16. Maximum strain (S) versus Young's modulus (Y) of PVDF-based actuator materials.

been shown to enhance its piezoelctric properties. Additionally, P(VDF-TrFE) exhibits a higher dielectric constant, lower Young's modulus and enhanced piezoelectric coefficients (d_{31} and d_{33}), compared with PVDF (see Table 1). Notably, very high d_{33} values (up to 63.5 pm V^{-1}) can be achieved by optimizing the VDF/TrFE molar ratio, as demonstrated in ref. 176.

Irradiating P(VDF-TrFE) with high-energy electrons and ions promotes RFE behavior, resulting in high transverse and longitudinal electrostrictive strains (S_3 and S_1 up to 5% and 4.4%, respectively). This process requires specialized equipment and has a low yield due to the undesirable damage.

While addressed only in a few reports, PVDF copolymer with CTFE can exhibit strain responses of above 5% and energy densities of above 1 J cm^{-3} (attributable to its high Young's modulus),[191] exceeding both PVDF and P(VDF-TrFE). Converting the CTFE units into CH═CF double bonds (DB) further produces P(VDF-DB) that exhibits relaxor ferroelectric behavior. P(VDF-DB) produces the highest strains ($S_3 > 10\%$) among all the reviewed materials and high energy densities (>3 J cm^{-3}), but requires high field strengths to achieve that (>250 V μm^{-1}).[39]

P(VDF-HFP) exhibits comparable strains (up to 4.1% at 50 V μm^{-1}) the to P(VDF-CTFE) and irradiated P(VDF-TrFE) at three to four times lower field strengths (see Table 1), attributable to its dominantly electrostrictive response.[164] This suggests that significantly higher strains are possible near the E_b (reported at 700 V μm^{-1} in).[199] Electrospun P(VDF-HFP) nanofiber mats produce similar strains to the bulk material at significantly lower driving fields (ca 17x lower E), while the low Young's modulus means reduced energy density (up to 0.22 J cm^{-3} in).[196]

6.1.3. Terpolymers

Similarly to P(VDF-HFP) and irradiated P(VDF-TrFE), PVDF terpolymers with an additional bulky monomer (CTFE, CFE and HFP) exhibit a nonlinear, but significantly stronger electromechanical response than PVDF and P(VDF-TrFE) due to their dominantly electrostrictive behavior (see Section 2.1.2). P(VDF-TrFE-CTFE) has been reported to exhibit the highest strains among terpolymers (S_3 of up to 9% at 200 V μm^{-1}),[188] while P(VDF-TrFE-CFE) exhibits the highest energy densities (1.1 J cm^{-3}) and coupling efficiencies (0.55), attributable to the higher ε_r, E_b, and Y (see Table 2). Both the longitudinal and transverse strain responses of these materials have been extensively studied and have been shown to strongly depend on the synthesis methods, composition, and post-processing.[106,107,188,210,214,224,230] The only study on P(VDF-TrFE-HFP) reported strains of up to 2.8% at 70 V μm^{-1},[221] requiring further investigation into its performance at higher fields similar to other terpolymers (see Table 2).

Additional incorporation of FA monomers into P(VDF-TrFE-CFE) produced P(VDF-TrFE-CFE-FA) tetrapolymer[40] that exhibits similar strains (6% at 80 V μm^{-1}) and higher coupling efficiencies ($k_{33} = 0.88$) than the original terpolymer[214,223,236,337] at significantly lower driving fields. Therefore, tetrapolymer synthesis and characterization is anticipated to produce more high-performing classes of RFE materials.

6.1.4. Composites

Incorporation of piezoceramic fillers into PVDF and its copolymers enhances their crystallinity, dielectric properties (e.g., ε_r up to 181 at 1 kHz in)[283] and piezoelectric response (d_{33} up to 100 pm V^{-1} in).[281] Fabrication of such composites is complicated by the elaborate anti-parallel poling process and results in reduced flexibility due to the high required filler concentrations. Till date, most of the reported studies focus on PZT-based ceramic fillers, and no studies have investigated employing PVDF terpolymers as matrix material (see Table 3).

Ceramic TiO_2 nanofillers in TiO_2/PVDF composites produced exceptionally high strains (S_3 of up to 8.1 at 40 V μm^{-1}), coupling efficiencies (k_{33} of up to 0.88) and energy densities

($11.3\,J\,cm^{-3}$).[286,289] Despite the reduced E_b, the reported U_S is significantly higher than other PVDF-based materials.

Incorporation of other fillers (conductive, metal-organic, and OS particles) in PVDF-based matrices enhances the electroactive phase crystallization and dielectric constant, as explained in Section 4.1. The composites basing on conductive and metal-organic fillers produce high strains at significantly lower electric fields (e.g., S_3 of up to 5.1% at $50\,V\,\mu m^{-1}$,[304] 4.1% at $23\,V\,\mu m^{-1}$,[308] and 1.91% at $13\,V\,\mu m^{-1}$[88]) and retain the mechanical flexibility of the matrix, with SWCNTs/P(VDF-TrFE) also achieving high coupling efficiency of 0.88.[304] However, the maximum strains remain inferior to the pure polymer matrix due to the 4× to 20× decrease in breakdown field strength (see Table 4). Breakdown strength of MWCNTs/PVDF has been shown to improve via mechanical rolling (130 to $340\,V\,\mu m^{-1}$)[305] and insulating encapsulation of MWCNTs (see core-shell structures in Section 4.2.6),[314,315] even beyond the strength of pure PVDF.[311] So far, both approaches have only been studied on the PVDF matrix. Strain and energy density of P(VDF-HFP) nanofiber mats improve upon PANI filler addition respectively by 2× (3.65% at $<12\,V\,\mu m^{-1}$) and 37× ($0.03\,J\,cm^{-3}$),[105] although the energy density remains below the bulk polymer values due to low Young's moduli.[105,196]

6.1.5. Blends

Blending P(VDF-TrFE-CTFE) and P(VDF-TrFE-CFE) with plasticizers (DEHP, DINP, Palamoll 652) results in extreme dielectric permittivity (up to 4800 at 0.1 Hz[224]) and significantly reduced Young's modulus (1.6× to 6×, see Table 5). The high permittivity has been ascribed to the MWS effect and plasticizer seepage,[331] and the improved low-field ($\leq 30\,V\,\mu m^{-1}$) strains are explainable by $M \propto (\varepsilon_r \varepsilon_0)/Y$ (see Section 2.1.2). However, the performance is limited by the reduced breakdown strength (up to 2×[237]) and plasticizer leakage,[331] while the dynamic response has not been studied. The highest strains of 2% (S_3) were reported for DEHP/P(VDF-TrFE-CFE) at low fields of $10\,V\,\mu m^{-1}$[326]), while their energy densities remained two to four orders of magnitude lower than in pure terpolymers (see Table 5).

Contrary to the plasticized polymers, the 2-polymer blends exhibit increased Young's modulus (see Table 5), resulting in enhanced energy densities and coupling efficiencies compared to the pure polymers.[235,236,337] The blends exhibit comparable maximum strains to the base polymers without deterioration in breakdown strength, except for P(VDF-HFP)/P(VDF-TrFE) that produces significantly higher strains than P(VDF-TrFE).[334] Transduction and dielectric properties have been studied for a limited amount of combinations of polymers (Section 4.3.2), leaving many unexplored permutations, such as P(VDF-TrFE-CTFE) or P(VDF-TrFE-HFP) combinations with (one or multiple) other terpolymers or copolymers.

6.2. Actuators

6.2.1. Design, Materials, and Applications

PVDF-based actuator types and configurations are summarized in **Figure 17**a. They include bending cantilevers (unimorph and bimorph), bending membranes (unimorph), dilating membranes, tubular actuators (coaxial and rolled), and plate and stack actuators. Multilayer designs have been employed in cantilever actuators, unimorph diaphagms, rolled tubular structures, and stack configuration. Over 70% of the reviewed devices utilize a unimorph configuration (benders and diaphragms), highlighting its versatility and ease of fabrication.

The reported actuators base on a multitude of pure polymers and their modification, as shown in Figure 17b. Their electrodes were based on metallic (Au, Ag, Cu, Al), carbon-based (grease, CB), polymeric (PEDOT:PSS), ceramic (ITO), and composite (CB/PDMS, MWCNTs/silicone) materials, as summarized in Table 6, 7, and 8. Flexible substrates, when present, consist of PET, PI, PEN, PC, PVDF, P(VDF-TrFE) and P(VDF-TrFE), Scotch tape, paper, or metallic passive layers (Cu and Ni-Fe foils). However, many of the PVDF-based materials (see Section 3) that exhibit strong electromechanical transduction have not yet been employed in actuators, including P(VDF-HFP) and P(VDF-DB) copolymers, P(VDF-TrFE-HFP) terpolymer, P(VDF-TrFE-CFE-FA) tetrapolymer, and composites with piezoceramic fillers.

Utilization of PVDF-based actuators has been proposed most commonly in the fields of optics, microfluidics and haptics, as illustrated in Figure 17c. The materials further offer a strong potential for soft robotics and wearable applications, showing similar strains and energy densities to DE actuators (see Figure 13, 15, and 16),[30] but at lower activation voltages. In soft robotics, they have been proposed for actuating a locomotion unit[364], origami structures,[372] and wings of a robotic butterfly.[331] Among wearable devices, PVDF and P(VDF-TrFE) have been extensively studied as sensors,[382] but not yet as actuators. Compared with other smart materials and conventional actuators that have been studied for wearables,[383–385] the PVDF-based actuators are anticipated to enable favorable trade-offs between bandwidth, strain, size, and activation voltage.

6.2.2. Manufacturing

Actuator manufacturing begins with either the active layer or the substrate and consists of deposition, assembly and treatment steps. When starting with the active layer, the fabrication bases on a purchased or fabricated membrane (e.g., solution-casting, melt-pressing, extrusion) and typically involves the steps of active layer processing (e.g., annealing, poling, stretching), application of electrodes (e.g., physical vapor deposition, brushing, printing), and assembly of the finished layers (with epoxy or adhesive tapes). This strategy has been used to produce bimorph,[356] unimorph,[230,299,371] tubular,[228] and stack[378] actuators. When starting with the substrate, individual functional layers are incrementally deposited via spin-coating, spray-coating, 3D printing, inkjet-printing, screen-printing, stencil-printing, or doctor blading. Actuators have been produced using either one[161,225,242,243,302,366] or multiple techniques.[239,241,364,368] Emergence of additive manufacturing has led to its growing application in actuator production[242,243] and is anticipated to further grow its role in the field.

EAP layer fabrication is a key step in actuator manufacturing, with appropriate methods depending on the specific EAP material and the intended actuator geometry. Solution casting is the most

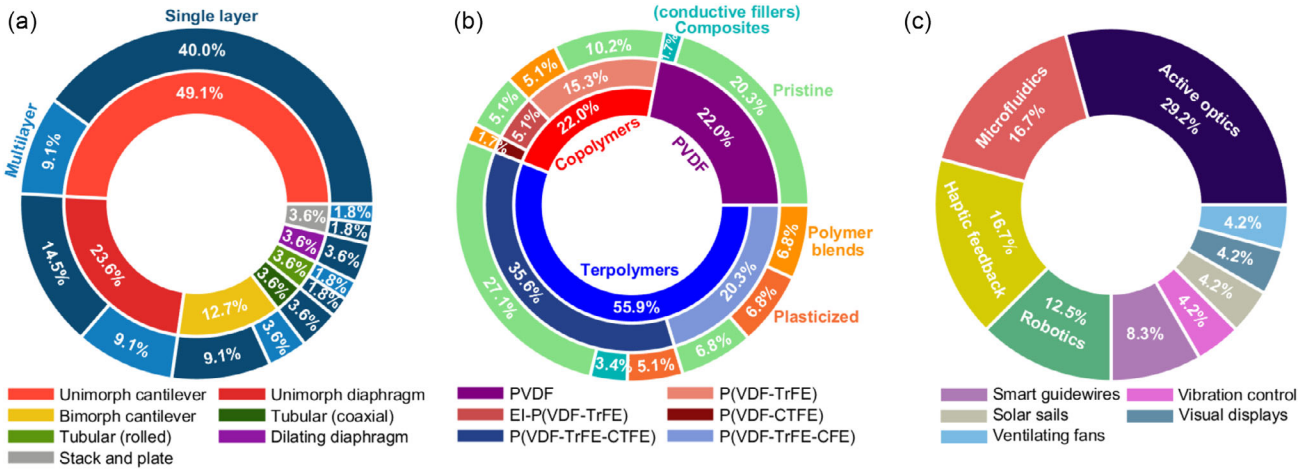

Figure 17. Graphic summary of the reported PVDF-based actuators: a) transducer configurations, b) employed materials, and c) proposed application domains.

commonly used method for PVDF-based FPs, as it is simple to implement, compatible with most materials, very accessible, and can produce very thin EAP layers (1–1.5 μm).[233,234,372,376,378,380] Drawbacks of solution casting include limited freedom in geometry and residual porosity.[192,195] Other accessible methods for EAP fabrication include spin-coating,[240,241,364] screen-printing,[225] and stencil-printing,[239] that exhibit similar characteristics to solution casting, but have been employed less frequently. Digital printing methods overcome the masking constraints by directly applying the required patterns of thin EAP layers.[242,243,366] Depending on the technique, the inks may require meticulous rheology optimization to ensure their printability,[242] which is more challenging for higher FP concentrations and filler contents. Specialized techniques that have been used for the fabrication of FP layers include electrospinning, which directly produces stretched and poled polymer fibers (enhanced transduction, but increased porosity and reduced stiffness)[105,196,231,374] and melt extrusion, which enables direct formation of hollow structures for tubular actuators.[379]

Electrodes of the actuators need to be sufficiently conductive and compliant to apply electric field to the EAP layer and allow it to deform. PVD methods have been used to produce very thin (typically tens of nm) metal electrodes, either directly on FPs[215,230,234,378] or in combination with Cr/Ti adhesion layers.[367] However, PVD requires custom masks to shape the electrode and is limited in the selection of compatible materials. Screen-printing and spray-coating have been used to deposit conductive polymer electrodes (PEDOT:PSS),[225,377] but also require masking. Additive manufacturing techniques are mask-free and have been used to produce fine electrode patterns of various materials, including Ag and CB nanoparticles,[239–242,365,366] MWCNTs/silicone composites[373] and PEDOT:PSS.[355] As a limitation, they may require pre- and post-processing steps, such as ink formulation, surface preparation, drying, and sintering.[239,240,242]

6.2.3. Performance

The most commonly reported performance indicator is the actuator displacement (see Table 6, 7, and 8). While displacement depends on the excitation frequency, it is often reported only for a single operating condition (quasi-static, dynamic, or resonant), making comparison challenging.

Comparison of bending cantilever actuator displacements can be facilitated by normalizing their tip deflection to compensate for differences in length (δ/L). **Figure 18** plots the normalized deflections of the reviewed cantilever actuators against the respective driving field strengths. In quasi-static conditions ($E \leq 50\,\mathrm{V\,\mu m^{-1}}$), PVDF bimorph and P(VDF-TrFE-CFE) multilayer unimorph actuators achieve the highest δ/L of 0.35[355] and 0.3,[373] respectively, followed by PVDF ($\delta/L = 0.18$),[357] DEHP/P(VDF-TrFE-CTFE) ($\delta/L = 0.15$),[120] and P(VDF-TrFE-CTFE) films and nanofibers-based unimorphs ($\delta/L = 0.08$–0.11).[120,374] In resonant operation, the double-supported PVDF bimorphs[354] achieve highest δ/L of 0.45 ($13.3\,\mathrm{V\,\mu m^{-1}}$), followed by single- and dual-layer P(VDF-TrFE-CTFE) unimorphs at 0.33 ($60\,\mathrm{V\,\mu m^{-1}}$)[239] and 0.2 ($40\,\mathrm{V\,\mu m^{-1}}$),[243] respectively.

Actuator's blocking forces (see Section 2.2) are reported less frequently, and the highest values of up to 1.3 and 1.1 N were produced by tubular actuators of P(VDF-TrFE-CFE)[228] and P(VDF-CTFE)/P(VDF-TrFE-CFE).[380] Bending cantilevers produce significantly lower forces, with studies reporting up to 26 mN for P(VDF-TrFE-CTFE)[372] and 20 mN for P(VDF-TrFE-CFE)[373] multilayer unimorphs.

Ferroelectric polymer actuators often operate close to the dielectric breakdown strength, requiring high activation fields (typically 10–150 $\mathrm{V\,\mu m^{-1}}$[40,219,231]) and driving voltages. Employing thinner active layers allows to reduce the driving voltages ($E = V/t_a$), but deteriorates the actuation capabilities due to the reduced EAP volume. Multilayer actuators overcome this challenge by stacking several actuator layers on top of one another and connecting them electrically in parallel, a common practice in piezoceramic[386,387] and dielectric elastomer actuators.[388–398] This approach has received less attention than the single layer structures (see Figure 17a).

Performance of the bending cantilever actuators (forces and deflections) is strongly dependent on their constituent materials and layer thicknesses,[129,130,239,364] as explained in Section 2.2.2.

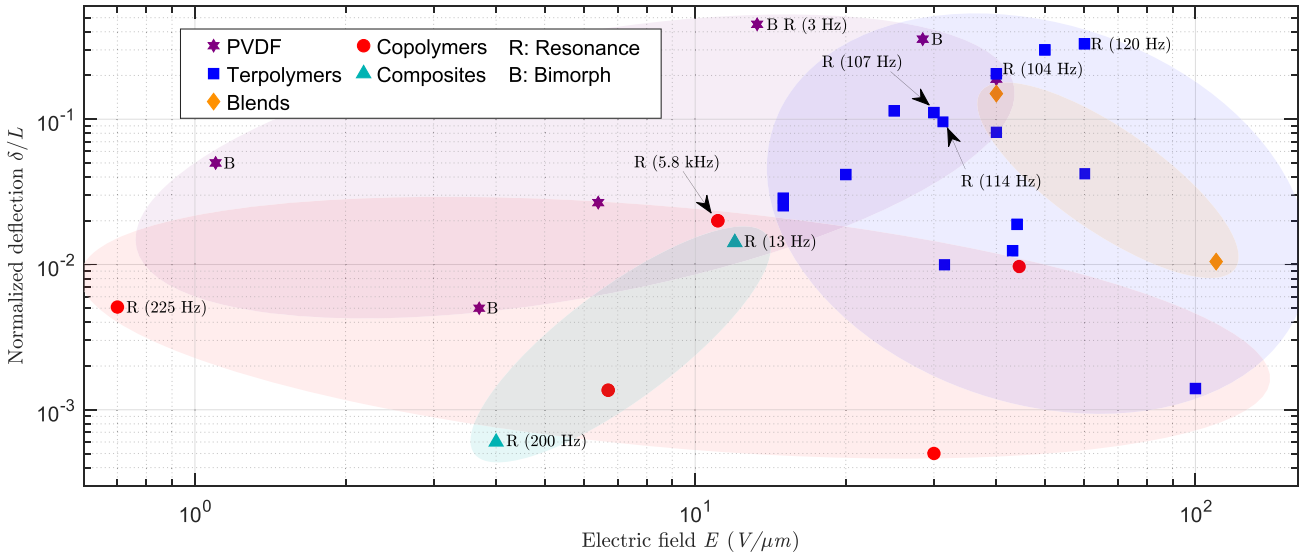

Figure 18. Comparison of normalized deflection (δ/L) and activation fields (E) for PVDF-based bending cantilevers.

Since the designs are mostly not optimized, the reported bending actuators exhibit modest performance (e.g., high material strains do not necessarily produce high tip deflections), which could be significantly improved by optimizing the morphology.

7. Conclusions

This work reviews and summarizes the research in electromechanical transduction properties of PVDF-based ferroelectric materials and actuators. The materials are divided into PVDF-based polymers (PVDF, its co-, ter-, and tetra-polymers), their composites (with ceramic, conductive, organometallic, and organosilicate fillers), and blends (with plasticizers and other polymers). The review addresses the key factors that contribute to transduction performance, including dielectric permittivity, Young's modulus, strain, electrostrictive and piezoelectric coefficients, energy density, breakdown strength, and coupling efficiency. The reported actuators are classified as unimorph and bimorph bending cantilevers, unimorph diaphragms, dilating diaphragms, plates, stacks, and tubular actuators. Evaluation is conducted in terms of quasi-static and dynamic displacement, blocking force and activating electric field strength. The review indicates several unexplored opportunities, both in the material and actuator design.

While pure PVDF polymer requires elaborate stretching and poling steps to produce strains of up to 0.88% (3.7 V μm^{-1}) and energy densities of up to 0.0024 J cm^{-3}, the copolymers exhibit higher performance and are easier to process. P(VDF-TrFE), P(VDF-CTFE), and P(VDF-HFP) respectively exhibit strains of up to 3.5% (190 V μm^{-1}), 5.5% (220 V μm^{-1}), and 4.1% (50 V μm^{-1}), and energy densities of up to 0.42, 1.1, and 0.92 J cm^{-3}. Double-bonded P(VDF-DB) have been synthesized from P(VDF-CTFE), attaining strains of up to 13.4% (275 V μm^{-1}) and energy densities of up to 3.1 J cm^{-3}, the highest among all reviewed materials. Irradiating P(VDF-TrFE) with high-energy electrons induces RFE behavior, enabling strains of up to 5% (146 V μm^{-1}, 0.92 J cm^{-3}). Electromechanical transduction of P(VDF-DB) and P(VDF-HFP) was studied well below their breakdown strength, indicating potentially much higher performance.

Terpolymers of PVDF exhibit strong electromechanical transduction without specific post-processing requiements. The P(VDF-TrFE-CTFE), P(VDF-TrFE-CFE), and P(VDF-TrFE-HFP) are synthesized by introducing a bulky monomer into P(VDF-TrFE) and respectively exhibit strains of up to 9% (200 V μm^{-1}, 0.51 J cm^{-3}), 7% (170 V μm^{-1}, 1.1 J cm^{-3}), and 2.8% (70 V μm^{-1}). Reports on P(VDF-TrFE-HFP) are very limited, and further investigation is required at higher field strengths. The recently reported P(VDF-TrFE-CFE-FA) tetrapolymer exhibits strains of up to 6% (80 V μm^{-1}, 0.4 J cm^{-3}) and a coupling efficiency of up to 0.88, which is among the highest figures of the reviewed materials and EAPs in general. This indicates that further research into tetrapolymers may produce a new class of high-performance RFE materials.

Introducing fillers into PVDF polymers yields composites with enhanced electromechanical properties. The reported ceramic fillers are mostly PZT-based and produce increased piezoelectric and dielectric properties (ε_r of up to 181 at 1 kHz and d_{33} up to 100 pm V^{-1}), but require elaborate anti-parallel poling. Electrothermal actuation in TiO_2/PVDF composites achieved the highest energy densities among the reviewed materials (up to 11.3 J cm^{-3} at 40 V μm^{-1}), despite the reduced breakdown strength. Composites basing on conductive and metal-organic fillers respectively exhibit improved low-field strains of 5.1% in SWCNTs/P(VDF-TrFE) (50 V μm^{-1}, 0.74 J cm^{-3}) and 1.91% in CuPC/EI-P(VDF-TrFE) (13 V μm^{-1}, 0.13 J cm^{-3}), at the cost of decreased breakdown strength. The SWCNTs/P(VDF-TrFE) composite further exhibits exceptional coupling efficiency of up to 0.88, alike the tetrapolymer and TiO_2/PVDF composite. Employing core-shell structures of conductive-insulating materials has been demonstrated to improve E_b in PVDF composites and are anticipated to have a similar effect in copolymer and terpolymer composites.

Blending P(VDF-TrFE-CTFE) and P(VDF-TrFE-CFE) terpolymers with plasticizers (DEHP, DINP, and Palamoll 652) significantly enhanced the low-field strains (up to 2%, 10 V μm^{-1}, 0.007 J cm^{-3} in DEHP/P(VDF-TrFE-CFE) blends) while decreasing both the breakdown strength and Young's modulus. In contrast, two-polymer blends show higher maximum strains (up to 5% in P(VDF-TrFE)/P(VDF-CTFE), 170 V μm^{-1}) and energy densities (up to 0.73 J cm^{-3} in P(VDF-CTFE)/P(VDF-TrFE-CFE), 150 V μm^{-1}) due to the increased film stiffness and unaffected breakdown strength. Therefore, the unexplored permutations of high-strain polymers, such as P(VDF-HFP), P(VDF-TrFE-HFP), and P(VDF-TrFE-CTFE) may attain further improvement in transduction properties.

The most commonly reported actuators are bending cantilevers (unimorph and bimorph), followed by unimorph diaphragms and tubular actuators. In contrast, stacked and dilating diaphragm actuators have received little attention. Both single- and multilayer designs have been implemented, whereas the former are more common. Most of the reported devices base either on P(VDF-TrFE-CTFE) or P(VDF-TrFE-CFE) terpolymers, owing to availability and minimal post-processing requirements. The highest quasi-static normalized displacements (δ/L) were reported for PVDF bimorph (0.35 at 28.5 V μm^{-1}) and P(VDF-TrFE-CFE) unimorph (0.3 at 50 V μm^{-1}) cantilevers. The highest δ/L in resonant operation was reported for PVDF double-supported bimorph (0.45 at 13.3 V μm^{-1}, 3 Hz) and P(VDF-TrFE-CTFE) unimorph (0.33 at 60 V μm^{-1}, ≈120 Hz) cantilevers. Actuator forces are reported rarely, and the highest figures of up to 1.3 N were produced by tubular P(VDF-TrFE-CFE) actuators. Superior materials do not necessarily translate into better actuator performance due to unoptimized layer thicknesses. Design optimization is therefore anticipated to significantly increase actuator performance and utilization outlooks in emerging technologies.

Conflict of Interest

The authors declare no conflict of interest.

Keywords

actuators, electromechanical transduction, ferroelectric polymers, performance, poly(vinylidene fluoride)

Received: June 24, 2025
Revised: November 10, 2025
Published online:

[1] E. A. Sideris, H. C. de Lange, A. Hunt, An ionic polymer metal composite (ipmc)-driven linear peristaltic microfluidic pump, *IEEE Rob. Autom. Lett.* **2020**, *5*, 6788.
[2] A. K. Price, K. M. Anderson, C. T. Culbertson, Demonstration of an integrated electroactive polymer actuator on a microfluidic electrophoresis device, *Lab on a Chip* **2009**, *9*, 2076.
[3] A. Zaszczynska, A. Gradys, P. Sajkiewicz, Progress in the applications of smart piezoelectric materials for medical devices, *Polymers* **2020**, *12*, 2754.
[4] P. Motreuil-Ragot, A. Hunt, D. Kasi, B. Brajon, A. van den Maagdenberg, V. Orlova, M. Mastrangeli, P. M. Sarro, Enabling actuation and sensing in organs-on-chip using electroactive polymers, in *2020 3rd IEEE Inter. Conf. on Soft Robotics (RoboSoft)*, IEEE, New Haven, CT, USA **2020**, pp. 530–535.
[5] Z. Chen, A review on robotic fish enabled by ionic polymer–metal composite artificial muscles, *Rob. Biomimetics* **2017**, *4*, 24.
[6] Y. Tang, L. Qin, X. Li, C.-M. Chew, J. Zhu, A frog-inspired swimming robot based on dielectric elastomer actuators, in *2017 IEEE/RSJ Inter. Conf. on Intelligent Robots and Systems (IROS)*, IEEE **2017**, pp. 2403–2408.
[7] X. Ji, X. Liu, V. Cacucciolo, M. Imboden, Y. Civet, A. E. Haitami, S. Cantin, Y. Perriard, H. Shea, An autonomous untethered fast soft robotic insect driven by low-voltage dielectric elastomer actuators, *Sci. Rob.* **2019**, *4*, eaaz6451.
[8] S. Bahl, H. Nagar, I. Singh, S. Sehgal, Smart materials types, properties and applications: A review, *Mater. Today Proc.* **2020**, *28*, 1302, International Conference on Aspects of Materials Science and Engineering.
[9] L. Hu, Q. Zhang, X. Li, M. J. Serpe, Stimuli-responsive polymers for sensing and actuation, *Mater. Horiz.* **2019**, *6*, 1774.
[10] F. Carpi, R. Kornbluh, P. Sommer-Larsen, G. Alici, Electroactive polymer actuators as artificial muscles: are they ready for bioinspired applications?, *Bioinspiration Biomimetics* **2011**, *6*, 045006.
[11] Y. Bar-Cohen, Electroactive polymers as an enabling materials technology, *Proc. Inst. Mech. Eng., Part G* **2007**, *221*, 553.
[12] Y. Bar-Cohen, Q. Zhang, Electroactive polymer actuators and sensors, *MRS Bulletin* **2008**, *33*, 173.
[13] M. Su, Y. Song, Printable smart materials and devices: Strategies and applications, *Chem. Rev.* **2022**, *122*, 5144, 34415152.
[14] Y. Wu, Y. Ma, H. Zheng, S. Ramakrishna, Piezoelectric materials for flexible and wearable electronics: A review, *Mater. Des.* **2021**, *211*, 110164.
[15] M. Annabestani, M. Fardmanesh, Ionic electro active polymer-based soft actuators and their applications in microfluidic micropumps, microvalves, and micromixers: a review, preprint arXiv:1904.07149, 2019.
[16] F. Hu, Y. Xue, J. Xu, B. Lu, Pedot-based conducting polymer actuators, *Front. Rob. AI* **2019**, *6*, 114.
[17] Z. Liu, Y. D. Liu, Q. Shi, Y. Liang, Electroactive dielectric polymer gels as new-generation soft actuators: a review, *J. Mater. Sci.* **2021**, *56*, 14943.
[18] J. D. W. Madden, N. A. Vandesteeg, P. A. Anquetil, P. G. A. Madden, A. Takshi, R. Z. Pytel, S. R. Lafontaine, P. A. Wieringa, I. W. Hunter, Artificial muscle technology: physical principles and naval prospects. *IEEE J. Oceanic Eng.* **2004**, *29*, 706.
[19] W. MohdIsa, A. Hunt, S. H. HosseinNia, Sensing and self-sensing actuation methods for ionic polymer–metal composite (ipmc): A review. *Sensors* **2019**, *19*, 3967.
[20] L. Bay, K. West, P. Sommer-Larsen, S. Skaarup, M. Benslimane, A conducting polymer artificial muscle with 12% linear strain. *Adv. Mater.* **2003**, *15*, 310.
[21] K. Oguro, N. Fujiwara, K. Asaka, K. Onishi, S. Sewa, In *Smart Structures and Materials 1999: Electroactive Polymer Actuators and Devices*, Vol. *3669*, SPIE, Bellingham, WA, USA **1999**, pp. 64–71.
[22] J. D. Madden, P. G. Madden, I. Warwick Hunter, *Smart Structures and Materials 2001: Electroactive Polymer Actuators and Devices*, Vol. *4329*, SPIE, Bellingham, WA, USA **2001**, pp. 72–83.
[23] Y. Bar-Cohen, Electroactive polymers (eap) as actuators for potential future planetary mechanisms, in *Proceedings. 2004 NASA/DoD Conf. on Evolvable Hardware, 2004*, IEEE, Seattle, WA, USA **2004**, pp. 309–317.
[24] Y. Bar-Cohen, Eap as artificial muscles: progress and challenges, *Smart Struct. Mater. Electro. Polym. Actuat. Devices EAPAD* **2004**, *5385*, 10.

[25] Y. Bar-Cohen, V. F. Cardoso, C. Ribeiro, S. Lanceros-Méndez, *Advanced Piezoelectric Materials*, *Second Edition*, (Ed: K. Uchino), Woodhead Publishing, Cambridge, UK **2017**, pp. 319–352.
[26] J. Su, J. S. Harrison, T. L. St Clair, Y. Bar-Cohen, S. Leary, Electrostrictive grafr elastomers and applications, *MRS Online Proc. Lib. OPL* **1999**, *600*, 131.
[27] A. Khan, F. R. Khan, H. Soo Kim, Electro-active paper as a flexible mechanical sensor, actuator and energy harvesting transducer: A review, *Sensors* **2018**, *18*, 3474.
[28] R. Pelrine, R. Kornbluh, Q. Pei, J. Joseph, High-speed electrically actuated elastomers with strain greater than 100%, *Science* **2000**, *287*, 836.
[29] R. Pelrine, R. Kornbluh, J. Joseph, R. Heydt, Q. Pei, S. Chiba, High-field deformation of elastomeric dielectrics for actuators, *Mater. Sci. Eng. C* **2000**, *11*, 89.
[30] R. Shankar, T. K. Ghosh, R. J. Spontak, Dielectric elastomers as next-generation polymeric actuators, *Soft Matter.* **2007**, *3*, 1116.
[31] L. J. Romasanta, M. A. López-Manchado, R. Verdejo, Increasing the performance of dielectric elastomer actuators: A review from the materials perspective, *Prog. Polym. Sci.* **2015**, *51*, 188.
[32] J. Biggs, K. Danielmeier, J. Hitzbleck, J. Krause, T. Kridl, S. Nowak, E. Orselli, X. Quan, D. Schapeler, W. Sutherland, J. Wagner, Electroactive polymers: Developments of and perspectives for dielectric elastomers, *Angew. Chem. Int. Ed.* **2013**, *52*, 9409.
[33] R. Kanno, T. Nagai, J. Shintake, Rapid fabrication method for soft devices using off-the-shelf conductive and dielectric acrylic elastomers, *Adv. Intell. Syst.* **2021**, *3*, 2000173.
[34] L. Liu, Y. Huang, Y. Zhang, E. Allahyarov, Z. Zhang, F. Lv, L. Zhu, Understanding reversible maxwellian electroactuation in a 3m vhb dielectric elastomer with prestrain, *Polymer* **2018**, *144*, 150.
[35] Y. Wang, X. Ma, Y. Jiang, W. Zang, P. Cao, M. Tian, N. Ning, L. Zhang, Dielectric elastomer actuators for artificial muscles: A comprehensive review of soft robot explorations, *Res. Chem. Mater.* **2022**, *1*, 308.
[36] G. Gallucci, Y. Wu, M. Tichem, A. Hunt, (Ed: J. D. W. Madden, S. S. Seelecke, A. Ladegaard Skov), In *Electroactive Polymer Actuators and Devices (EAPAD) XXVI*, volume *12945*, page 129450I. International Society for Optics and Photonics, SPIE, **2024**.
[37] W. Lehmann, H. Skupin, C. Tolksdorf, E. Gebhard, R. Zentel, P. Krüger, M. Lösche, F. Kremer, Giant lateral electrostriction in ferroelectric liquid-crystalline elastomers, *Nature* **2001**, *410*, 447.
[38] M. O. Saed, R. H. Volpe, N. A. Traugutt, R. Visvanathan, N. A. Clark, C. M. Yakacki, High strain actuation liquid crystal elastomers via modulation of mesophase structure, *Soft Matter.* **2017**, *13*, 7537.
[39] Z. Zhang, X. Wang, S. Tan, Q. Wang, Superior electrostrictive strain achieved under low electric fields in relaxor ferroelectric polymers, *J. Mater. Chem. A* **2019**, *7*, 5201.
[40] X. Chen, H. Qin, X. Qian, W. Zhu, B. Li, B. Zhang, W. Lu, R. Li, S. Zhang, L. Zhu, F. D. dos Santos, J. Bernholc, Q. M. Zhang, Relaxor ferroelectric polymer exhibits ultrahigh electromechanical coupling at low electric field, *Science* **2022**, *375*, 1418.
[41] Z.-C. Jiang, Q. Liu, Y.-Y. Xiao, Y. Zhao, Liquid crystal elastomers for actuation: A perspective on structure-property-function relation, *Prog. Polym. Sci.* **2024**, *153*, 101829.
[42] Y. Xiao, J. Wu, Y. Zhang, Recent advances in the design, fabrication, actuation mechanisms and applications of liquid crystal elastomers, *Soft Sci.* **2023**, *3*, 11.
[43] R. S. Kularatne, H. Kim, J. M. Boothby, T. H. Ware, Liquid crystal elastomer actuators: Synthesis, alignment, and applications, *J. Polym. Sci. Part B: Polym. Phys.* **2017**, *55*, 395.
[44] A. Gruzdenko, I. Dierking, Liquid crystal-based actuators, *Front. Soft Matter.* **2022**, *2*, 1052037.
[45] H. Jiang, C. Li, X. Huang, Actuators based on liquid crystalline elastomer materials, *Nanoscale* **2013**, *5*, 5225.
[46] D. Mistry, N. A. Traugutt, K. Yu, C. M. Yakacki, Processing and reprocessing liquid crystal elastomer actuators, *J. Appl. Phys.* **2021**, *129*, 130901.
[47] R. Pelrine, P. Sommer-Larsen, R. D. Kornbluh, R. Heydt, G. Kofod, Q. Pei, P. Gravesen, In *Smart Structures and Materials 2001: Electroactive Polymer Actuators and Devices*, Vol. *4329*, SPIE, Bellingham, WA, USA **2001**, pp. 335–349.
[48] A. O'Halloran, F. O'Malley, P. McHugh, A review on dielectric elastomer actuators, technology, applications, and challenges, *J. Appl. Phys.* **2008**, *104*, 071101.
[49] P. Brochu, Q. Pei, Advances in dielectric elastomers for actuators and artificial muscles, *Macromol. Rapid Commun.* **2010**, *31*, 10.
[50] Y. Guo, L. Liu, Y. Liu, J. Leng, Review of dielectric elastomer actuators and their applications in soft robots, *Adv. Intell. Syst.* **2021**, *3*, 2000282.
[51] Q. Zhang, W. Yu, J. Zhao, C. Meng, S. Guo, A review of the applications and challenges of dielectric elastomer actuators in soft robotics, *Machines* **2025**, *13*101.
[52] Y. Qiu, E. Zhang, R. Plamthottam, Q. Pei, Dielectric elastomer artificial muscle: Materials innovations and device explorations, *Accounts of Chem. Res.* **2019**, *52*, 316.
[53] J.-H. Youn, S. M. Jeong, G. Hwang, H. Kim, K. Hyeon, J. Park, K.-U. Kyung, Dielectric elastomer actuator for soft robotics applications and challenges, *Appl. Sci.* **2020**, *10*, 640.
[54] U. Gupta, L. Qin, Y. Wang, H. Godaba, J. Zhu, Soft robots based on dielectric elastomer actuators: a review, *Smart Mater. Struct.* **2019**, *28*, 103002.
[55] C. Tang, B. Du, S. Jiang, Z. Wang, X.-J. Liu, H. Zhao, A review on high-frequency dielectric elastomer actuators: Materials, dynamics, and applications, *Adv. Intell. Syst.* **2024**, *6*, 2300047.
[56] M. Ghevondyan, M. Davtyan, M. Aghayan, Dielectric elastomer actuators: medical applications review, *Discover Mater.* **2025**, *5*, 43.
[57] P. Banet, N. Zeggai, J. Chavanne, G. T. M. Nguyen, L. Chikh, C. Plesse, M. Almanza, T. Martinez, Y. Civet, Y. Perriard, O. Fichet, Evaluation of dielectric elastomers to develop materials suitable for actuation, *Soft Matter.* **2021**, *17*, 10786.
[58] T. Lu, C. Ma, T. Wang, Mechanics of dielectric elastomer structures: A review, *Extreme Mech. Lett.* **2020**, *38*, 100752.
[59] G.-Y. Gu, J. Zhu, L.-M. Zhu, X. Zhu, A survey on dielectric elastomer actuators for soft robots, *Bioinspiration Biomimetics* **2017**, *12*, 011003.
[60] Y. Zhao, L.-J. Yin, S.-L. Zhong, J.-W. Zha, Z.-M. Dang, Review of dielectric elastomers for actuators, generators and sensors, *IET Nanodielectrics* **2020**, *3*, 99.
[61] H. Kawai, The piezoelectricity of poly (vinylidene fluoride), *Jpn. J. Appl. Phys.* **1969**, *8*, 975.
[62] Y. Murata, K. Tsunashima, J. Umemura, N. Koizumi, Ferroelectric properties of polyamides consisting of hepta-and nonamethylenediamines, *IEEE Trans. Dielectr. Electr. Insul.* **1998**, *5*, 96.
[63] T. Nagasawa, Y. Murata, K. Tsunashima, Y. Morishima, S. Yano, N. Koizumi, Amorphous ferroelectric polyamide blends, *Macromolecules* **2000**, *33*, 2302.
[64] Z. Z. Ounaies, J. A. Young, J. O. Simpson, B. L. Farmer, Dielectric properties of piezoelectric polyimides, *MRS Online Proc. Library* **1996**, 53–58.
[65] Y. Tajitsu, Piezoelectricity of chiral polymeric fiber and its application in biomedical engineering, *IEEE Trans. Ultrason. Eng.* **2008**, *55*, 1000.
[66] J. Y.-H. Kim, A. Cheng, Y.-C. Tai, Parylene-c as a piezoelectric material, in *2011 IEEE 24th Inter. Conf. on Micro Electro Mechanical Systems*, IEEE, Cancun, Mexico **2011**, pp. 473–476.
[67] J. Y.-H. Kim, M. Nandra, Y.-C. Tai, Cantilever actuated by piezoelectric parylene-c, in *2012 IEEE 25th Inter. Conf. on Micro Electro Mechanical Systems (MEMS)*, IEEE, Paris, France **2012**, pp. 1141–1144.

[68] P. Martins, A. C. Lopes, S. Lanceros-Mendez, Electroactive phases of poly (vinylidene fluoride): Determination, processing and applications, *Prog. Polym. Sci.* **2014**, *39*, 683.
[69] P. Saxena, P. Shukla, A comprehensive review on fundamental properties and applications of poly (vinylidene fluoride)(pvdf), *Adv. Compos. Hybrid Mater.* **2021**, *4*, 8.
[70] D. M. Nivedhitha, S. Jeyanthi, Polyvinylidene fluoride, an advanced futuristic smart polymer material: A comprehensive review, *Polym. Adv. Technol.* **2023**, *34*, 474.
[71] C. Ribeiro, C. M. Costa, D. M. Correia, J. O. João Nunes-Pereira, P. Martins, R. Gonçalves, V. F. Cardoso, S. Lanceros-Méndez, Electroactive poly (vinylidene fluoride)-based structures for advanced applications, *Nat. Protocols* **2018**, *13*, 681.
[72] L. Wu, Z. Jin, Y. Liu, H. Ning, X. Liu, Alamusi, and Ning Hu. Recent advances in the preparation of pvdf-based piezoelectric materials, *Nanotechnol. Rev.* **2022**, *11*, 1386.
[73] G. Kalimuldina, N. Turdakyn, I. Abay, A. Medeubayev, A. Nurpeissova, D. Adair, Z. Bakenov, A review of piezoelectric pvdf film by electrospinning and its applications, *Sensors* **2020**, *20*, 5214.
[74] W. Xia, Z. Zhang, Pvdf-based dielectric polymers and their applications in electronic materials, *IET Nanodielectr.* **2018**, *1*, 17.
[75] L. Zhu, Exploring strategies for high dielectric constant and low loss polymer dielectrics, *J. Phys. Chem. Lett.* **2014**, *5*, 3677.
[76] Y. Jiang, M. Zhou, Z. Shen, X. Zhang, H. Pan, Y.-H. Lin, Ferroelectric polymers and their nanocomposites for dielectric energy storage applications, *APL Mater.s* **2021**, *9*, 020905.
[77] X. Hu, K. Yi, J. Liu, B. Chu, High energy density dielectrics based on pvdf-based polymers, *Energy Technol.* **2018**, *6*, 849.
[78] J. C. Barbosa, J. P. Dias, S. Lanceros-Méndez, C. M. Costa, Recent advances in poly (vinylidene fluoride) and its copolymers for lithium-ion battery separators. *Membranes* **2018**, *8*, 45.
[79] J. Yan, M. Liu, Y. G. Jeong, W. Kang, L. Li, Y. Zhao, N. Deng, B. Cheng, G. Yang, Performance enhancements in poly(vinylidene fluoride)-based piezoelectric nanogenerators for efficient energy harvesting, *Nano Energy* **2019**, *56*, 662.
[80] X. Chen, X. Han, Q.-D. Shen, Pvdf-based ferroelectric polymers in modern flexible electronics, *Adv. Electron. Mater.* **2017**, *3*, 1600460.
[81] S. Guo, X. Duan, M. Xie, K. C. Aw, Q. Xue, Composites, fabrication and application of polyvinylidene fluoride for flexible electromechanical devices: A review, *Micromachines* **2020**, *11*, 1076.
[82] C. M. Costa, V. F. Cardoso, P. Martins, D. M. Correia, R. Gonçalves, P. Costa, V. Correia, C. Ribeiro, M. M. Fernandes, P. M. Martins, S. Lanceros-Méndez, Smart and multifunctional materials based on electroactive poly(vinylidene fluoride): Recent advances and opportunities in sensors, actuators, energy, environmental, and biomedical applications, *Chem. Rev.* **2023**, *123*, 11392.
[83] S. Sukumaran, S. Chatbouri, D. Rouxel, E. Tisserand, F. Thiebaud, T. Ben Zineb, Recent advances in flexible pvdf based piezoelectric polymer devices for energy harvesting applications, *J. Intell. Mater. Syst. Struct.* **2021**, *32*, 746.
[84] G. H. Haertling, Ferroelectric ceramics: History and technology, *J. Am. Ceram. Soc.* **1999**, *82*, 797.
[85] A. Preumont, Actuators, piezoelectric materials, and active structures, in *Vibration Control of Active Structures: an Introduction*, Springer, Netherlands, Dordrecht **2002**, pages 37–74.
[86] E. Aksel, J. L. Jones, Advances in lead-free piezoelectric materials for sensors and actuators, *Sensors* **2010**, *10*, 1935.
[87] S. Lustig, D. Elata, Ambiguous definitions of the piezoelectric coupling factor, *J. Intell. Mater. Syst. Struct.* **2020**, *31*, 1689.
[88] Q. M. Zhang, H. Li, M. Poh, F. Xia, Z-Y Cheng, H. Xu, C. Huang, An all-organic composite actuator material with a high dielectric constant, *Nature* **2002**, *419*, 284.
[89] S. A. K. M. Tadigadapa, K. Mateti, Piezoelectric mems sensors: state-of-the-art and perspectives, *Meas. Sci. Technol.* **2009**, *20*, 092001.
[90] G. Liu, S. Zhang, W. Jiang, W. Cao, Losses in ferroelectric materials, *Mater. Sci. Eng. R: Rep.* **2015**, *89*, 1.
[91] D. Bogdal, *Polymer Science: A Comprehensive Reference*, Elsevier, Amsterdam, Netherlands **2012**, pp. 981–1027.
[92] X. Liu, D. Zhu, J. Lin, Y. Zhang, Temperature and frequency dependence of the dynamic viscoelastic properties of silicone rubber, *Polymers* **2023**, *15*, 3005.
[93] X. Zhang, J. Jiang, Z. Shen, Z. Dan, M. Li, Y. Lin, C.-W. Nan, L. Chen, Y. Shen, Polymer nanocomposites with ultrahigh energy density and high discharge efficiency by modulating their nanostructures in three dimensions, *Adv. Mater.* **2018**, *30*, 1707269.
[94] Z. Pan, M. Wang, J. Chen, B. Shen, J. Liu, J. Zhai, Largely enhanced energy storage capability of a polymer nanocomposite utilizing a core-satellite strategy, *Nanoscale* **2018**, *10*, 16621.
[95] R. E. Newnham, V. Sundar, R. Yimnirun, J. Su, Q. M. Zhang, Electrostriction: nonlinear electromechanical coupling in solid dielectrics, *J. Phys. Chem. B* **1997**, *101*, 10141.
[96] R. E. Pelrine, R. D. Kornbluh, J. P. Joseph, Electrostriction of polymer dielectrics with compliant electrodes as a means of actuation, *Sens. Actuators, A* **1998**, *64*, 77.
[97] J. Li, N. Rao, Micromechanics of ferroelectric polymer-based electrostrictive composites, *J. Mech. Phys. Solids* **2004**, *52*, 591.
[98] M. Lallart, J.-F. Capsal, G. Sebald, P.-J. Cottinet, D. Guyomar, Converse electrostrictive effect in dielectric polymers, *Sens. Actuators B Chem.* **2014**, *190*, 259.
[99] I. Diaconu, A. David, D. Dorohoi, An experimental investigation of electroactive polyurethane, *J. Optoelectron. Adv. Mater.* **2005**, *7*, 2797.
[100] K. Wongtimnoi, B. Guiffard, A. B.-V. de Moortèle, L. Seveyrat, C. Gauthier, J.-Y. Cavaillé, Improvement of electrostrictive properties of a polyether-based polyurethane elastomer filled with conductive carbon black, *Compos. Sci. Technol.* **2011**, *71*, 885.
[101] Z. Suo, Theory of dielectric elastomers, *Acta Mech. Solida Sin.* **2010**, *23*, 549.
[102] V. Sundar, R. E. Newnham, Electrostriction and polarization, *Ferroelectrics* **1992**, *135*, 431.
[103] T. Furukawa, N. Seo, Electrostriction as the origin of piezoelectricity in ferroelectric polymers, *Jpn. J. Appl. Phys.* **1990**, *29*, 675.
[104] T. Wongwirat, Z. Zhu, G. Rui, R. Li, P. Laoratanakul, H. He, H. Manuspiya, L. Zhu, Origins of electrostriction in poly(vinylidene fluoride)-based ferroelectric polymers, *Macromolecules* **2020**, *53*, 10942.
[105] N. Tohluebaji, C. Putson, N. Muensit, J. Yuennan, Electrostrictive and structural properties of poly (vinylidene fluoride-hexafluoropropylene) composite nanofibers filled with polyaniline (emeraldine base), *Polymers* **2021**, *13*, 3250.
[106] G. S. Buckley, C. M. Roland, R. Casalini, A. Petchsuk, T. C. Chung, Electrostrictive properties of poly(vinylidenefluoride trifluoroethylenechlorotrifluoroethylene), *Chem. Mater.* **2002**, *14*, 2590.
[107] J. T. Garrett, C. M. Roland, A. Petchsuk, T. C. Chung, Electrostrictive behavior of poly(vinylidene fluoride-trifluoroethylene-chlorotrifluoroethylene), *Appl. Phys. Lett.* **2003**, *83*, 1190.
[108] R. Yimnirun, S. M.-L. Eury, V. Sundar, P. J. Moses, S.-J. Jang, R. E. Newnham, Electrostriction measurements on low permittivity dielectric materials, *J. Eur. Ceram. Soc.* **1999**, *19*, 1269.
[109] S. Eury, R. Yimnirun, V. Sundar, P. J. Moses, S.-J. Jang, R. E. Newnham, Converse electrostriction in polymers and composites, *Mater. Chem. Phys.* **1999**, *61*, 18.
[110] F. M. Guillot, E. Balizer, Electrostrictive effect in polyurethanes, *J. Appl. Polym. Sci.* **2003**, *89*, 399.

[111] F. Li, L. Jin, Z. Xu, S. Zhang, Electrostrictive effect in ferroelectrics: An alternative approach to improve piezoelectricity, *Appl. Phys. Rev.* **2014**, *1*, 011103.
[112] Y. Liu, Q. Wang, Ferroelectric polymers exhibiting negative longitudinal piezoelectric coefficient: Progress and prospects, *Adv. Sci.* **2020**, *7*, 1902468.
[113] T. Furukawa, J. Xun Wen, Electrostriction and piezoelectricity in ferroelectric polymers, *Jpn. J. Appl. Phys.* **1984**, *23*, L677.
[114] K. Wang, T. Godfroid, D. Robert, A. Preumont, Adaptive shell spherical reflector actuated with pvdf-trfe thin film strain actuators, *Actuators* **2021**, *10, 7*.
[115] M. E. Lines, A. M. Glass, *Principles and Applications of Ferroelectrics and Related Materials*, Oxford university press, Oxford, UK **2001**.
[116] M. G. Broadhurst, G. T. Davis, J. E. McKinney, R. E. Collins, Piezoelectricity and pyroelectricity in polyvinylidene fluoride—a model, *J. Appl. Phys.* **1978**, *49*, 4992.
[117] C. L. Hom, S. M. Pilgrim, N. Shankar, K. Bridger, M. Massuda, S. R. Winzer, Calculation of quasi-static electromechanical coupling coefficients for electrostrictive ceramic materials, *IEEE Trans. Ultrason. Eng.* **1994**, *41*, 542.
[118] T.-B. Xu, Z.-Y. Cheng, T. Mai, Y. Lu, Q. M. Zhang, Electromechanical coupling factor of electrostrictive p(vdf-trfe) copolymer, in *2000 IEEE Ultrasonics Symp. Proceedings. An Inter. Symp. (Cat. No.0°CH37121)*, IEEE, San Juan, Puerto Rico **2000**, Vol. *2*, pp. 997–1000.
[119] X. D. Zhang, C. A. Rogers, A macroscopic phenomenological formulation for coupled electromechanical effects in piezoelectricity, *J. Intell. Mater. Syst. Struct.* **1993**, *4*, 307.
[120] N. D. Schiava, K. Thetpraphi, M.-Q. Le, P. Lermusiaux, A. Millon, J.-F. Capsal, P.-J. Cottinet, Enhanced figures of merit for a high-performing actuator in electrostrictive materials, *Polymers* **2018**, *10*, 263.
[121] W. Zhang, S. Ahmed, S. Masters, J. Hong, Z. Ounaies, M. Frecker, Finite element analysis of electroactive and magnetoactive coupled behaviors in multi-field origami structures, *J. Intell. Mater. Syst. Struct.* **2018**, *29*, 3983.
[122] M. Lallart, C. Richard, P. Sukwisut, L. Petit, D. Guyomar, N. Muensit, Electrostrictive bending actuators: Modeling and experimental investigation, *Sens. Actuators, A* **2012**, *179*, 169.
[123] J. Wang, W. Li, L. Qin, J. Zhang, P. Wei, Effects of electrodes and protective layers on the electromechanical characteristics of piezoelectric stack actuators, *Adv. Compos. Lett.* **2019**, *28*, 0963693519877419.
[124] H. J. Xiang, Z. F. Shi, Static analysis for multi-layered piezoelectric cantilevers, *Int. J. Solids Struct.* **2008**, *45*, 113.
[125] E. Edqvist, E. Hedlund, B. Lundberg, Quasi-static and dynamic electromechanical response of piezoelectric multilayer cantilever beams, *Sens. Actuators, A* **2010**, *157*, 198.
[126] M. Goldfarb, N. Celanovic, Modeling piezoelectric stack actuators for control of micromanipulation, *IEEE Control Syst. Mag.* **1997**, *17*, 69.
[127] R. R. Munnig Schmidt, G. Schitter, A. Rankers, *The design of high performance mechatronics-: High-Tech functionality by multidisciplinary system integration*, Ios Press, Amsterdam, Netherlands **2020**.
[128] K. S. Tran, H. V. Phan, H. Y. Lee, Y. Kim, H. C. Park, Blocking force of a piezoelectric stack actuator made of single crystal layers (pmn-29pt), *Smart Mater. Struct.* **2016**, *25*, 095038.
[129] Q.-M. Wang, X.-H. Du, B. Xu, L. E. Cross, Electromechanical coupling and output efficiency of piezoelectric bending actuators, *IEEE Trans. Ultrason. Eng.* **1999**, *46*, 638.
[130] Q.-M. Wang, L. Eric Cross, Tip deflection and blocking force of soft pzt-based cantilever rainbow actuators, *J. Am. Ceram. Soc.* **1999**, *82*, 103.
[131] E. Fukada, T. Furukawa, Piezoelectricity and ferroelectricity in polyvinylidene fluoride, *Ultrasonics* **1981**, *19*, 31.
[132] F. Liu, N. Awanis Hashim, Y. Liu, M. R. Moghareh Abed, K. Li, Progress in the production and modification of pvdf membranes, *J. Membrane Sci.* **2011**, *375*, 1.
[133] J.-H. Bae, S.-H. Chang, Pvdf-based ferroelectric polymers and dielectric elastomers for sensor and actuator applications: a review, *Funct. Compos. Struct.* **2019**, *1*, 012003.
[134] A. J. Lovinger, Ferroelectric polymers, *Science* **1983**, *220*, 1115.
[135] T. Furukawa, Ferroelectric properties of vinylidene fluoride copolymers, *Phase Trans. A Multi. J.* **1989**, *18*, 143.
[136] K. Nakagawa, Y. Ishida, Estimation of amorphous specific volume of poly (vinylidene fluoride) as a function of temperature, *Kolloid-Zeitschrift und Zeitschrift für Polymere* **1973**, *251*, 103.
[137] K. Nakagawa, Y. Ishida, Annealing effects in poly(vinylidene fluoride) as revealed by specific volume measurements, differential scanning calorimetry, and electron microscopy, *J. Polym. Sci.: Polym. Phys. Ed.* **1973**, *11*, 2153.
[138] E. Koray Akdogan, M. Allahverdi, A. Safari, Piezoelectric composites for sensor and actuator applications, *IEEE Trans. Ultrason. Eng.* **2005**, *52*, 746.
[139] B. Ameduri, From vinylidene fluoride (vdf) to the applications of vdf-containing polymers and copolymers: Recent developments and future trends, *Chem. Rev.* **2009**, *109*, 6632.
[140] N. A. Shepelin, A. M. Glushenkov, V. C. Lussini, P. J. Fox, G. W. Dicinoski, J. G. Shapter, A. V. Ellis, New developments in composites, copolymer technologies and processing techniques for flexible fluoropolymer piezoelectric generators for efficient energy harvesting, *Energy Environ. Sci.* **2019**, *12*, 1143.
[141] E. Giannetti, Ferroelectric polymers, *Polym. Int.* **2001**, *50*, 10.
[142] A. Salimi, A. A. Yousefi, Ftir studies of b-phase crystal formation in stretched pvdf films, *Polym. Test* **2003**, *22*, 699.
[143] B.-E. E. Mohajir, N. Heymans, Changes in structural and mechanical behaviour of pvdf with processing and thermomechanical treatments. 1. change in structure, *Polymer* **2001**, *42*, 5661.
[144] B. Chu, X. Zhou, K. Ren, B. Neese, M. Lin, Q. Wang, F. Bauer, Q. M. Zhang, A dielectric polymer with high electric energy density and fast discharge speed, *Science* **2006**, *313*, 334.
[145] M. Wegener, W. Künstler, K. Richter, R. Gerhard-Multhaupt, Ferroelectric polarization in stretched piezo-and pyroelectric poly (vinylidene fluoride-hexafluoropropylene) copolymer films, *J. Appl. Phys.* **2002**, *92*, 7442.
[146] Alamusi, L. Wu, N. Hu, J. Yao, Y. Liu, H. Ning, X. Liu, W. Yuan, S. Fu, Improvement of the piezoelectricity of pvdf-trfe by carbon black, *Mater. Res. Express* **2018**, *6*, 025509.
[147] F. Bauer, Pvf2 polymers: ferroelectric polarization and piezoelectric properties under dynamic pressure and shock wave action, *Ferroelectrics* **1983**, *49*, 231.
[148] J. Gomes, J. Serrado Nunes, V. Sencadas, S. Lanceros-Méndez, Influence of the β-phase content and degree of crystallinity on the piezo-and ferroelectric properties of poly (vinylidene fluoride), *Smart Mater. Struct.* **2010**, *19*, 065010.
[149] J. M. Kenney, S. C. Roth, Room temperature poling of poly (vinylidene fluoride) with deposited metal electrodes, *J. Res. Nat. Bur. Stand.* **1979**, *84*, 447.
[150] T. Furukawa, G. E. Johnson, Measurements of ferroelectric switching characteristics in polyvinylidene fluoride, *Appl. Phys. Lett.* **1981**, *38*, 1027.
[151] B. P. Mahale, S. A. Gangal, D. S. Bodas, Pvdf based micro actuator, in *2012 1st Inter. Symp. on Physics and Technology of Sensors (ISPTS-1)*, IEEE, Pune, India **2012**, pp. 59–62.
[152] M. Womes, E. Bihler, W. Eisenmenger, Dynamics of polarization growth and reversal in pvdf films, *IEEE Trans. Electr. Insul.* **1989**, *24*, 461.

[153] B. Dickens, E. Balizer, A. S. DeReggi, S. C. Roth, Hysteresis measurements of remanent polarization and coercive field in polymers, *J. Appl. Phys.* **1992**, *72*, 4258.
[154] H. Wang, Q. M. Zhang, L. E. Cross, A. O. Sykes. Piezoelectric, dielectric, and elastic properties of poly (vinylidene fluoride/trifluoroethylene), *J. Appl. Phys.* **1993**, *74*, 3394.
[155] G. M. Sessler, Piezoelectricity in polyvinylidenefluoride, *J. Acoust. Soc. Am.* **1981**, *70*, 1596.
[156] P. Martins, J. Serrado Nunes, G. Hungerford, D. Miranda, A. Ferreira, V. Sencadas, S. Lanceros-Méndez, Local variation of the dielectric properties of poly(vinylidene fluoride) during the α- to β-phase transformation, *Phys. Lett. A* **2009**, *373*, 177.
[157] H. Ohigashi, Electromechanical properties of polarized polyvinylidene fluoride films as studied by the piezoelectric resonance method, *J. Appl. Phys.* **1976**, *47*, 949.
[158] R. G. Kepler, R. A. Anderson, Piezoelectricity and pyroelectricity in polyvinylidene fluoride, *J. Appl. Phys.* **1978**, *49*, 4490.
[159] B. Neese, Y. Wang, B. Chu, K. Ren, S. Liu, Q. M. Zhang, C. Huang, J. West, Piezoelectric responses in poly(vinylidene fluoride/hexafluoropropylene) copolymers, *App. Phys. Lett.* **2007**, *90*, 242917.
[160] E. L. Nix, I. M. Ward, The measurement of the shear piezoelectric coefficients of polyvinylidene fluoride, *Ferroelectrics* **1986**, *67*, 137.
[161] E. D. Burnham-Fay, T. Le, J. A. Tarbutton, J. D. Ellis, Strain characteristics of additive manufactured polyvinylidene fluoride (pvdf) actuators, *Sens. Actuat. A Phys.* **2017**, *266*, 85.
[162] K. Omote, H. Ohigashi, K. Koga, Temperature dependence of elastic, dielectric, and piezoelectric properties of "single crystalline"-films of vinylidene fluoride trifluoroethylene copolymer, *J. Appl. Phys.* **1997**, *81*, 2760.
[163] Z. Li, Y. Wang, Z.-Y. Cheng, Electromechanical properties of poly (vinylidene-fluoride-chlorotrifluoroethylene) copolymer, *Appl. Phys. Lett.* **2006**, *88*, 062904.
[164] X. Lu, A. Schirokauer, J. Scheinbeim, Giant electrostrictive response in poly (vinylidene fluoride-hexafluoropropylene) copolymers, *IEEE Trans. Ultrason. Eng.* **2000**, *47*, 1291.
[165] P.-H. Ducrot, I. Dufour, C. Ayela, Optimization of pvdf-trfe processing conditions for the fabrication of organic mems resonators, *Sci. Rep.* **2016**, *6*, 1.
[166] K. Koga, H. Ohigashi, Piezoelectricity and related properties of vinylidene fluoride and trifluoroethylene copolymers, *J. Appl. Phys.* **1986**, *59*, 2142.
[167] F. J. Baltá Calleja, A. González Arche, T. A. Ezquerra, C. Santa Cruz, F. Batallán, B. Frick, E. López Cabarcos, *Structure and Properties of Ferroelectric Copolymers of Poly(vinylidene Fluoride)*, Springer Berlin Heidelberg, Berlin, Heidelberg **1993**, pp. 1–48.
[168] G. D. Jones, R. A. Assink, T. R. Dargaville, P. M. Chaplya, R. L. Clough, J. M. Elliott, J. W. Martin, D. M. Mowery, M. Christopher Celina, *Characterization, performance and optimization of pvdf as a piezoelectric film for advanced space mirror concepts*, Technical Report SAND2005-6842, Sandia National Laboratories, Albuquerque, NM, USA, and Livermore, CA, USA **2005**.
[169] A. Jain, S. Jayanth Kumar, D. Roy Mahapatra, V. T. Rathod, Development of p (vdf-trfe) films and its quasi-static and dynamic strain response, *Int. J. Eng. Res. Technol.* **2013**, *2*, 2598.
[170] M. Kobayashi, Y. Chatani, K. Tashiro, K. Takano, H. Tadokoro, Structural study on ferroelectric phase transition of vinylidene fluoride-trifluoroethylene copolymers (iii) dependence of transitional behavior on vdf molar content, *Ferroelectrics* **1984**, *57*, 297.
[171] Z.-Y. Cheng, V. Bharti, T. Mai, T.-B. Xu, Q. M. Zhang, T. Ramotowski, K. A. Wright, R. Ting, Effect of high energy electron irradiation on the electromechanical properties of poly (vinylidene fluoride-trifluoroethylene) 50/50 and 65/35 copolymers, *IEEE Trans. Ultrason. Eng.* **2000**, *47*, 1296.
[172] K. Koga, N. Nakano, T. Hattori, H. Ohigashi, Crystallization, field-induced phase transformation, thermally induced phase transition, and piezoelectric activity in P(vinylidene fluoride-TrFE) copolymers with high molar content of vinylidene fluoride, *J. Appl. Phys.* **1990**, *67*, 965.
[173] H. Ohigashi, Piezoelectric polymers–materials and manufacture, *Jpn. J. Appl. Phys.* **1985**, *24*, 23.
[174] K. Tashiro, H. Kaito, M. Kobayashi, Structural changes in ferroelectric phase transitions of vinylidene fluoride-tetrafluoroethylene copolymers: 1. vinylidene fluoride content dependence of the transition behavior, *Polymer* **1992**, *33*, 2915.
[175] A. J. Lovinger, G. T. Davis, T. Furukawa, M. G. Broadhurst, Crystalline forms in a copolymer of vinylidene fluoride and trifluoroethylene (52/48 mol%), *Macromolecules* **1982**, *15*, 323.
[176] Y. Liu, H. Aziguli, B. Zhang, W. Xu, W. Lu, J. Bernholc, Q. Wang, Ferroelectric polymers exhibiting behaviour reminiscent of a morphotropic phase boundary, *Nature* **2018**, *562*, 96.
[177] Y. Liu, B. Zhang, W. Xu, A. Haibibu, Z. Han, W. Lu, J. Bernholc, Q. Wang, Chirality-induced relaxor properties in ferroelectric polymers. *Nat. Mater.* **2020**, *19*, 1169.
[178] L. Eric Cross, Relaxor ferroelectrics, *Ferroelectrics* **1987**, *76*, 241.
[179] A. K. Tagantsev, Vogel-fulcher relationship for the dielectric permittivity of relaxor ferroelectrics, *Phys. Rev. Lett.* **1994**, *72*, 1100.
[180] R. Pirc, R. Blinc, Vogel-fulcher freezing in relaxor ferroelectrics, *Phys. Rev. B* **2007**, *76*, 020101.
[181] X. Bai, H. Li, X. Chu, M. Liu, H. Li, H. Wang, X. Sun, S. Yan, The tuning of crystallization behavior of ferroelectric poly(vinylidene fluoride-co-trifluoroethylene), *J. Polym. Sci.* **2024**, *62*, 1742.
[182] Y. Li, W. Feng, L. Meng, K. M. Tse, Z. Li, L. Huang, Z. Su, S. Guo, Investigation on in-situ sprayed, annealed and corona poled pvdf-trfe coatings for guided wave-based structural health monitoring: From crystallization to piezoelectricity, *Mater. Des.* **2021**, *199*, 109415.
[183] T. Yagi, Y. Higashihata, K. Fukuyama, J. Sako, Piezoelectric properties of rolled vinylidene fluoride and trifluoroethylene copolymer, *Ferroelectrics* **1984**, *57*, 327.
[184] H. Ohigashi, K. Koga, M. Suzuki, T. Nakanishi, K. Kimura, N. Hashimoto, Piezoelectric and ferroelectric properties of p (vdf-trfe) copolymers and their application to ultrasonic transducers, *Ferroelectrics* **1984**, *60*, 263.
[185] R. S. Dahiya, M. Valle, G. Metta, L. Lorenzelli, S. Pedrotti, *Sensors*, IEEE, New York, NY, USA, **2008**, pp. 490–493.
[186] X. Hu, M. You, N. Yi, X. Zhang, Y. Xiang, Enhanced piezoelectric coefficient of pvdf-trfe films via in situ polarization, *Front. Energy Res.* **2021**, *9*, 621540.
[187] J. Seo, J. Y. Son, W.-H. Kim, Structural and ferroelectric properties of p (vdf-trfe) thin films depending on the annealing temperature, *Mater. Lett.* **2019**, *238*, 294.
[188] B. Qiao, X. Wang, S. Tan, W. Zhu, Z. Zhang, Synergistic effects of maxwell stress and electrostriction in electromechanical properties of poly (vinylidene fluoride)-based ferroelectric polymers, *Macromolecules* **2019**, *52*, 9000.
[189] J. Belovickis, M. Ivanov, Svirskas, V. Samulionis, J. Banys, A. V. Solnyshkin, S. A. Gavrilov, K. N. Nekludov, V. V. Shvartsman, M. V. Silibin, Dielectric, ferroelectric, and piezoelectric investigation of polymer-based p (vdf-trfe) composites, *Phys. Status Solidi b* **2018**, *255*, 1700196.
[190] H. L. W. Chan, M. C. Cheung, C. L. Choy, Study on batio3/p (vdf-trfe) 0–3 composites, *Ferroelectrics* **1999**, *224*, 113.
[191] Z. Li, Y. Wang, Z.-Y. Cheng, *Smart Structures and Materials 2005: Electroactive Polymer Actuators and Devices (EAPAD)* (Ed: Y. Bar-Cohen), *5759*, International Society for Optics and Photonics, SPIE **2005**, pp. 405–413.

[192] R. E. Sousa, J. C. C. Ferreira, C. M. Costa, A. V. Machado, M. M. Silva, S. Lanceros-Mendez, Tailoring poly(vinylidene fluoride-co-chlorotrifluoroethylene) microstructure and physicochemical properties by exploring its binary phase diagram with dimethylformamide, *J. Polym. Sci. Part B: Polym. Phys.* **2015**, *53*, 761.
[193] X. He, K. Yao, B. Keen Gan, Phase transition and properties of a ferroelectric poly (vinylidene fluoride-hexafluoropropylene) copolymer, *J. Appl. Phys.* **2005**, *97*, 084101.
[194] Y. Huan, Y. Liu, Y. Yang, Simultaneous stretching and static electric field poling of poly (vinylidene fluoride-hexafluoropropylene) copolymer films, *Polym. Eng. Sci.* **2007**, *47*, 1630.
[195] R. E. Sousa, J. Nunes-Pereira, J. C. C. Ferreira, C. M. Costa, A. V. Machado, M. M. Silva, S. Lanceros-Mendez, Microstructural variations of poly(vinylidene fluoride co-hexafluoropropylene) and their influence on the thermal, dielectric and piezoelectric properties, *Polym. Test.* **2014**, *40*, 245.
[196] N. Tohluebaji, C. Putson, N. Muensit, High electromechanical deformation based on structural beta-phase content and electrostrictive properties of electrospun poly (vinylidene fluoride-hexafluoropropylene) nanofibers, *Polymers* **1817**, *11*, 2019.
[197] A. C. Jayasuriya, A. Schirokauer, J. I. Scheinbeim, Crystal-structure dependence of electroactive properties in differently prepared poly (vinylidene fluoride/hexafluoropropylene) copolymer films, *J. Polym. Sci. Part B: Polym. Phys.* **2001**, *39*, 2793.
[198] W. Künstler, M. Wegener, M. Seiß, R. Gerhard-Multhaupt, Preparation and assessment of piezo-and pyroelectric poly (vinylidene fluoride-hexafluoropropylene) copolymer films. *Appl. Phys. A* **2001**, *73*, 641.
[199] X. Zhou, X. Zhao, Z. Suo, C. Zou, J. Runt, S. Liu, S. Zhang, Q. M. Zhang, Electrical breakdown and ultrahigh electrical energy density in poly (vinylidene fluoride-hexafluoropropylene) copolymer, *Appl. Phys. Lett.* **2009**, *94*, 162901.
[200] Q. M. Zhang, Z.-Y. Cheng, V. Bharti, Relaxor ferroelectric behavior in high-energy electron-irradiated poly (vinylidene fluoride-trifluoroethylene) copolymers, *Appl. Phys. A* **2000**, *70*, 307.
[201] Z.-Y. Cheng, H. Xu, T. X. Mai, T. C. Mike Chung, Q. Ming Zhang, R. Y. Ting, *Smart structures and materials 2001: Electroactive polymer actuators and devices*, Vol. *4329*, SPIE, Bellingham, WA, USA **2001**, pp. 106–116.
[202] Q. M. Zhang, V. Bharti, X. Zhao, Giant electrostriction and relaxor ferroelectric behavior in electron-irradiated poly (vinylidene fluoride-trifluoroethylene) copolymer, *Science* **1998**, *280*, 2101.
[203] Z.-Y. Cheng, V. Bharti, T.-B. Xu, S. Wang, Q. M. Zhang, T. Ramotowski, F. Tito, R. Ting, Transverse strain responses in electrostrictive poly (vinylidene fluoride-trifluoroethylene) films and development of a dilatometer for the measurement, *J. Appl. Phys.* **1999**, *86*, 2208.
[204] Y. Liu, H. Tong, C. Li, W. Qi, H. Zhou, Y. Liu, Morphotropic phase boundary in irradiated ferroelectric polymers, *Adv. Mater.* **2025**, *37*, 2502099.
[205] L. Yang, X. Li, E. Allahyarov, P. L. Taylor, Q. M. Zhang, L. Zhu, Novel polymer ferroelectric behavior via crystal isomorphism and the nanoconfinement effect, *Polymer* **2013**, *54*, 1709.
[206] Z.-Y. Cheng, D. Olson, H. Xu, F. Xia, J. S. Hundal, Q. M. Zhang, F. B. Bateman, G. J. Kavarnos, T. Ramotowski, Structural changes and transitional behavior studied from both micro-and macroscale in the high-energy electron-irradiated poly (vinylidene fluoride- trifluoroethylene) copolymer, *Macromolecules* **2002**, *35*, 664.
[207] H. Xu, G. Shanthi, V. Bharti, Q. M. Zhang, T. Ramotowski, Structural, conformational, and polarization changes of poly (vinylidene fluoride- trifluoroethylene) copolymer induced by high-energy electron irradiation, *Macromolecules* **2000**, *33*, 4125.
[208] Z.-Y. Cheng, Q. M. Zhang, F. B. Bateman, Dielectric relaxation behavior and its relation to microstructure in relaxor ferroelectric polymers: High-energy electron irradiated poly (vinylidene fluoride–trifluoroethylene) copolymers, *J. Appl. Phys.* **2002**, *92*, 6749.
[209] F. Bauer, Relaxor fluorinated polymers: novel applications and recent developments, *IEEE Trans. Dielectr. Electr. Insul.* **2010**, *17*, 1106.
[210] Z. Han, Y. Liu, X. Chen, W. Xu, Q. Wang, Enhanced piezoelectricity in poly(vinylidene fluoride-co-trifluoroethylene-co-chlorotrifluoroethylene) random terpolymers with mixed ferroelectric phases, *Macromolecules* **2022**, *55*, 2703.
[211] C. Li, Y. Liu, B. Li, Z. Yuan, T. Yang, Y. Liu, H. Gao, L. Xu, X. Yu, Q. Luo, S. Tang, M. Yao, Y. Gong, Z. Fei, L.-Q. Chen, H. Zhang, H. Zhou, Q. Wang, Enhanced energy storage in high-entropy ferroelectric polymers, *Nat. Mater.* **2025**, *24*, 1066–1073.
[212] H. Xu, Dielectric properties and ferroelectric behavior of poly (vinylidene fluoride-trifluoroethylene) 50/50 copolymer ultrathin films, *J. Appl. Polym. Sci.* **2001**, *80*, 2259.
[213] V. Bharti, X.-Z. Zhao, Q. M. Zhang, T. Romotowski, F. Tito, R. Ting, Ultrahigh field induced strain and polarization response in electron irradiated poly (vinylidene fluoride-trifluoroethylene) copolymer, *Mater. Res. Innov.* **1998**, *2*, 57.
[214] C. Huang, R. Klein, F. Xia, H. Li, Q. M. Zhang, F. Bauer, Z. Y. Cheng, Poly (vinylidene fluoride-trifluoroethylene) based high performance electroactive polymers, *IEEE Tran. Dielectr. Electr. Insul.* **2004**, *11*, 299.
[215] Z.-Y. Cheng, V. Bharti, T.-B. Xu, H. Xu, T. Mai, Q. M. Zhang, Electrostrictive poly (vinylidene fluoride-trifluoroethylene) copolymers, *Sens. Actuat. A: Phys.* **2001**, *90*, 138.
[216] F. Xia, Y. K. Wang, H. Li, C. Huang, Y. Ma, Q. M. Zhang, Z.-Y. Cheng, F. B. Bateman, Influence of the annealing conditions on the polarization and electromechanical response of high-energy-electron-irradiated poly(vinylidene fluoride trifluoroethylene) copolymer, *J. Polym. Sci. Part B: Polym. Phys.* **2003**, *41*, 797.
[217] P.-Y. Mabboux, K. K. Gleason, 19f nmr characterization of electron beam irradiated vinylidene fluoride–trifluoroethylene copolymers, *J. Fluor.Chem.* **2002**, *113*, 27.
[218] V. Bharti, H. S. Xu, G. Shanthi, Q. M. Zhang, K. Liang, Polarization and structural properties of high-energy electron irradiated poly (vinylidene fluoride-trifluoroethylene) copolymer films, *J. Appl. Phys.* **2000**, *87*, 452.
[219] H. Xu, Z.-Y. Cheng, D. Olson, T. Mai, Q. M. Zhang, G. Kavarnos, Ferroelectric and electromechanical properties of poly (vinylidene-fluoride–trifluoroethylene–chlorotrifluoroethylene) terpolymer, *Appl. Phys. Lett.* **2001**, *78*, 2360.
[220] F. Xia, Z.-Y. Cheng, H. S. Xu, H. F. Li, Q. M. Zhang, G. J. Kavarnos, R. Y. Ting, G. G. Abdul-Sadek, K. D. Belfield, High electromechanical responses in a poly (vinylidene fluoride–trifluoroethylene–chlorofluoroethylene) terpolymer, *Adv. Mater.* **2002**, *14*, 1574.
[221] H. Xu, D. Shen, Q. Zhang, Structural and ferroelectric response in vinylidene fluoride/trifluoroethylene/hexafluoropropylene terpolymers, *Polymer* **2007**, *48*, 2124.
[222] Z. Cheng, Q. Zhang, Field-activated electroactive polymers, *MRS Bulletin.* **2008**, *33*, 183.
[223] R. J. Klein, F. Xia, Q. M. Zhang, F. Bauer, Influence of composition on relaxor ferroelectric and electromechanical properties of poly (vinylidene fluoride-trifluoroethylene-chlorofluoroethylene), *J. Appl. Phys.* **2005**, *97*, 094105.
[224] J.-F. Capsal, J. Galineau, M.-Q. Le, F. D. D. Santos, P.-J. Cottinet, Enhanced electrostriction based on plasticized relaxor ferroelectric p (vdf-trfe-cfe/ctfe) blends, *J. Polym. Sci. B: Polym. Phys.* **2015**, *53*, 1368.

[225] P. Lheritier, S. Noel, N. Vaxelaire, F. D. D. Santos, E. Defay, Actuation efficiency of polyvinylidene fluoride-based co-and ter-polymers, *Polymer* **2018**, *156*, 270.
[226] A. Petchsuk, T. C. Chung, Synthesis and electric property of vdf/trfe/hfp terpolymers, *MRS Online Proc. Library OPL* **1999**, *600*, 53.
[227] R. J. Klein, J. J. Runt, Q. M. Zhang, Influence of crystallization conditions on the microstructure and electromechanical properties of poly (vinylidene fluoride- trifluoroethylene- chlorofluoroethylene) terpolymers, *Macromolecules* **2003**, *36*, 7220.
[228] T. Levard, P. J. Diglio, S.-G. Lu, C. D. Rahn, Q. M. Zhang, Core-free rolled actuators for braille displays using p (vdf–trfe–cfe), *Smart Mater. Struct.* **2011**, *21*, 012001.
[229] Q. Chen, B. Chu, X. Zhou, Q. M. Zhang, Effect of metal-polymer interface on the breakdown electric field of poly (vinylidene fluoride-trifluoroethylene-chlorofluoroethylene) terpolymer, *Appl. Phys. Lett.* **2007**, *91*, 062907.
[230] Q. Liu, C. Richard, J.-F. Capsal, Control of crystal morphology and its effect on electromechanical performances of electrostrictive p (vdf-trfe-ctfe) terpolymer, *Eur. Polym. J.* **2017**, *91*, 46.
[231] R. D'Annibalie, A. Zucchelli, R. Carloni, The effect of morphology on poly (vinylidene fluoride-trifluoroethylene-chlorotrifluoroethylene)-based soft actuators: Films and electrospun aligned nanofiber mats, *Sens. Actuat. A: Phys.* **2022**, *333*, 113255.
[232] C. Huang, Q. Zhang, Enhanced dielectric and electromechanical responses in high dielectric constant all-polymer percolative composites, *Adv. Funct. Mater.* **2004**, *14*, 501.
[233] N. D. K. Tu, M.-S. Noh, Y. Ko, J.-H. Kim, C. Y. Kang, H. Kim, Enhanced electromechanical performance of p (vdf-trfe-ctfe) thin films hybridized with highly dispersed carbon blacks, *Compos. Part B: Eng.* **2018**, *152*, 133.
[234] K. Thetpraphi, S. Chaipo, W. Kanlayakan, P.-J. Cottinet, M. Q. Le, L. Petit, D. Audigier, J. Kuhn, G. Moretto, J.-F. Capsal, Advanced plasticized electroactive polymers actuators for active optical applications: live mirror, *Adv. Eng. Mater.* **2020**, *22*, 1901540.
[235] Q. V. Duong, C. Park, Y. Lee, S. Lee, T. T. Nguyen, V. P. Nguyen, K. Lee, F. D. D. Santos, C. Park, S. Tae Choi, High-temperature electromechanical actuation of relaxor ferroelectric polymers blended with normal ferroelectric polymer, *Giant* **2024**, *17*, 100208.
[236] S. Zhang, B. Neese, K. Ren, B. Chu, Q. M. Zhang, Microstructure and electromechanical responses in semicrystalline ferroelectric relaxor polymer blends, *J. Appl. Phys.* **2006**, *100*.
[237] N. D. Schiava, F. Pedroli, K. Thetpraphi, A. Flocchini, M.-Q. Le, P. Lermusiaux, J.-F. Capsal, P.-J. Cottinet, Effect of beta-based sterilization on p (vdf-trfe-cfe) terpolymer for medical applications, *Sci. Rep.* **2020**, *10*, 8805.
[238] I. J. Kim, K. Y. Cho, E. Kim, Y. J. Kwon, M. Y. Shon, B.-I. Park, S. Yu, J. Hong Lee, Development of high dielectric electrostrictive pvdf terpolymer blends for enhanced electromechanical properties, *Nanomaterials* **2020**, *11*, 6.
[239] G. Gallucci, V. Jaarsma, and A. Hunt. (Ed: J. D. W. Madden, S. S. Seelecke, A. Ladegaard Skov), In *Electroactive Polymer Actuators And Devices (EAPAD) XXVI*, volume *12945*, page 1294503. International Society for Optics and Photonics, SPIE, **2024**.
[240] K. K. Keith Baelz, A. Hunt, P (vdf-trfe-ctfe) actuators with inkjet printed electrodes, in *2019 7th Inter. Conf. on Control, Mechatronics and Automation (ICCMA)*, IEEE, Delft, Netherlands **2019**, pp. 327–332.
[241] K. Keith Baelz and A. Hunt, (Ed: H. R. Shea, I. A. Anderson, and J. D. W. Madden, editors, *Electroactive Polymer Actuators and Devices (EAPAD) XXV*, volume *12482*, page 124820P. International Society for Optics and Photonics, SPIE, **2023**.
[242] S. A. Sekar, A. Hunt, Inkjet printing p(vdf-trfe-ctfe) actuators for large bending strains, *Smart Mater. Struct.* **2024**, *33*, 025036.
[243] S. IJssel de Schepper, A. Hunt, An airbrush 3d printer: Additive manufacturing of relaxor ferroelectric actuators, *Addit. Manuf.* **2024**, *81*, 103982.
[244] C. M. Roland, J. T. Garrett, R. Casalini, D. F. Roland, P. G. Santangelo, S. B. Qadri, Mechanical and electromechanical properties of vinylidene fluoride terpolymers, *Chem. Mater.* **2004**, *16*, 857.
[245] S. Zhang, N. Zhang, C. Huang, K. Ren, Q. M. Zhang, Microstructure and electromechanical properties of carbon nanotube/poly (vinylidene fluoride—trifluoroethylene—chlorofluoroethylene) composites, *Adv. Mater.* **2005**, *17*, 1897.
[246] S.-H. Yao, J.-K. Yuan, T. Zhou, Z.-M. Dang, J. Bai, Stretch-modulated carbon nanotube alignment in ferroelectric polymer composites: Characterization of the orientation state and its influence on the dielectric properties, *J. Phys. Chem. C* **2011**, *115*, 20011.
[247] K. Y. Cho, A. R. Cho, Y. J. Lee, C. M. Koo, S. M. Hong, S. S. Wang, H. G. Yoon, K. Y. Baek, in *Key Engineering Materials*, Vol. *605*, Trans Tech Publications, Zürich, Switzerland **2014**, pp. 335–339.
[248] B. Guiffard, L. Seveyrat, G. Sebald, D. Guyomar, Enhanced electric field-induced strain in non-percolative carbon nanopowder/polyurethane composites, *J. Phys.s D: Appl. Phys.* **2006**, *39*, 3053.
[249] I. Graz, M. Krause, S. Bauer-Gogonea, S. Bauer, S. P. Lacour, B. Ploss, M. Zirkl, B. Stadlober, S. Wagner, Flexible active-matrix cells with selectively poled bifunctional polymer-ceramic nanocomposite for pressure and temperature sensing skin, *J. Appl. Phys.* **2009**, *106*, 034503.
[250] A. Chiolerio, P. Rivolo, S. Porro, S. Stassi, S. Ricciardi, P. Mandracci, G. Canavese, K. Bejtka, C. Fabrizio Pirri, Inkjet-printed pedot: Pss electrodes on plasma-modified pdms nanocomposites: quantifying plasma treatment hardness, *Rsc Adv.* **2014**, *4*, 51477.
[251] J.-K. Yuan, S.-H. Yao, Z.-M. Dang, A. Sylvestre, M. Genestoux, J. Bai1, Giant dielectric permittivity nanocomposites: realizing true potential of pristine carbon nanotubes in polyvinylidene fluoride matrix through an enhanced interfacial interaction, *J. Phys. Chem. C* **2011**, *115*, 5515.
[252] S. Begum, H. Ullah, A. Kausar, M. Siddiq, M. Adeel Aleem, Fabrication of epoxy functionalized mwcnts reinforced pvdf nanocomposites with high dielectric permittivity, low dielectric loss and high electrical conductivity, *Compos. Sci. Technol.* **2018**, *167*, 497.
[253] Y. Niu, K. Yu, Y. Bai, H. Wang, Enhanced dielectric performance of batio 3/pvdf composites prepared by modified process for energy storage applications, *IEEE Trans. Ultrason. Eng.* **2015**, *62*, 108.
[254] R. Tamura, E. Lim, T. Manaka, M. Iwamoto, Analysis of pentacene field effect transistor as a maxwell-wagner effect element, *J. Appl. Phys.* **2006**, *100*, 114515.
[255] W. Cao, R. Gerhardt, Calculation of various relaxation times and conductivity for a single dielectric relaxation process, *Solid State Ionics* **1990**, *42*, 213.
[256] S. D. Vacche, Y. Leterrier, V. Michaud, D. Damjanovic, A. B. Aebersold, J.-A. E. Månson, Effect of interfacial interactions on the electromechanical response of poly (vinylidene fluoride-trifluoroethylene)/batio3 composites and its time dependence after poling, *Compos. Sci. Technol.* **2015**, *114*, 103.
[257] G. Perrier, A. Bergeret, Maxwell–wagner–sillars relaxations in polystyrene–glass-bead composites, *J. Appl. Phys.* **1995**, *77*, 2651.
[258] A. C. Lopes, C. Miguel Costa, R. S. i Serra, I. C. Neves, J. L. Gomez Ribelles, S. Lanceros-Méndez, Dielectric relaxation, ac conductivity and electric modulus in poly (vinylidene fluoride)/nay zeolite composites, *Solid State Ionics* **2013**, *235*, 42.
[259] X. Xia, Z. Zhong, G. J. Weng, Maxwell–wagner–sillars mechanism in the frequency dependence of electrical conductivity and dielectric

permittivity of graphene-polymer nanocomposites, *Mech. Mater.* **2017**, *109*, 42.
[260] P. Hedvig, *Dielectric Spectroscopy of Polymers*, Wiley, New York, NY, USA **1977**.
[261] K. G. Gatos, J. G. Martinez Alcazar, G. C. Psarras, R. Thomann, J. Karger-Kocsis, Polyurethane latex/water dispersible boehmite alumina nanocomposites: Thermal, mechanical and dielectrical properties, *Compos. Sci. Technol.* **2007**, *67*, 157.
[262] R. H. Boyd, F. Liu, Dielectric spectroscopy of semicrystalline polymers, in *Dielectric Spectroscopy of Polymeric Materials* (Eds: J. P. Runt, J. J. Fitzgerald), American Chemical Society, Washington, DC **1997**, pp. 107–136.
[263] P. A. M. Steeman, J. van Turnhout, Dielectric Properties of Inhomogeneous Media, in *Broadband Dielectric Spectroscopy* (Eds: F. Kremer, A. Schönhals), Springer, Berlin **2003**, pp. 495–522.
[264] D. S. Kalika, Dielectric Spectroscopy of Crystalline Polymers and Blends, in *Handbook of Low and High Dielectric Constant Materials and Their Applications* (Ed: H. S. Nalwa), Academic Press, Burlington **1999**, pp. 275–327.
[265] J. Y. Li, L. Zhang, S. Ducharme, Electric energy density of dielectric nanocomposites, *Appl. Phys. Lett.* **2007**, *90*, 132901.
[266] G. Polizos, E. Tuncer, V. Tomer, I. Sauers, C. A. Randall, E. Manias, *Nanoscale Spectroscopy With Applications*, CRC Press, Boca Raton, FL, USA **2018**, pp. 93–130.
[267] Z.-M. Dang, L. Wang, Y. I. Yin, Q. Zhang, Q.-Q. Lei, Giant dielectric permittivities in functionalized carbon-nanotube/electroactive-polymer nanocomposites, *Adv. Mater.* **2007**, *19*, 852.
[268] C.-W. Nan, Physics of inhomogeneous inorganic materials, *Prog. Mater. Sci.* **1993**, *37*, 1.
[269] J. Yuan, Percolation of carbon nanomaterials for high-k polymer nanocomposites, *Chin. Chem. Lett.* **2017**, *28*, 2036.
[270] C.-W. Nan, Y. Shen, J. Ma, Physical properties of composites near percolation, *Annu. Rev. Mater. Res.* **2010**, *40*, 131.
[271] A. L. Efros, B. I. Shklovskii, Critical behaviour of conductivity and dielectric constant near the metal-non-metal transition threshold, *Physica Status Solidi b* **1976**, *76*, 475.
[272] T. Yamada, T. Ueda, T. Kitayama, Piezoelectricity of a high-content lead zirconate titanate/polymer composite, *J. Appl. Phys.* **1982**, *53*, 4328.
[273] K. L. Ng, H. L. W. Chan, C. Loong Choy, Piezoelectric and pyroelectric properties of pzt/p (vdf-trfe) composites with constituent phases poled in parallel or antiparallel directions, *IEEE Trans. Ultrason. Eng.* **2000**, *47*, 1308.
[274] C. Zhang, H. Sun, Q. Zhu, Preparation and property enhancement of poly (vinylidene fluoride) (pvdf)/lead zirconate titanate (pzt) composite piezoelectric films, *J. Electron. Mater.* **2021**, *50*, 6426.
[275] P. Sampathkumar, P. Gowdhaman, S. Sundaram, V. Annamalai, A review on pzt-polymer composites: dielectric and piezoelectric properties, *Nano Vision* **2013**, *3*, 223.
[276] K. Uchino, *Advanced Piezoelectric Materials*, Elsevier, Amsterdam, Netherlands **2017**, pp. 353–382.
[277] X. Cai, C. Zhong, S. Zhang, H. Wang, A surface treating method for ceramic particles to improve the compatibility with pvdf polymer in 0-3 piezoelectric composites, *J. Mater. Sci. Lett.* **1997**, *16*, 253.
[278] X.-D. Chen, D.-B. Yang, Y.-D. Jiang, Z.-M. Wu, D. Li, F.-J. Gou, J.-D. Yang, 0–3 piezoelectric composite film with high d33 coefficient, *Sens. Actuat. A: Phys.* **1998**, *65*, 194.
[279] V. Tiwari, G. Srivastava, Structural, dielectric and piezoelectric properties of 0–3 pzt/pvdf composites, *Ceram. Int.* **2015**, *41*, 8008.
[280] T. Siponkoski, M. Nelo, J. Palosaari, J. Peräntie, M. Sobocinski, J. Juuti, H. Jantunen, Electromechanical properties of pzt/p (vdf-trfe) composite ink printed on a flexible organic substrate, *Compos. Part B: Eng.* **2015**, *80*, 217.
[281] M. Dietze, M. Es-Souni, Large area thick films of pvdf-trfe and relaxor-ceramics for piezo-and pyroelectric applications, *Macromol. Mater. Eng.* **2019**, *304*, 1900538.
[282] M. Wegener, K. Arlt, Pzt/p(vdf-hfp) 0–3 composites as solvent-cast thin films: preparation, structure and piezoelectric properties, *J. Phys. D: Appl. Phys.* **2008**, *41*, 165409.
[283] Y. J. Choi, M.-J. Yoo, H.-W. Kang, H.-G. Lee, S. H. Han, S. Nahm, Dielectric and piezoelectric properties of ceramic-polymer composites with 0–3 connectivity type, *J. Electroceram.* **2013**, *30*, 30.
[284] B. Ploss, B. Ploss, F. G. Shin, H. L. W. Chan, C. L. Choy, Pyroelectric or piezoelectric compensated ferroelectric composites, *Appl. Phys. Lett.* **2000**, *76*, 2776.
[285] K. H. Lam, H. L. W. Chan, Piezoelectric and pyroelectric properties of 65pmn-35pt/p(vdf-trfe) 0–3 composites, *Compos. Sci. Technol.* **2005**, *65*, 1107.
[286] Y. Liu, Y. Zhou, H. Qin, T. Yang, X. Chen, L. Li, Z. Han, K. Wang, B. Zhang, W. Lu, L.-Q. Chen, J. Bernholc, Q. Wang Electro-thermal actuation in percolative ferroelectric polymer nanocomposites, *Nat. Mater.* **2023**, *22*, 873.
[287] E. Kar, N. Bose, S. Das, N. Mukherjee, S. Mukherjee, Enhancement of electroactive β phase crystallization and dielectric constant of pvdf by incorporating geo 2 and sio 2 nanoparticles, *Phys. Chem. Chem. Phys.* **2015**, *17*, 22784.
[288] Y. Liu, T. Yang, B. Zhang, T. Williams, Y.-T. Lin, L. Li, Y. Zhou, W. Lu, Seong H. S. H. Kim, L.-Q. Chen, J. Bernholc, Q. Wang, Structural insight in the interfacial effect in ferroelectric polymer nanocomposites, *Adv. Mater.* **2020**, *32*, 2005431.
[289] Polymer actuation using a joule-heating-induced ferroelectric phase transition, *Nat. Mater.* **2023**, *22*, 814.
[290] C. Li, H. Qin, Y. Zhou, T. Yang, X. Chen, L. Li, Z. Yuan, K. Wang, B. Zhang, W. Lu, L.-Q. Chen, Y. Liu, J. Bernholc, Q. Wang, Strain-induced polar interfaces in ferroelectric polymer nanocomposites, *Adv. Funct. Mater.* **2025**, *35*, 2421825.
[291] M. Lallart, P.-J. Cottinet, L. Lebrun, B. Guiffard, D. Guyomar, Evaluation of energy harvesting performance of electrostrictive polymer and carbon-filled terpolymer composites, *J. Appl. Phys.* **2010**, *108*, 034901.
[292] X. Yin, J.-F. Capsal, D. Guyomar, A comprehensive investigation of poly (vinylidene fluoride-trifluoroethylene-chlorofluoroethylene) terpolymer nanocomposites with carbon black for electrostrictive applications, *Appl. Phys. Lett.* **2014**, *104*, 052913.
[293] N. Guo, S. A. DiBenedetto, P. Tewari, M. T. Lanagan, M. A. Ratner, T. J. Marks, Nanoparticle, size, shape, and interfacial effects on leakage current density, permittivity, and breakdown strength of metal oxide- polyolefin nanocomposites: experiment and theory, *Chem. Mater.* **2010**, *22*, 1567.
[294] K. Kunz, B. Krause, B. Kretzschmar, L. Juhasz, O. Kobsch, W. Jenschke, M. Ullrich, P. Pötschke, Direction dependent electrical conductivity of polymer/carbon filler composites, *Polymers* **2019**, *11*, 591.
[295] M. S. Shaffer, A. H. Windle, Fabrication and characterization of carbon nanotube/poly (vinyl alcohol) composites, *Adv. Mater.* **1999**, *11*, 937.
[296] M. Martin-Gallego, R. Verdejo, M. Khayet, J. M. O. de Zarate, M. Essalhi, M. A. Lopez-Manchado, Thermal conductivity of carbon nanotubes and graphene in epoxy nanofluids and nanocomposites, *Nanoscale Res. Lett.* **2011**, *6*, 1.
[297] Z. Xu, J. Zhang, M. Shan, Y. Li, B. Li, J. Niu, B. Zhou, X. Qian, Organosilane-functionalized graphene oxide for enhanced antifouling and mechanical properties of polyvinylidene fluoride ultrafiltration membranes, *J. Memb. Sci.* **2014**, *458*, 1.
[298] A. Ramaratnam, N. Jalili, Novel carbon nanotube reinforced electroactive polymer sensors for structural vibration control, *ASME Int. Mech. Eng. Congr. Expo.* **2004**, *47063*, 533.

[299] S. Sharafkhani, M. Kokabi, High performance flexible actuator: Pvdf nanofibers incorporated with axially aligned carbon nanotubes, *Compos. Part B: Eng.* **2021**, *222*, 109060.
[300] M. Panahi-Sarmad, B. Zahiri, M. Noroozi, Graphene-based composite for dielectric elastomer actuator: A comprehensive review, *Sens. Actuat. A: Phys.* **2019**, *293*, 222.
[301] J. Zhang, X. Wang, X. Chen, X. Xia, G. J. Weng, Piezoelectricity enhancement in graphene/polyvinylidene fluoride composites due to graphene-induced $\alpha \rightarrow \beta$ crystal phase transition, *Energy Convers. Manag.* **2022**, *269*, 116121.
[302] T. H. T. Fook, J. H. Jeon, P. See Lee, Transparent flexible polymer actuator with enhanced output force enabled by conductive nanowires interlayer, *Adv. Mater. Technol.* **2020**, *5*, 1900762.
[303] N. Levi, R. Czerw, S. Xing, P. Iyer, D. L. Carroll, Properties of polyvinylidene difluoride- carbon nanotube blends, *Nano Lett.* **2004**, *4*, 1267.
[304] K. Y. Cho, H. Park, H.-J. Kim, X. H. Do, C. M. Koo, S. S. Hwang, H. G. Yoon, K.-Y. Baek, Highly enhanced electromechanical properties of pvdf-trfe/swcnt nanocomposites using an efficient polymer compatibilizer, *Compos. Sci. Technol.* **2018**, *157*, 21.
[305] L. Yang, J. Qiu, H. Ji, K. Zhu, J. Wang, Enhanced electrical properties of multiwalled carbon nanotube/poly (vinylidenefluoride) films through a rolling process, *J. Mater. Sci.: Mater. Electron.* **2014**, *25*, 2126.
[306] F. Wen, Z. Xu, W. Xia, X. Wei, Z. Zhang, High dielectric permittivity and low dielectric loss nanocomposites based on poly (vdf–trfe–ctfe) and graphene nanosheets, *J. Adv. Dielectr.* **2013**, *3*, 1350010.
[307] L. Seveyrat, A. Chalkha, D. Guyomar, L. Lebrun, Preparation of graphene nanoflakes/polymer composites and their performances for actuation and energy harvesting applications, *J. Appl. Phys.* **2012**, *111*, 104904.
[308] A. Javadi, Y. Xiao, W. Xu, S. Gong, Chemically modified graphene/p (vdf-trfe-cfe) electroactive polymer nanocomposites with superior electromechanical performance, *J. Mater. Chem.* **2012**, *22*, 830.
[309] J. Xu, C. P. Wong, Effects of the low loss polymers on the dielectric behavior of novel aluminum-filled high-k nano-composites, in *9th Inter. Symp. on Advanced Packaging Materials: Processes, Properties and Interfaces (IEEE Cat. No. 04TH8742). 2004 Proc.*, IEEE, Atlanta, GA, USA **2004**, pp. 158–170.
[310] Y. Shen, Y. H. Lin, C.-W. Nan, Interfacial effect on dielectric properties of polymer nanocomposites filled with core/shell-structured particles, *Adv. Funct. Mater.* **2007**, *17*, 2405.
[311] L. Yang, J. Qiu, H. Ji, K. Zhu, J. Wang, Enhanced dielectric and ferroelectric properties induced by tio2@ mwcnts nanoparticles in flexible poly (vinylidene fluoride) composites, *Compos. Part A: Appl. Sci. Manuf.* **2014**, *65*, 125.
[312] H. Feng, W. Ma, Z.-K. Cui, X. Liu, J. Gu, S. Lin, Q. Zhuang, Core/shell-structured hyperbranched aromatic polyamide functionalized graphene nanosheets-poly (p-phenylene benzobisoxazole) nanocomposite films with improved dielectric properties and thermostability, *J. Mater. Chem. A* **2017**, *5*, 8705.
[313] L. Yang, H. Ji, K. Zhu, J. Wang, J. Qiu, Dramatically improved piezoelectric properties of poly(vinylidene fluoride) composites by incorporating aligned tio2@mwcnts, *Compos. Sci. Technol.* **2016**, *123*, 259.
[314] L. Yang, M. Cheng, W. Lyu, M. Shen, J. Qiu, H. Ji, Q. Zhao, Tunable piezoelectric performance of flexible pvdf based nanocomposites from mwcnts/graphene/mno2 three-dimensional architectures under low poling electric fields, *Compos. Part A: Appl. Sci. Manuf.* **2018**, *107*, 536.
[315] L. Yang, Q. Zhao, Y. Hou, R. Sun, M. Cheng, M. Shen, S. Zeng, H. Ji, J. Qiu, High breakdown strength and outstanding piezoelectric performance in flexible pvdf based percolative nanocomposites through the synergistic effect of topological-structure and composition modulations, *Compos. Part A: Appl. Sci. Manuf.* **2018**, *114*, 13.
[316] X. Liang, S. Yu, R. Sun, S. Luo, J. Wan, Z. Zhuang, Microstructure and dielectric behavior of the three-phase ag@ sio2/batio3/pvdf composites with high permittivity, *J. Mater. Res.* **2012**, *27*, 991.
[317] J.-W. Wang, Q.-D. Shen, C.-Z. Yang, Q.-M. Zhang, High dielectric constant composite of p (vdf- trfe) with grafted copper phthalocyanine oligomer, *Macromolecules* **2004**, *37*, 2294.
[318] J.-W. Wang, Q.-D. Shen, H.-M. Bao, C.-Z. Yang, Q. M. Zhang, Microstructure and dielectric properties of p (vdf- trfe- cfe) with partially grafted copper phthalocyanine oligomer, *Macromolecules* **2005**, *38*, 2247.
[319] C. Geng, J. Wang, Q. Zhang, Q. Fu, New piezoelectric damping composites of poly (vinylidene fluoride) blended with clay and multi-walled carbon nanotubes. *Polym. Int.* **2012**, *61*, 934.
[320] Y. Y. Zhang, S. L. Jiang, Y. Yu, G. Xiong, Q. F. Zhang, G. Z. Guang, Phase transformation mechanisms and piezoelectric properties of poly (vinylidene fluoride)/montmorillonite composite, *J. Appl. Polym. Sci.* **2012**, *123*, 2595.
[321] F.-A. He, K. Lin, D.-L. Shi, H.-J. Wu, H.-K. Huang, J.-J. Chen, F. Chen, K.-H. Lam, Preparation of organosilicate/pvdf composites with enhanced piezoelectricity and pyroelectricity by stretching, *Compos. Sci. Technol.* **2016**, *137*, 138.
[322] C. Löwe, X. Zhang, G. Kovacs, Dielectric elastomers in actuator technology, *Adv. Eng. Mater.* **2005**, *7*, 361.
[323] C. Renard, D. Wang, Y. Yang, S. Xiong, C.-Y. Shi, Z.-M. Dang, Plasticized thermoplastic polyurethanes for dielectric elastomers with improved electromechanical actuation, *J. Appl. Polym. Sci.* **2017**, *134*, 45123.
[324] F. Galantini, F. Carpi, G. Gallone, Effects of plasticization of a soft silicone for dielectric elastomer actuation, *Smart Mater. Struct.* **2013**, *22*, 104020.
[325] J. M. Davies, R. F. Miller, W. F. Busse, Dielectric properties of plasticized polyvinyl chloride, *J. Am. Chem. Soc.* **1941**, *63*, 361.
[326] J.-F. Capsal, J. Galineau, M. Lallart, P.-J. Cottinet, D. Guyomar, Plasticized relaxor ferroelectric terpolymer: Toward giant electrostriction, high mechanical energy and low electric field actuators, *Sens. Actuat. A: Phys.* **2014**, *207*, 25.
[327] G. Wypych, Effect of Plasticizers on Properties of Plasticized Materials, in *>Handbook of Plasticizers*, 4th Ed. (Ed: G. Wypych), ChemTec Publishing, Toronto **2023**, pp. 229–311.
[328] G. C. Psarras, *Dielectric Polymer Materials for High-Density Energy Storage* (Ed: Z.-M. Dang), William Andrew Publishing, Norwich, NY, USA **2018**, pp. 11–57.
[329] M. Q. Le, J.-F. Capsal, J. Galineau, F. Ganet, X. Yin, M. D. Yang, J.-F. Chateaux, L. Renaud, C. Malhaire, P.-J. Cottinet, R. Liang, All-organic electrostrictive polymer composites with low driving electrical voltages for micro-fluidic pump applications, *Sci. Rep.* **2015**, *5*, 1.
[330] X. Yin, Q. Liu, J. Galineau, P.-J. Cottinet, D. Guyomar, J.-F. Capsal, Enhanced electromechanical performances in plasticizer modified electrostrictive polymers, *Eur. Polym. J.* **2016**, *76*, 88.
[331] N. D. Schiava, M.-Q. Le, J. Galineau, F. D. D. Santos, P.-J. Cottinet, J.-F. Capsal, Influence of plasticizers on the electromechanical behavior of a p (vdf-trfe-ctfe) terpolymer: Toward a high performance of electrostrictive blends, *J. Polym. Sci. Part B: Polym. Phys.* **2017**, *55*, 355.
[332] Q. Gao, J. I. Scheinbeim, B. A. Newman, Ferroelectric properties of nylon 11 and poly(vinylidene fluoride) blends, *J. Polym. Sci. Part B: Polym. Phys.* **1999**, *37*, 3217.
[333] Q. Gao, J. I. Scheinbeim, Dipolar intermolecular interactions, structural development, and electromechanical properties in ferroelectric polymer blends of nylon-11 and poly(vinylidene fluoride), *Macromolecules* **2000**, *33*, 7564.

[334] A. C. Jayasuriya, A. Schirokauer, J. I. Scheinbeim, *Smart Structures and Materials 2001: Electroactive Polymer Actuators and Devices*, (Ed: Yoseph Bar-Cohen), *4329*, International Society for Optics and Photonics, SPIE **2001**, pp. 125–130.
[335] Z. Li, Y. Wang, Z.-Y. Cheng, Thermal and electric properties of p (vdf-trfe) and p (vdf-ctfe) copolymer blends, *MRS Online Proc. Libr.* **2004**, *856*, BB12.
[336] Q. V. Duong, V. P. Nguyen, F. D. D. Santos, S. Tae Choi, Localized fretting-vibrotactile sensations for large-area displays, *ACS Appl. Mater. Interfaces* **2019**, *11*, 33292.
[337] Lee J. L. J. Gorny, S.-G. Lu, S. Liu, M. Lin, Electromechanical properties of relaxor ferroelectric p(vdf-trfe-cfe)-p(vdf-ctfe) blends, *IEEE Trans. Ultrason. Eng.* **2013**, *60*, 441.
[338] V. Bharti, H. Hu, Z. Y. Cheng, T. Mai, Q. M. Zhang, Quantitative analysis of structural, relaxational and electrostrictive properties of pvdf-trfe/pmma films irradiated with high-energy electrons, *IEEE Trans. Dielectr. Electr. Insul.* **2001**, *8*, 718.
[339] B. Chu, B. Neese, M. Lin, X. Zhou, Q. Chen, Q. M. Zhang, in *Technical Proceedings of the 2008 Clean Technology Conf. and Trade Show*, TechConnect Briefs, Boston, MA, USA **2008**, pp. 499–502.
[340] K. H. Stark, C. G. Garton, Electric strength of irradiated polythene, *Nature* **1955**, *176*, 1225.
[341] G. Casar, X. Li, Q. M. Zhang, V. Bobnar, Influencing dielectric properties of relaxor polymer system by blending vinylidene fluoride–trifluoroethylene-based terpolymer with a ferroelectric copolymer, *J. Appl. Phys.* **2014**, *115*, 104101.
[342] A. Ullah, A. ur Rahman, C. Won Ahn, M.-U. Rahman, A. Ullah, Z.-U. Rehman, M. Javid Iqbal, I. W. Kim, Enhancement of dielectric and energy density properties in the pvdf-based copolymer/terpolymer blends, *Polym. Eng. Sci.* **2015**, *55*, 1396.
[343] X. Zhang, Y. Shen, Z. Shen, J. Jiang, L. Chen, C.-W. Nan, Achieving high energy density in pvdf-based polymer blends: Suppression of early polarization saturation and enhancement of breakdown strength, *ACS Appl. Mater. Interfaces* **2016**, *8*, 27236.
[344] H. Ohigashi, R. Shigenari, Kokai 49–84798, Toray Industries, Inc., Japan, **1974**, 47–128115.
[345] H. Sussner, D. Michas, A. Assfalg, S. Hunklinger, K. Dransfeld, Piezoelectric effect in polyvinylidene fluoride at high frequencies, *Phys. Lett. A* **1973**, *45*, 475.
[346] M. Tamura, T. Yamaguchi, T. Oyaba, T. Yoshimi, Electroacoustic transducers with piezoelectric high polymer films, *J. Audio Eng. Soc* **1975**, *23*, 21.
[347] D. Brandt, G. Bohannan, H. Schmidt, M. Mooibroek, Piezoelectric polymer actuators for active vibration isolation in space applications, *Ferroelectrics* **1999**, *224*, 211.
[348] R. Pérez, M. Král, H. Bleuler, Study of polyvinylidene fluoride (pvdf) based bimorph actuators for laser scanning actuation at khz frequency range, *Sens. Actuat. A Phys.* **2012**, *183*, 84.
[349] J. T. Polasik, V. Hugo Schmidt, *Smart Structures And Materials 2005: Electroactive Polymer Actuators And Devices (EAPAD)*, Vol. *5759*, SPIE, Bellingham, WA, USA **2005**, pp. 114–120.
[350] M. Toda, S. Osaka, E. O. Johnson, A new electromotional device, *RCA Eng.* **1979**, *25*, 24.
[351] M. M. Toda, S. S. Osaka, Vibrational fan using the piezoelectric polymer pvf 2, *Proc. IEEE* **1979**, *67*, 1171.
[352] M. Toda, Elastic properties of piezoelectric PVF2, *J. Appl. Phys.* **1980**, *51*, 4673.
[353] M. Toda, Voltage-induced large amplitude bending device-pvf2 bimorph-its properties and applications, *Ferroelectrics* **1981**, *32*, 127.
[354] S. Osaka, M. Toda, S. Tosima, Large area display element using pvf2bimorph with double-support structure, *Ferroelectrics* **1980**, *23*, 115.
[355] V. Hugo Schmidt, L. Lediaev, J. Polasik, J. Hallenberg, Piezoelectric actuators employing pvdf coated with flexible pedot-pss polymer electrodes, *IEEE Trans. Dielectr. Electr. Insul.* **2006**, *13*, 1140.
[356] Y. Z. Liu, Z. W. Hao, J. X. Yu, X. R. Zhou, P. See Lee, Y. Sun, Z. C. Mu, F. L. Zeng, A high-performance soft actuator based on a poly(vinylidene fluoride) piezoelectric bimorph, *Smart Mater. Struct.* **2019**, *28*, 055011.
[357] Q. Chen, D. Natale, B. Neese, K. Ren, M. Lin, Q. M. Zhang, M. Pattom, K. W. Wang, *Electroactive Polymer Actuators And Devices (EAPAD) 2007*, Vol. *6524*, SPIE, Bellingham, WA, USA **2007**, pp. 491–501.
[358] Y. Fu, E. C. Harvey, M. K. Ghantasala, G. M. Spinks, Design, fabrication and testing of piezoelectric polymer pvdf microactuators, *Smart Mater. Struct.* **2005**, *15*, S141.
[359] T. Sato, H. Ishida, O. Ikeda, Adaptive pvdf piezoelectric deformable mirror system, *Appl. Opt.* **1980**, *19*, 1430.
[360] Y. Zhang, H. Niu, S. Xie, X. Zhang, Numerical and experimental investigation of active vibration control in a cylindrical shell partially covered by a laminated pvdf actuator, *Smart Mater. Struct.* **2008**, *17*, 035024.
[361] Y. Zhang, X. Zhang, S. Xie, Adaptive vibration control of a cylindrical shell with laminated pvdf actuator, *Acta Mech.* **2010**, *210*, 85.
[362] N. Snis, E. Edqvist, U. Simu, S. Johansson, Monolithic fabrication of multilayer p(vdf-trfe) cantilevers, *Sens. Actuat. A: Phys.* **2008**, *144*, 314.
[363] E. Edqvist, N. Snis, S. Johansson, Gentle dry etching of p(vdf-trfe) multilayer micro actuator structures by use of an inductive coupled plasma, *J. Micromechan. and MicroEng.* **2007**, *18*, 015007.
[364] E. Edqvist, E. Hedlund, Design and manufacturing considerations of low-voltage multilayer p(vdf-trfe) actuators, *J. Micromechan. and MicroEng.* **2009**, *19*, 115019.
[365] O. O. Pabst, J. J. Perelaer, E. E. Beckert, U. S. Schubert, R. Eberhardt, A. Tünnermann, *Electroactive Polymer Actuators and Devices (EAPAD) 2011*, Vol. *7976*, SPIE, Bellingham, WA, USA **2011**, pp. 717–722.
[366] O. Pabst, J. Perelaer, E. Beckert, U. S. Schubert, R. Eberhardt, A. Tünnermann, All inkjet-printed piezoelectric polymer actuators: Characterization and applications for micropumps in lab-on-a-chip systems, *Organ. Electron.* **2013**, *14*, 3423.
[367] K. Patterson, S. Pellegrino, Ultralightweight deformable mirrors, *Appl. Opt.* **2013**, *52*, 5327.
[368] K. Wang, T. Godfroid, D. Robert, and A. Preumont, Electrostrictive PVDF-TrFE Thin Film Actuators for the Control of Adaptive Thin Shell Reflectors, *Actuators* **2020**, *9*, 53.
[369] F. Xia, S. Tadigadapa, Q. M. Zhang, Electroactive polymer based microfluidic pump, *Sens. Actuat. A: Phys.* **2006**, *125*, 346.
[370] T.-B. Xu, Z.-Y. Cheng, H. Xu, W. Chen, K. Uchino, Q. Ming Zhang, *Smart Structures and Materials 2001: Electroactive Polymer Actuators and Devices*, Vol. *4329*, SPIE, Bellingham, WA, USA **2001**, pp. 133–140.
[371] T.-B. Xu, Z.-Y. Cheng, Q. M. Zhang, High-performance micromachined unimorph actuators based on electrostrictive poly (vinylidene fluoride–trifluoroethylene) copolymer, *Appl. Phys. Lett.* **2002**, *80*, 1082.
[372] S. Ahmed, Z. Ounaies, E. A. F. Arrojado, Electric field-induced bending and folding of polymer sheets, *Sens. Actuat. A: Phys.* **2017**, *260*, 68.
[373] K. Kadooka, H. Imamura, M. Taya, Experimentally verified model of viscoelastic behavior of multilayer unimorph dielectric elastomer actuators, *Smart Mater. Struct.* **2016**, *25*, 105028.
[374] R. D'Anniballe, G. Selleri, L. Wierenga, A. Zucchelli, D. Fabiani, R. Carloni, Soft composite actuators of poly(vinylidene fluoride-trifluoroethylene-chlorotrifluoroethylene)-based nanofibers and polydimethylsiloxane: Fabrication, electromechanical characterization, and dynamic modeling, *Mater. Des.* **2023**, *236*, 112467.

[375] R. D'Anniballe, N. Erdmann, G. Selleri, R. Carloni, Dynamic modeling of p(vdf-trfe-ctfe)-based soft actuators via echo state networks, in *2022 IEEE/ASME Inter. Conf. on Advanced Intelligent Mechatronics (AIM)*, IEEE, Hampton, VA, USA **2022**, pp. 118–124.
[376] S. T. Choi, J. O. Kwon, F. Bauer, Multilayered relaxor ferroelectric polymer actuators for low-voltage operation fabricated with an adhesion-mediated film transfer technique, *Sens. Actuat. A: Phys.* **2013**, *203*, 282.
[377] W.-E. Ju, Y.-J. Moon, C.-H. Park, S. Tae Choi, A flexible tactile-feedback touch screen using transparent ferroelectric polymer film vibrators, *Smart Mater. Struct.* **2014**, *23*, 074004.
[378] K. Thetpraphi, M. Q. Le, A. Houachtia, P.-J. Cottinet, L. Petit, D. Audigier, J. Kuhn, G. Moretto, J.-F. Capsal, Surface correction control based on plasticized multilayer p(vdf-trfe-cfe) actuator—live mirror, *Adv. Opt. Mater.* **2019**, *7*, 1900210.
[379] F. ea Ganet, M.-Q. Le, J. F. Capsal, P. Lermusiaux, L. Petit, A. Millon, P. J. Cottinet, Development of a smart guide wire using an electrostrictive polymer: option for steerable orientation and force feedback, *Sci. Rep.* **2015**, *5*, 18593.
[380] S. G. Lu, X. Chen, T. Levard, P. J. Diglio, L. J. Gorny, C. D. Rahn, Q. M. Zhang, Large displacement in relaxor ferroelectric terpolymer blend derived actuators using al electrode for braille displays, *Sci. Rep.* **2015**, *5*, 11361.
[381] H. Tian, C. Guo, X. Li, S. Wang, Y. Xin, H. Sun, C. Wang, The use of polyvinylidene fluoride (pvdf) films as sensors for vibration measurement: A brief review, *Ferroelectrics* **2016**, *502*, 28.
[382] Y. Chen, X. Zhang, C. Lu, Flexible piezoelectric materials and strain sensors for wearable electronics and artificial intelligence applications, *Chem. Sci.* **2024**, *15*, 16436.
[383] C. Peng, Y. Chen, B. Yang, Z. Jiang, Y. Liu, Z. Liu, L. Zhou, L. Tang, Recent advances of soft actuators in smart wearable electronic-textile, *Adv. Mater. Technol.* **2024**, *9*, 2400079.
[384] C. Pacchierotti, S. Sinclair, M. Solazzi, A. Frisoli, V. Hayward, D. Prattichizzo, Wearable haptic systems for the fingertip and the hand: Taxonomy, review, and perspectives, *IEEE Trans. Haptics* **2017**, *10*, 580.
[385] V. Hayward, O. R. Astley, M. Cruz-Hernandez, D. Grant, G. Robles-De-La-Torre, Haptic interfaces and devices, *Sens. Rev.* **2004**, *24*, 16.
[386] J. Pritchard, C. R. Bowen, F. Lowrie, Multilayer actuators, *British Ceram. Trans.* **2001**, *100*, 265.
[387] S. Takahashi, Multilayer piezoelectric ceramic actuators and their applications, *Jpn. J. Appl. Phys.* **1985**, *24*, 41.
[388] G. Kovacs, L. Düring, S. Michel, G. Terrasi, Stacked dielectric elastomer actuator for tensile force transmission, *Sens. Actuat. A: Phys.* **2009**, *155*, 299.
[389] G. Kovacs, L. Düring, *Electroactive Polymer Actuators and Devices (EAPAD) 2009*, Vol. *7287*, SPIE, Bellingham, WA, USA **2009**, pp. 106–120.
[390] W. Lai, A. F. Bastawros, W. Hong, S.-J. Chung, Fabrication and analysis of planar dielectric elastomer actuators capable of complex 3-d deformation, in *2012 IEEE Inter. Conf. on Robotics and Automation*, IEEE, Saint Paul, MN, USA **2012**, pp. 4968–4973.
[391] S. Ahmed, Z. Ounaies, M. Frecker, Investigating the performance and properties of dielectric elastomer actuators as a potential means to actuate origami structures, *Smart Mater. Struct.* **2014**, *23*, 094003.
[392] F. Carpi, C. Salaris, D. De Rossi, Folded dielectric elastomer actuators, *Smart Mater. Struct.* **2007**, *16*, S300.
[393] G.-K. Lau, S. C.-K. Goh, L.-L. Shiau, Dielectric elastomer unimorph using flexible electrodes of electrolessly deposited (eld) silver, *Sens. Actuat. A: Phys.* **2011**, *169*, 234.
[394] H. Fu, Y. Jiang, J. Lv, Y. Huang, Z. Gai, Y. Liu, P. S. Lee, H. Xu, D. Wu, Multilayer dielectric elastomer with reconfigurable electrodes for artificial muscle, *Adv. Sci.* **2023**, *10*, 2206094.
[395] M. Duduta, R. J. Wood, D. R. Clarke, Multilayer dielectric elastomers for fast, programmable actuation without prestretch, *Adv. Mater.* **2016**, *28*, 8058.
[396] S. Su, T. He, H. Yang, 3d printed multilayer dielectric elastomer actuators, *Smart Mater. Struct.* **2023**, *32*, 035021.
[397] O. A. Araromi, A. T. Conn, C. S. Ling, J. M. Rossiter, R. Vaidyanathan, S. C. Burgess, Spray deposited multilayered dielectric elastomer actuators, *Sens. Actuat. A: Phys.*, Solid-State Sensors, Actuators and Microsystems Workshop **2011**, *167*, 459.
[398] M. Duduta, E. Hajiesmaili, H. Zhao, R. J. Wood, D. R. Clarke, Realizing the potential of dielectric elastomer artificial muscles, *Proc. Natl. Acad. Sci.* **2019**, *116*, 2476.

Giulio Gallucci received his master's degree in nanotechnology engineering from 'La Sapienza' University of Romein 2022. He is currently a Ph.D. student in the Department of Precision and Microsystems Engineering at Delft University of Technology. His research focuses on smart material structures and strategies to enhance transduction performance in electroactive polymer actuators.

Andres Hunt is an assistant professor in the Departmentof Precision and Microsystems Engineering at Delft University of Technology. His research focuses on high-performance functional materials, actuators, and additive manufacturing methods to enable embedding actuation, sensing, and other intelligent functionalities into engineering materials, structures, and devices.